UNIVERSIDADE BEIRA INTERIOR

Development of micro/nano cellulose-based biodegradable materials using 3D computational simulation

José António Silva Mendes

Dissertação para obtenção do Grau de Mestre em
Biotecnologia
(2º ciclo de estudos)

Orientadora: Professora Doutora Joana Maria Rodrigues Curto

Outubro de 2023

Declaração de Integridade

Eu, José António Silva Mendes, que abaixo assino, estudante com o número de inscrição M11316 de Biotecnologia da Faculdade de Ciências da Saúde, declaro ter desenvolvido o presente trabalho e elaborado o presente texto em total consonância com o **Código de Integridades da Universidade da Beira Interior**.

Mais concretamente afirmo não ter incorrido em qualquer das variedades de Fraude Académica, e que aqui declaro conhecer, que em particular atendi à exigida referenciação de frases, extratos, imagens e outras formas de trabalho intelectual, e assumindo assim na íntegra as responsabilidades da autoria.

Universidade da Beira Interior, Covilhã 09/ 10 / 2023

Assinado por: **José António Silva Mendes**
Num. de Identificação: 15479764
Data: 2023.10.09 13:10:14+01'00'

CHAVE MÓVEL

Acknowledgments

A year of hard work and commitment to this project has allowed me to grow personally and professionally. This would not have been possible without the support of certain people who inspired me to believe in my potential. Therefore, I would like to thank them.

Since my second year of bioengineering, Professor Doctor Joana Maria Rodrigues Curto has allowed me to grow as a researcher by sharing her laboratory, industrial, and professional knowledge. Her motivation, support, and search for new challenges outside the box made me leave my comfort zone and risk going beyond my capabilities.

I want to thank Canna Forest Lda. for their confidence in our work and partnership throughout this project.

To the FibEnTech Research Unit, its Coordinator, Professor Doutor Paulo Fiadeiro, and the researchers and professors of the Chemistry Department of the University of Beira Interior, without them, it would not be possible to have access to the laboratories and equipment for carrying out the experimental work.

Special thanks to my friend, MSc João Medeiros, for his assistance in obtaining and characterizing hemp fibers in the laboratory and for all the companionship created over the last year of work. Also thank you, to PhD Flávia Morais, MSc Joana Moreira, MSc Sofia Oliveira, MSc Pedro Videira, and MSc João Velosa provided me with a good working environment, showing companionship and team spirit, as well as all available, in clarifying the various doubts that have arisen throughout the work. To the researchers at Fiber Materials and Environmental Technologies Laboratories and technical support from César Marques and Dr. Ana Paula Gomes in acquisition of Scanning Electron Microscope (SEM) images.

To all my Desertuna friends, thank you for your friendship, music, and support along this journey.

To all my other friends, especially Bruno Monteiro and Beatriz Ferreira, who were always there to support me in the good and bad times during these five years in Covilhã.

To my parents and sister for believing in me and encouraging me to face challenges, no matter how big they may appear to be. Thank you.

Finally, thank you to the financial support received from FCT, Foundation for Science and Technology for the funding of the FibEnTech-UBI Research Unit, project UIDB/00195/2020.

Resumo

O aumento drástico de plásticos de uso único (PUU) produzidos a partir matérias de origem fóssil não biodegradáveis contribuiu para o crescimento da poluição constituindo um problema ambiental. As preocupações com o meio ambiente e o desenvolvimento de produtos biodegradáveis a partir de fontes renováveis, especificamente o desenvolvimento de embalagens sustentáveis utilizando fibras de celulose de diferentes fontes vegetais, representam um desafio multidisciplinar no qual esta investigação está inserida.

Selecionaram-se para este estudo fibras de *Eucalyptus* globulus branqueado, *Picea* abies não branqueado e fibras de cânhamo produzidas em laboratório. As fibras foram avaliadas quanto à sua morfologia e biometria, e foram produzidas estruturas laboratorialmente com diversas misturas e tratamentos mecânicos no PFI. As suas propriedades estruturais, mecânicas, óticas e químicas foram caracterizadas experimentalmente, utilizando metodologias e seguindo as respetivas normas ISO. As fibras e estruturas por elas formadas foram simuladas utilizando modelos de simulação computacional em 3D. A compostagem foi avaliada e utilizada para a realização testes de biodegradabilidade através de uma metodologia desenvolvida para ser utilizada tanto em laboratório, como nas indústrias do setor, tendo sido recolhidos dados para o efeito.

A comparação das fibras de referência revelou que as fibras de *softwood* são aproximadamente três vezes mais longas que as fibras de *hardwood*. Em termos de largura, as fibras de *softwood* são cerca de duas vezes mais largas que as fibras de *hardwood*. No geral, o aumento da refinação resultou num aumento na fibrilação e nos elementos finos da amostra. Como resultado, a espessura dos *handsheets* foi reduzida em 62% (HW) e 60% (SW) quando comparadas às folhas feitas com fibras não refinadas. Uma maior compactação e maiores ligações entre fibras contribuíram para uma estrutura mais coesa e reforçada, como evidenciado pelo aumento exponencial no índice de tração e no módulo de elasticidade das estruturas refinadas. As características das fibras de cânhamo foram semelhantes às fibras de *Picea abies*, mas um pouco mais longas. O índice de tração aumentou em 62,33% e o módulo de elasticidade em 40,50% numa combinação otimizada de fibra de cânhamo com fibras de eucalipto. Além disso, os estudos de biodegradação avaliaram o efeito da compostagem após 28 e 60 dias, indicando que as estruturas refinadas se biodegradaram mais rapidamente do que as restantes amostras, uma vez que os seus valores de perda de massa foram superiores

Uma combinação otimizada na estrutura fibrosa contendo fibras de celulose em micro e nanoescala permitiu produzir uma matriz 3D porosa que poderá ser usada em embalagens inovadoras. Nesta rede, as fibras de celulose em microescala proporcionam resistência e estabilidade. Em contraste, as fibras de celulose em nanoescala criam uma estrutura com mais ligações interfibras, o que pode favorecer propriedades de resistência e estabilidade trazendo vantagens para as funções pretendidas. As unidades estruturais porosas formadas por fibras de celulose em micro e nanoescala foram representadas por simulação computacional 3D, considerando os valores de entrada da caracterização das fibras.

Por fim, a metodologia experimental e computacional proposta mostrou-se uma excelente ferramenta no desenvolvimento e otimização de estruturas 3D para obtenção de protótipos laboratoriais que poderão ser utilizados em embalagens de alimentos de uma forma mais sustentável.

Palavras-chave

Biodegradação, Embalagens moldadas, Celulose micro/nano fibrilada, Materiais à base de celulose, Otimização, Simulação computacional

Abstract

The dramatic increase in single-use plastic (SUP) made from fossil-derived materials that are not biodegradable has contributed to the emergence of pollution as an environmental issue. Concerns regarding the environment and the development of biodegradable products from renewable sources, specifically the development of sustainable packaging using cellulose fibers from different plant sources, represent a multidisciplinary challenge for this investigation.

Fibers from bleached *Eucalyptus* globulus, unbleached *Picea* abies, and hemp fibers produced in the laboratory were selected for this study. The fibers were evaluated for their morphology and biometry, and structures were produced in the laboratory with different mixtures and mechanical treatments at the PFI. Its structural, mechanical, optical, and chemical properties were experimentally characterized using methodologies and following the respective ISO standards. The fibers and structures formed by them were simulated using 3D computer simulation models. Composting was used to conduct biodegradability tests using a methodology developed to be used both in the laboratory and later in the sector's industries, having collected data for this purpose.

The comparison of the reference fibers revealed that softwood fibers are approximately three times longer than hardwood fibers. In terms of width, softwood fibers are about twice as wide as hardwood fibers. In general, the increase in refining resulted in a rise in fibrillation and fine elements within the sample. As a result, the handsheets' thickness was reduced by 62% (HW) and 60% (SW) compared to handsheets made with unrefined fibers. Higher compaction and increased interfiber bonds contribute to a more cohesive and reinforced structure, as evidenced by the exponential increase in refined structures' tensile index and elastic modulus. The characteristics of hemp fibers were similar to *Picea* abies fibers but a little longer. The tensile index increased by 62,33% and the elastic modulus by 40,50% in an optimized combination of hemp fiber and eucalyptus fibers. Furthermore, biodegradation studies evaluated the effect of composting after 28 and 60 days, indicating that the refined structures biodegraded more quickly than the remaining samples since their mass loss values were the highest.

An optimized combination of a fibrous structure containing micro and nanoscale cellulose fibers produced a porous 3D matrix that could be used for innovative packaging. In this network, the microscale cellulose fibers provide resistance and stability. In contrast, the nanoscale cellulose fibers create a structure with more interfiber bonds, which may provide resistance and stability properties advantageous for the intended functions. The porous structural units formed by cellulose fibers in micro and nanoscale were represented by 3D computational simulation, considering the input values of the fiber characterization and the output values.

Finally, the proposed experimental and computational methodology proved an excellent tool for developing and optimizing 3D structures for obtaining laboratory prototypes that could be used in more sustainable food packaging.

Keywords

Cellulose-based materials, Micro/nanofibrillated cellulose, Molded packaging, Computational simulation, Optimization, Biodegradation

Index

Chapter I Introduction 1

1. Introduction 3
1.1. Motivation 4
1.2. Objectives 4

Chapter II Bibliographic Revision 7

2. Bibliographic Revision 9
2.1. Biotechnology 9
2.1.1. Nanotechnology 9
2.2. Cellulose 11
2.2.1. Cellulose Structure 11
2.2.2. Nanocellulose 14
2.2.2.1. Nanofibrillated Cellulose 14
2.2.2.2. Additives 17
2.3. The Emerging of Eco-Friendly Packaging 20
2.3.1. Concerns Regarding Packaging based on Fossil Resources 20
2.3.2. Sources of Cellulose Fibers 21
2.3.3. The New Generation of Biodegradable and Biobased Materials for Food Packaging 23
2.3.3.1. The Modernization of Food Packaging 23
2.3.3.2. Benchmarking 23
2.3.3.3. New Trends in Food Packaging 24
2.3.3.4. Molded Packaging Manufacturing Methodology 28
2.3.4. Life Cycle Assessment 30
2.4. Optimization using Advanced Computational tools 31
2.4.1. Molecular Modeling 31
2.4.2. The Evolution of Models to Simulate and Optimize Fiber Materials 32
2.4.3. Simulation of Fiber and Structures 33
2.4.4. Data Mining Techniques 36
2.4.4.1. Decision/Regression Trees 36
2.4.4.2. Multiple Linear Regressions (MLR) 36
2.4.4.3. Artificial Neural Networks (ANN) 37
2.4.5. Simulation using Finite Element Method (FEM) 38

Chapter III Materials and Methods 39

3. Materials and Methods 41
3.1. Materials 41
3.1.1. Cellulose Fiber 41
3.1.1.1. Cellulose Fiber Reference 41
3.1.1.2. Micro/nanofibrillated Cellulose Fiber Additive 41
3.1.1.3. Hemp Fibers 41
3.1.2. Biodegradability Studies 42
3.1.2.1. Cellulose Fiber Reference 42
3.1.2.2. Cellulose Fiber under Investigation 42
3.1.2.3. Laboratory Scale Composting 42
3.1.3. Benchmarking 42
3.2. Equipments 43
3.3. Methods 44
3.3.1. Forming Handsheets for Physical Tests of Pulp 45
3.3.1.1. Selection of Pulp Samples 45
3.3.1.2. Dry Mass Content 45
3.3.1.3. Desintegration Operation 45
3.3.1.4. Pulp Samples Homogenization 46
3.3.1.5. Production of Cellulose Fiber Structures 46
3.3.1.6. Pulp Samples Modification Process 46
3.3.1.7. Pulp Samples Formulations 47
3.3.2. Pulp Suspension Evaluation 48
3.3.2.1. Morfi Analyzer 48
3.3.2.2. Optical Microscope 48
3.3.2.3. Evaluation of Pulp Drainability using ºSR method 48
3.3.3. Hemp Fiber Extraction 49
3.3.3.1. Sample Preparation 49
3.3.3.2. Cooking Step 49
3.3.3.3. Bleaching Step 50
3.3.4. Characterization of Hemp Fibers 50
3.3.4.1. Production of Cellulose Fiber Structures with Hemp Fiber Incorporation 50
3.3.5. Fibers Structures Characterization 51
3.3.5.1. Structural Properties 51
3.3.5.2. Optical Properties 51
3.3.5.2.1. Whiteness 52

3.3.5.2.2. Opacity 52
3.3.5.3. Mechanical Properties 52
3.3.5.4. Morphological Characterization using Scanning Electron Microscopy (SEM) 52
3.3.5.5. Chemical Characterization using Infrared Spectroscopy by FTIR-ATR 53
3.3.5.6. Evaluation of Liquid Spreading Area 54
3.3.6. Laboratory Scale Composting Assays 55
3.3.7. Computational Studies 57

Chapter IV Results and Discussion 59

4. Results and Discussion 61
4.1. Evaluation of Reference Fibers using Characterization Methods 61
4.1.1. Fiber Suspension Characterization 61
4.1.1.1. Fiber Morphology 61
4.1.1.2. Fiber Morphology using a Fiber Analyzer, the Morfi® 63
4.1.1.3. Evaluation of Pulp Drainability using the Schopper-Riegler Degree Method 69
4.1.2. Fiber Handsheets Characterization 69
4.1.2.1. Structural Properties 69
4.1.2.2. Mechanical Properties 72
4.1.2.3. Optical Properties 73
4.1.2.4. Morphological Characterization using Image Analysis by SEM 74
4.1.2.5. Chemical Characterization using Infrared Spectroscopy by FTIR-ATR 77
4.1.2.6. Optimization of Fibrous Materials on Liquid Retention/ Absorption 80
4.2. Evaluation of Hemp Fibers using Characterization Methods 81
4.2.1. Fiber Suspension Characterization 81
4.2.1.1. Fiber Morphology 81
4.2.1.2. Fiber Morphology using a Fiber Analyzer, the Morfi® 82
4.3. Evaluation of Hemp Fibers Mixture 85
4.3.1. Fiber Suspension Characterization 85
4.3.1.1. Fiber Morphology 85
4.3.1.2. Fiber Morphology using a Fiber Analyzer, the Morfi® 85
4.3.2. Fiber Handsheets Characterization 88
4.3.2.1. Structural Properties 88
4.3.2.2. Mechanical Properties 89
4.3.2.3. Optical Properties 91

4.4. Biodegradability Evaluation of Fibrous Structures 91
4.4.1. Visual Evaluation of Fibrous Structures 92
4.4.2. Evaluation by Loss of Mass of Fibrous Structures 94
4.5. Optimization using Advanced Computational Tolls 95
4.5.1. Molecular Modeling 95
4.5.2. Computational Simulation Studies for Structure Optimization 96
4.5.2.1. Simulation of Fiber Deposition of Reference Fibers without Mechanical Treatment 97
4.5.2.2. Simulation of Fiber Deposition of Hemp Fibers without Mechanical Treatment 99
4.5.2.3. Simulation of Fiber Deposition of Reference Fibers Mixture 100
4.5.2.4. Simulation of Fiber Mixture Deposition of Reference Fibers with Hemp fibers and Micro/nano-fibrillated cellulose 101

Chapter V Conclusions and Futures Perspectives 105

5. Conclusions and Futures Perspectives 107

Chapter VI Bibliography 111

Appendix I

Appendix A. Publication List III
Appendix B. Data obtained from the Characterization of the Reference Fibers V
Appendix C. Data obtained from the Characterization of the Hemp Fibers VIII
Appendix D. Data obtained from the Characterization of the Industrial Tissue Paper with Hemp Fibers IX

List of Figures

Chapter II Bibliographic Revision

Figure 2.1 - Variety of nanotechnology applications (adapted from (Nasrollahzadeh et al., 2019)). 10
Figure 2.2 – In (a) the linear and (b) cyclic molecular structures of the glucose monomer, as well as the (c) structure of the natural polymer cellulose and monomeric cellobiose unit (adapted from (Klemm et al., 2005)). 12
Figure 2.3 - The primary C6-OH (with "tg-conformation" to cellulose I crystal structure) and secondary C2-OH and C3-OH groups in the glucosyl unit indicate the hydrophilic and hydrophobic planes of cellulose molecule in 3D (adapted from (Isogai et al., 2018)).....12
Figure 2.4 - Schematic representation of the hierarchical structure of cellulose from the micro to the nano molecular scales (adapted from (T. Li et al., 2021)). 13
Figure 2.5 - Schematization of nanocellulose extraction from lignocellulosic plants (adapted from (Phanthong et al., 2018)).....15
Figure 2.6 - Representation of the selective oxidation mechanism of C6 of the primary hydroxyl groups of cellulose measured by 2,2,6,6-tetramethylpiperidine-1-oxyl (TIME) (adapted from (Isogai et al., 2011)). 16
Figure 2.7 -The effect on the combination of MFC/NFC additive with pulp fibers (adapted from (A. Li et al., 2021)). 19
Figure 2.8 - Statistics on packaging waste generated and recycled in the 27 of European Union (EU) Member States and some non-member countries (adapted from(Eurostat, 2022)). 20
Figure 2.9 - Schematic overview of novel cellulose fiber-based packaging materials (adapted from (Schenker et al., 2021; Semple et al., 2022)). 22
Figure 2.10 – Subdivision of different materials and packaging with current economic value for companies. 24
Figure 2.11 – Schematic diagram of a smart packaging, highlighting the differences between active packaging and intelligent packaging (adapted from (Salgado et al., 2021)). 26
Figure 2.12 - Illustration of the typical production procedure for various kinds of molded pulp products (adapted from (Zhang et al., 2022)).....28
Figure 2.13 -Life Cycle Assessment of molded cellulose packaging (adapted from (Didone et al., 2017)). 30
Figure 2.14 - A timeline of the different approaches that have been introduced and implemented for fibrous materials over time (adapted from (Morais, 2017)).....33
Figure 2.15 – An illustration that demonstrates the fibers' sequential deposition in a 3D matrix, followed by plain extraction and fiber bending to conform to the underlying structure (adapted from (Curto et al., 2011)). 34
Figure 2.16 – A 3D fiber and structural characterization is given in the first section (left), and a 3D modeling approach is described in the second (right). The fibers are modeled with realistic parameters based on experimental analysis to perform these computational simulation investigations. The fibers are randomly deposited, (a) one at a time, (b) without depositing on others because the fibers' space will not be overlaid, and (c) inside a spatial arrangement (indicated by the user) in the 3D matrix to create the 3D computational structure (adapted from (Morais & Curto, 2022a)). 35
Figure 2.17 – Example of an architecture of ANN analysis (adapted from (Morais & Curto, 2022b)). 37
Figure 2.18 – Schematic of the methodology used to study the replacement of natural fibers in PCB, using experimental methods and computational tools (adapted from (Velosa et al., 2023)).....38

Chapter III Materials and Methods

Figure 3.1 - Experimental and computational methodology developed throughout the study. 44
Figure 3.2 – Methodology applied in the laboratory for hemp fiber extraction (a) after separating the main stems from the secondary ones, (b) two types of cutting were applied, one with scissors and the other using a mill, resulting in (c) stems with 2-3 cm length and (d) stems with 0.5-2 cm length. 49
Figure 3.3 - Interactions of a beam of light when it hits a paper surface (adapted from (Sousa, 2012)). 52
Figure 3.4 - Illustration of an (a) ATR accessory for FTIR spectrometer and (b) schematization of the evanescent wave at the interface of an ATR crystal (into (a)) (adapted from (Jafari, 2017)). 53
Figure 3.5 – Scheme of the optical system used for analysis over time of the interaction of liquid droplets on web fiber structures (adapted from (Mendes et al., 2013)). 54
Figure 3.6 – Methodology used to evaluate the biodegradability of structures produced in the laboratory. 55

Chapter IV Results and Discussion

Figure 4.1 - Microscopic images of hardwood fibers, namely, (a) unrefined, with a magnification of 40x, (b) PFI-refined at 3000 revolutions, and (c) PFI-refined at 6000 revolutions, both with a magnification of 100x. The orange arrows show the fine elements on the surface of the fibers. 62
Figure 4.2 - Microscopic images of softwood fibers, namely, (a) unrefined, with a magnification of 40x, (b) PFI-refined at 3000 revolutions, and (c) PFI-refined at 6000 revolutions, both with a magnification of 100x. The orange arrows show the fine elements on the surface of the fibers. 62
Figure 4.3 - Length weighted by length of reference fibers alone (hardwood or softwood) and mixture (90_HW_10_S, 80_HW_20_SW and 50HW_50SW). 63
Figure 4.4 - Length weighted by length of reference fibers only (hardwood or softwood) and mixture (90_HW_10_S, 80_HW_20_SW and 50HW_50SW). 64
Figure 4.5 - Length weighted by length of unrefined reference fibers (hardwood or softwood) and with PFI-refinements of: (1) 1000 revolutions (HW_MT_1 and SW_MT_1), (2) 3000 revolutions (HW_MT_3 and SW_MT_3), (3) 6000 revolutions (HW_MT_6 and SW_MT_6), (4) 12000 revolutions (HW_MT_12 at pH=12) and lastly (5) additive of micro/nanofibrillated cellulose. 65
Figure 4.6 - Fiber length weighted by length and width distributions of (a) unrefined HW fibers and (b) HW fibers PFI-refined at 6000 revolutions. 66
Figure 4.7 - Fiber length weighted by length and width distributions of (a) unrefined SW fibers and (b) SW fibers PFI-refined at 6000 revolutions. 67
Figure 4.8 - Fibrillation percentage of unrefined reference fibers (hardwood and softwood) and with PFI-refinements of: (1) 1000 revolutions (HW_MT_1 and SW_MT_1), (2) 3000 revolutions (HW_MT_3 and SW_MT_3), (3) 6000 revolutions (HW_MT_6 and SW_MT_6), (4) 12000 revolutions (HW_MT_12 at pH=12) and (5) additive of micro/nanofibrillated cellulose. 68
Figure 4.9 - Graph referring to the average thickness (mm) of HW and SW handsheets without PFI-refining (dark orange bars) and HW and SW handsheets PFI-refined at 1000 revolutions, 3000 revolutions and 6000 revolutions and the micro/nanofibrillated cellulose additive (light orange bars). 70
Figure 4.10 - Graph referring to the (a) bulk (cm^3/g) and (b) porosity (%) of HW and SW handsheets without PFI-refining (dark orange bars) and HW and SW handsheets PFI-refined at 1000 revolutions, 3000 revolutions and 6000 revolutions and the micro/nanofibrillated cellulose additive (light orange bars). 71

Figure 4.11 - Graph referring to the (a) tensile index (Nm/a) and (b) elastic modulus (MPa) of HW and SW handsheets without PFI-refining (dark orange bars) and HW and SW handsheets PFI-refined at 1000 revolutions, 3000 revolutions and 6000 revolutions and the Micro/nano-fibrillated cellulose additive (light orange bars). 73
Figure 4.12 - SEM images of structures of 100% HW fibers without mechanical treatments (a) random arrangement of the fibers magnified at 150x in the XY axis and (b) overlapping of the fibers on top of each other, in this case, the orange fiber on top, magnified at 500x in the XY axis. 75
Figure 4.13 - SEM images of structures of 100% SW fibers without mechanical treatments (a) random arrangement of the fibers magnified at 150x in the XY axis and (b) overlapping of the fibers on top of each other, providing support, for example the fiber highlighted in red, magnified at 500x in the XY axis..... 75
Figure 4.14 - SEM images of structures of 50% HW fibers and 50%SW fibers without mechanical treatments (a) random arrangement of fibers magnified at 150x in the XY axis and (b) thickness of structures, magnified at 50x in the Y axis. 76
Figure 4.15 - SEM images of structures of 100% HW fibers refined at 12000 revolutions (a) jelly-like appearance of the fiber with a very uniform and smooth surface magnified at 500x in the XY axis and (b) measurement of the width of some micro/nanofibrillated cellulose magnified at 6.00kx in the XY axis. 76
Figure 4.16 - FTIR-ATR spectra of the hansheets produced from (a) HW fibers and (b) SW fibers, both without any kind of additional mechanical treatment. 77
Figure 4.17 - FTIR-ATR spectrum comparison: (1) paper filter (black), (2) surface of coated of silicone paper (light blue), (3) coffee paper cup - outer layer (Red), (4) coffee paper cup (green) - inner layer and (5) nonwoven made of bamboo fibers (purple)..... 79
Figure 4.18 - Evolution of the liquid droplet spreading area over time in laboratory-made structures produced from industrial tissue paper (a) basis weight of 60 g/m², (b) basis weight of 120 g/m² and in a (c) commercial sample. 80
Figure 4.19 - Microscope images of hemp fibers with different separation methods and different concentrations of NaOH. Note that the top images have a 40x magnification and the bottom images a 100x magnification. In (a) cut hemp fibers subjected to a coking step at a 1M NaOH concentration, (b) milled hemp fibers and applied a coking step at a 1M NaOH concentration, and (c) milled hemp fibers with a coking step at a 2M NaOH concentration. 81
Figure 4.20 - Length weighted by length of hemp fibers. The dark orange bars represent fibers cut manually and with different concentrations of NaOH (0,5M, 1M, 2M). The light orange bars are milled fibers with different concentrations of NaOH (1M and 2M). 82
Figure 4.21 - Percentage of fibrillation of hemp fibers. The dark orange bars represent fibers cut manually and with different concentrations of NaOH (0,5M, 1M, 2M). The light orange bars are milled fibers with different concentrations of NaOH (1M and 2M). 83
Figure 4.22 - Fiber length weighted by length and width distributions of (a) cut manually hemp fiber cooked to 1M NaOH concentration and (b) milled hemp fiber cooked to 1M NaOH concentration. 84
Figure 4.23 - Microscope images of industrial tissue paper fibers at (a) 40x magnification and (b) 100x magnification. 85
Figure 4.24 - Length weighted by length of the reference fibers, namely HW and IT exclusively (dark orange bars) and mixture fibers 99_IT_1_HF, 90_IT_10_HF and 90_IT_10_HF_1 (light orange bars).....86
Figure 4.25 - Fiber length weighted by length and width distributions of (a) only IT, (b) 99_IT_1_HF, (c) 90_IT_10_HF and (d) 90 _IT_10_HF_1, respectively. 87
Figure 4.26 - Graphs referring to the thickness (mm) of the HW and IT handsheets (dark orange bars) and handsheets 99_IT_1_HF, 90_IT_10_HF and 90_IT_10_HF_1 (light orange bars). 88
Figure 4.27 - Graphs referring to the porosity (%) of the HW and IT handsheets (dark orange bars) and handsheets 99_IT_1_HF, 90_IT_10_HF and 90_IT_10_HF_1 (light orange bars). 89

Figure 4.28 - Graphs of the tensile index (Mn/a) of the HW and IT handsheets (dark orange bars) and fiber mixture handsheets 99_IT_1_HF, 90_IT_10_HF and 90_IT_10_HF_1 (light orange bars).....90
Figure 4.29 - Graphs of the tensile index (Mn/a) of the HW and IT handsheets (dark orange bars) and fiber mixture handsheets 99_IT_1_HF, 90_IT_10_HF and 90_IT_10_HF_1 (light orange bars).....90
Figure 4.30 - Images of samples of handsheets that had undergone a biodegradation by composting test before and after being buried for 28 days and 60 days..... 93
Figure 4.31 - Graphs evaluating the mass loss of the structures under study over time, (a) after 28 days and (b) after 60 days. 94
Figure 4.32 – Molecular structures in 2D and 3D of (a) dehydrovomifoliol (Samba et al., 2023) and (b) β-caryophyllene (Medeiros et al., 2023). Molecules made using ACD/ChemSketch by Mendes, J.A.S. and Medeiros, J.F.B.....96
Figure 4.33 - The simulation represents the deposition process of HW fiber with a length of 40 voxels and flexibility 3. The left side is the fiber deposition in voxels, and the right side represents the visualization of 3D structures. In (a) the initial stage, (b) the intermediate stage, and (c) the final stage..... 97
Figure 4.34 - SEM images of HW fibers, in blue are the deposition of fibers one by one, just like in the 3D simulation.....98
Figure 4.35 - The simulation represents the final stage in the deposition process of SW fiber with a length of 100 voxels and flexibility 3. The left side is the fiber deposition in voxels, and the right side represents the visualization of 3D structures. 99
Figure 4.36 - The simulation represents the final stage in the deposition process of HF that has a length of 130 voxels and a flexibility of 2. The left side is the fiber deposition in voxels and the right side represent the visualization of 3D structures. 99
Figure 4.37 - The simulation represents the final stage in the deposition process of HF (blue) and SW (pink) mixture that has a length of 40 and 100 voxels, respectively and the same flexibility of 3. The left side is the fiber deposition in voxels and the right side represent the visualization of 3D structures.....100
Figure 4.38 - SEM images of HW fibers (blue) and SW fibers (pink) are the deposition of fibers one by one, just like in the 3D simulation. 100
Figure 4.39 - The simulation represents the final stage in the deposition process of HW (blue) and HF (pink) mixture that has a length of 40 and 130 voxels and a flexibility of 3 and 2, respectively. The left side is the fiber deposition in voxels and the right side represent the visualization of 3D structures.....101
Figure 4.40 - The simulation represents the final stage in the deposition process of HW (blue), HF (pink), and the micro/nanofibrillated cellulose (red) mixture that has a length of 40, 130, and 30 voxels and flexibility of 3, 2 and 4, respectively. The left side is the fiber deposition in voxels, and the right side represents the visualization of 3D structures. 101

List of Tables

Chapter II Bibliographic Revision

Table 2.1 - Terminology and nomenclature of cellulose nanomaterials, with the distribution of their dimensions (adapted from (Osong et al., 2016)). 14

Chapter III Materials and Methods

Table 3.1 - List of equipments. 43
Table 3.2 - List of software. 43
Table 3.3 - DMC obtained for different materials used, as well as the time used for each one..... 45
Table 3.4 – List of fibrous structures PFI-refined in the laboratory. 47
Table 3.5 – List of fibrous formulation of the structures produced in the laboratory. 47
Table 3.6 - Reaction conditions and composition of the cooking liquor. 50
Table 3.7 - Composition and designation of structures produced containing hemp fibers. 51
Table 3.8 -Operating conditions for the FTIR-ATR method..... 54
Table 3.9 – Selected samples with their designation and detailed description. For each sample type, three samples were buried and removed after 28 days and 60 days, respectively. 56

Chapter IV Results and Discussion

Table 4.1 - Schopper-Riegler degree of pulps subject to different PFI-refinements.... 69
Table 4.2 – Optical characterization of the structures produced in the laboratory individually (HW or SW) and their mixtures (heterogeneous fibers) in the proportions HW:SW (90:10, 80:20, 50:50), both without any type of mechanical treatment. 74
Table 4.3 - Optical characterization of structures produced individually in the laboratory, namely hardwood and softwood handsheets PFI-refined at 1000 revolutions, 3000 revolutions and 6000 revolutions..... 74
Table 4. 4 - Graphs of the tensile index (Mn/a) of the HW and IT handsheets (dark orange bars) and handsheets 90_IT_1_HF, 90_IT_10_HF and 90_IT_10_HF_1. (light orange bars). 91
Table 4.5 - Conversion of length weighted by length (µm), real value, in number of voxels, simulated value, considering its dimensions. For Hardwood (HW), Softwood (HW), Hemp Fiber (HF) and Micro/nanofibrillated cellulose fibers (additive). 96

Appendix

Table B1.1 - Morphological characterization using Morfi® in homogeneous fibers (HW or SW) and in mixtures with each other (heterogeneous fibers) in the proportions HW:SW - 90:10, 80:20, 50:10, respectively. V
Table B1.2 - Morphological characterization using Morfi® on homogeneous fibers (HW or SW) to which a mechanical process (PFI-refined) has been applied. V
Table B2.1 - Structural characterization of homogeneous fibers (HW or SW) and mixtures with each other (heterogeneous fibers) in the proportions HW:SW - 50:50, 90:10, 80:20, 50:10, respectively. VI
Table B2.2 - Structural characterization of homogeneous fibers (HW or SW) to which a mechanical process (PFI-refinement) has been applied. VI

Table B3.1 – Mechanical characterization of homogeneous fibers (HW or SW) and mixtures with each other (heterogeneous fibers) in the proportions HW:SW - 50:50, 80:20,90:10,respectively.....VII
Table B3.2 - Structural characterization of homogeneous fibers (HW or SW) to which a mechanical process (PFI-refinement) has been applied. VII
Table C1.1 - Morphological characterization using Morfi® on hemp fibers. VIII
Table D1.1 - Structural characterization of homogeneous fibers (IT) and mixtures with hemp fiber (heterogeneous fibers) in the proportions IT:HF. IX
Table D2.1 - Structural characterization of homogeneous fibers (IT) and mixtures with hemp fiber (heterogeneous fibers) in the proportions IT:HF. IX

List of Abbreviations

ASA	Alkenyl Succinic Anhydrides
AKD	Alkyl Ketene Dimer
ANN	Artificial Neural Network
BC	Bacterial Cellulose
CNC	Cellulose Nanocrystals
DSDG	Division for Sustainable Development Goals
DDS	Drug Delivery Systems
FEM	Finite Element Method
FTIR-ATR	Fourier Transform Infrared Spectroscopy with Attenuated Total Reflectance
HW	Hardwood
HF	Hemp Fiber
IMFA	International Molded Fiber Association
ISO	International Organization for Standardization
LCA	Life Cycle Assessment
MT	Metric Tons
MFC/NFC	Micro/Nanofibrillated cellulose
MLR	Multiple Linear Regression
MIMO	Multiple-Input Multiple-Output
NC	Nanocellulose
NFC	Nanofibrillated Cellulose
PFC	Perfluorochemicals
PFOS	Perfluorooctane Sulfonate
PFOA	Perfluorooctanoic Acid
PLA	Poly(Lactic Acid)
PAM	Polyacrylamides
PAC	Polyaluminium Chloride
PEI	Polyethylenimine
PTFE	Polytetrafluoroethylene
PCB	Printed Circuit Board
RFID	Radio-Frequency Identification
RBA	Relative Bonding Area
R&D	Research and Development
SEM	Scanning Electron Microscopy
SR	Schopper-Riegler
SUP	Single Use Plastic
SW	Softwood
3D	Three Dimensions
TTI	Time-Temperature Indicators
2D	Two Dimensions
UV	Ultraviolet
UBI	University of Beira Interior
UF	Urea Formaldyde

Chapter I
Introduction

Introduction

Currently, using materials made from nonrenewable resources, such as synthetic fibers, in various industrial sectors is causing several environmental issues. Given their physical and thermal properties and low production costs, these have been the primary materials to be chosen. On the other hand, they are not biodegradable, meaning they have an extremely long lifetime, indicating a faster rate of accumulation than decomposition in landfills or the environment (Geyer et al., 2017; Li et al., 2016; Prata et al., 2020). For the same reason, over the next decade, a set of initiatives and investments will be implemented to move countries toward recovery and sustained economic growth, guided by a concept of sustainability influenced by the United Nations' Division for Sustainable Development Goals (DSDG) (United Nations, 2021).

In light of the previous arguments, this work suggests developing materials with micro/nanofibrillated cellulose for applications in molded food packaging. The reference fibers most commonly used in industry are *Eucalyptus* globulus and *Picea* abies fibers. However, hemp fibers will be studied and characterized as an innovative and differentiating factor in the current market, as they have morphological characteristics identical to *Picea* abies fibers. In addition, they are considered a sustainable and economically viable alternative to other fibers (such as linen and cotton) due to their cultivation without chemical pesticides, low water consumption, resistance, and reduced cultivation pressure on the soil. Through the use of a 3D simulator of fibrous web in MATLAB®, which had previously been validated by (Conceição et al., 2010; Curto et al., 2011). Due to its applicability and contribution to the optimization of materials, the connection between experimental and computational methods has attracted much attention from companies because it contributes to the efficiency of costs and resources.

Considering the European guidelines this work includes an initial study on the biodegradation of laboratory-produced structures through composting. Having obtained positive results, the investigation can be carried out further, with potential applications in the R&D Projects at FibEnTech-UBI

1.1. Motivation

The motivation of this work is to replace fossil-based package materials with more environmentally friendly alternatives, such as those made from materials based on cellulose that are derived from naturally renewable sources. Also combined with new areas of knowledge (such as biotechnology and bioengineering), it acts as a driving force to join the experimental knowledge with the computational data to produce the ideal combination of cellulose fibers on the micro and nanoscale. The optimization network of cellulose fibers at the micro and nanoscale helps to create a structure that provides strength and stability, fundamental characteristics in designing new food packaging to contain and protect food.

1.2. Objectives

The overall objective of this work is to develop cellulosic fiber-based structures suitable for biodegradable packaging materials. The aim is to use a combination of experimental methods and computational tools to obtain information, optimize the structures, and achieve an alternative to materials made from nonbiodegradable polymers. To reach this final objective, the specific goals of this work are:

- Produce in the laboratory structures made from cellulose fibers using kraft pulps from *Eucalyptus* globulus fibers and *Picea* abies fibers;
- Produce in the laboratory structures made from cellulose hemp fibers produced in the laboratory;
- Characterize the fibers biometry and morphology;
- Characterize the structural, mechanical, optical, and chemical properties of laboratory structures using ISO standards;
- Laboratory study of biodegradability of web fibrous structures;
- Make a benchmarking study with products in the market to compare to our structures;
- Simulate the 3D fibrous structures using a validated 3D MATLAB® simulator and comparation with the real ones with the help of SEM.

Chapter II
Bibliographic Revision

2. Bibliographic Revision

2.1. Biotechnology

Biotechnology will continue to be a significant driver of innovation in the twenty-first century. Concerns, including climate change, global food shortages, and public health administration, will influence the future of biotechnology (Cornelissen et al., 2021). Its versatility of applications in various health, food, and industrial sectors is based on biological knowledge and techniques capable of manipulating genetic, molecular, and cellular processes, improving human life quality (Jackson et al., 2021). The goal of biotechnological advancement has moved from the macro and microscale to the nanoscale. In this same context, the word "nanotechnology" begins appearing in the literature and the current project will be an example of such progress.

2.1.1. Nanotechnology

As the name suggests, nanotechnology is a research field based on the design, manufacturing, and characterization of a diversity of materials at the nanoscale (between 1 and 100 nm), exploring their physical-chemical characteristics as well as behaviors (Shahcheraghi et al., 2022). Given the many potentials, it is unsurprising that this field will significantly develop environmentally friendly and economically viable solutions in the coming years. In (Enescu et al., 2019) highlight nanotechnology's current advances and challenges in developing nanostructured materials, such as packaging, in the food and beverage industry.

In addition to the food industry, the agricultural sector benefits from nanotechnology. A farmer's use of these tools could improve soil quality, increase production, and reduce water usage, among other things (Vijayakumar et al., 2022). By 2050, the global population is projected to reach 10 billion people. Currently, nearly 815 million people worldwide are undernourished, and this number might grow to even more than 2 billion by 2050. Exploring nano solutions seems crucial to substantially reducing this number (Usman et al., 2020).

In a slightly different context, nanomedicine is dedicated to developing solutions and instruments to improve the current healthcare system. The use of nanomedicine for imaging, screening, diagnosis, targeted drug delivery systems, and efficient therapeutic approaches for severe diseases such as cancer and cardiovascular diseases is spotlighted — in particular (Sahu et al., 2021).

Figure 2.1 illustrates a variety of applications that are currently being investigated in different fields. As a result, the current study focuses on the possible benefits and drawbacks of using fibrous materials of natural origin at the nanoscale. One of them is cellulose, a biopolymer frequently used in the food industry for the transporting and packaging of food and beverages.

Figure 2.1 - Variety of nanotechnology applications (adapted from (Nasrollahzadeh et al., 2019)).

2.2. Cellulose

Several polymers are recognized for having unique characteristics that meet the population's needs. Among natural polymers, cellulose stands out for its sustainability, biodegradability, and biological safety (Morais & Curto, 2022c). As the most common polymer in the biosphere, cellulose has a worldwide production (and decomposition) rate of about $1{,}5 \times 10^{12}$ tons per year, identical to the planet's reserves of significant fossil and mineral sources (Heinze, 2015). The photosynthesis of plants mainly produces it; however, certain bacteria, for example, the gram-negative bacterial cultures of *Gluconacetobacter* (Muddasar et al., 2022; Picheth et al., 2017).

The desire for simple and environmentally friendly solutions, as well as the development of novel methodologies for the elaboration of food safety and storage systems based on natural fibers until they reach the consumer (Martins et al., 2018; Nascimento et al., 2021; Silva et al., 2020), led to the selection of cellulose as the biopolymer to be studied in the current study.

2.2.1. Cellulose Structure

Regardless of the origin of the cellulose, it always has the same conformation. Its empirical formula is $(C_6H_{10}O_5)_n$, where "n" represents the number of polymerizations, which varies based on the origin of the cellulose source (Muddasar et al., 2022). This linear polymer is made of a sequence of repetitions of glucose units interconnected by β -1,4-glycosidic bonds (Figure 2.2), this results in an alternating rotation of the cellulose chain axis at 180º, and the set that composes the repetition of the two glucose monomers are known as cellobiose (Heinze, 2015; Oprea & Voicu, 2020).

Analyzing the cellobiose structure, specifically its hydroxyl groups (-OH), two types of hydroxyl groups stand out: the primary alcohol at the C6 position and the secondary alcohol at the C2 and C3 positions. (Figure 2.2, c). Generally, secondary groups are controlled by inspiring steric and molecular factors instead of the reactivity of different hydroxyl groups, as with primary groups. The OH-O hydrogen bonding causes most cellulose intramolecular interactions (same cellular chain), but intermolecular interactions (different cellular chain) are also influenced by the weaker CH-O hydrogen bonding and Van der Waals interactions (Xi et al., 2013).

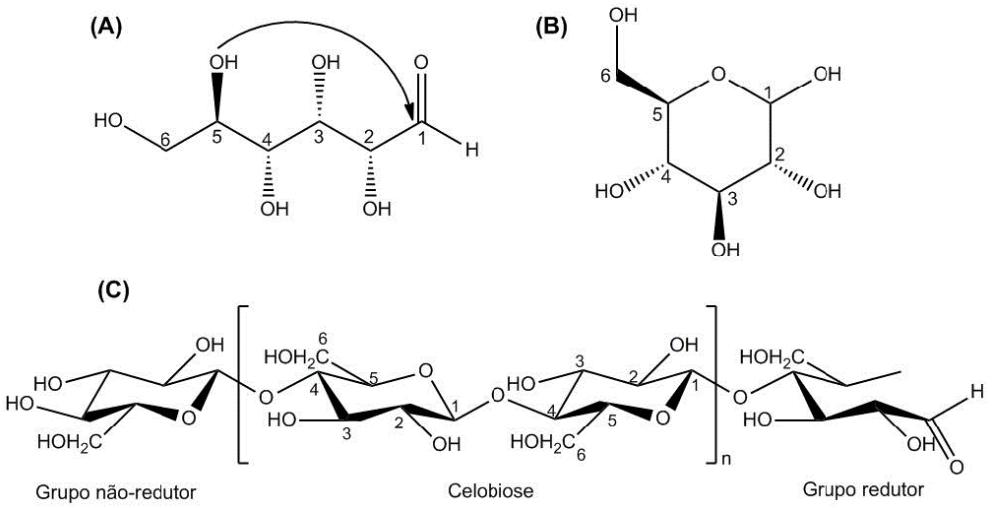

Figure 2.2 – In (a) the linear and (b) cyclic molecular structures of the glucose monomer, as well as the (c) structure of the natural polymer cellulose and monomeric cellobiose unit (adapted from (Klemm et al., 2005)).

Another aspect to take into account is the spatial arrangement of the hydroxyl groups and hydrogen atoms (Figure 2.3); – i.e., the -OH groups are found in the equatorial plane, while the -H atoms are axially oriented in the ring plane, resulting in distinct polarities; in other words, the presence of hydrophilic (parallel to the plane of the ring) and hydrophobic (opposite to the plane of the ring) sites perpendicular to the plane of the ring (Flauzino Neto, 2017; Xi et al., 2013). Understanding these aspects is relevant when designing and engineering food packaging because plant fibers are typically hydrophilic, allowing them to absorb moisture, fats, and oils (Semple et al., 2022). This topic will be discussed in more detail later.

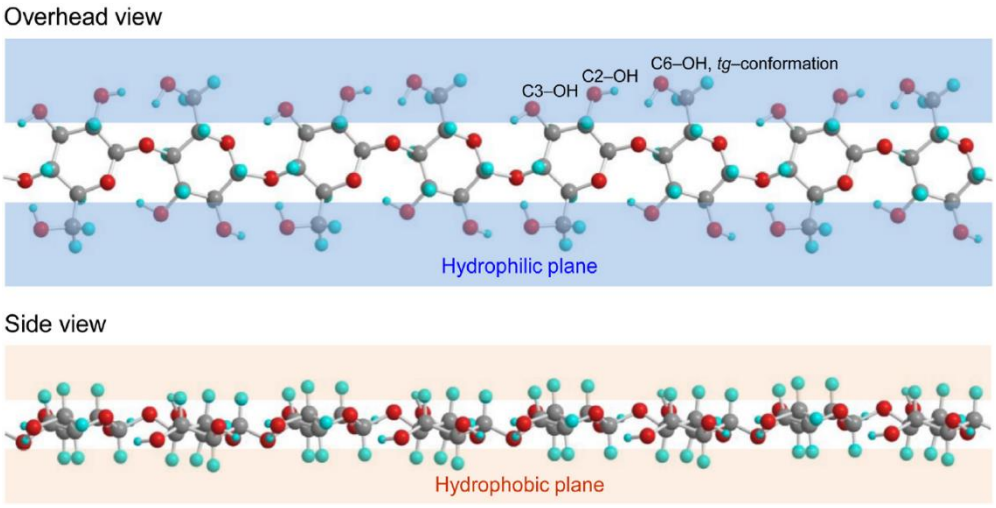

Figure 2.3 - The primary C6-OH (with "tg-conformation" to cellulose I crystal structure) and secondary C2-OH and C3-OH groups in the glucosyl unit indicate the hydrophilic and hydrophobic planes of cellulose molecule in 3D (adapted from (Isogai et al., 2018)).

The architectural structure of cellulose within lignocellulosic plants (plants containing cellulose, hemicellulose, and lignin in their constitution) can be divided into hierarchical levels (Figure 2.4). In other words, cellulose chains repeatedly aggregate into crystalline domains and amorphous regions (1 – 100 Å) to form microfibrils (10-100 nm) in the plant's cell wall, which then organize themselves again and generate larger fibers (1–100 μm) reaching the macroscopic scale (Eichhorn et al., 2010; Kovalenko, 2010; Tingaut et al., 2012). These levels need to be divided and separated to obtain various levels, such as microfibrillated cellulose (MFC) and nanofibrillated cellulose (NFC). The procedures in question can be performed mechanically, chemically and enzymatically (Sharma et al., 2019).

Recent efforts by researchers and corporations have focused on developing micro/nanofibrillated cellulose (MFC/NFC) applied in food packaging materials and optimizing different fibrous materials to improve their mechanical and barrier properties. Additionally, due to the fibrous structures' ability to retain and absorb substances, active substances can be incorporated, giving packaging its designation of active packaging. Such active substances can have antioxidant and antibacterial properties (Martins et al., 2018; Silva et al., 2020).

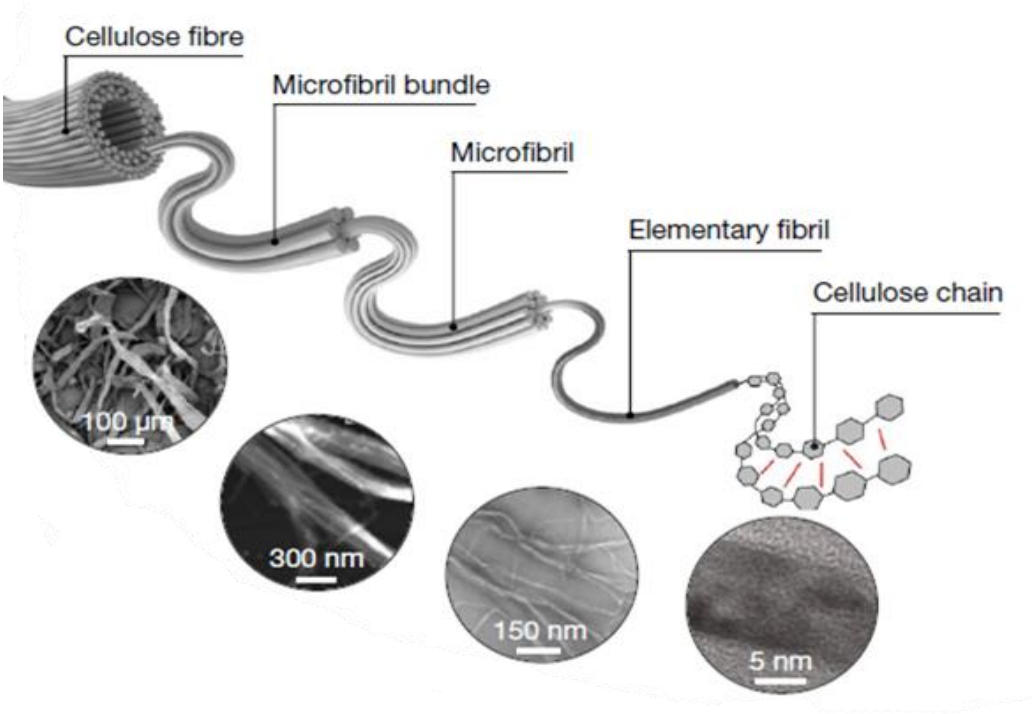

Figure 2.4 - Schematic representation of the hierarchical structure of cellulose from the micro to the nano molecular scales (adapted from (T. Li et al., 2021)).

2.2.2. Nanocellulose

As the term suggests, nanocellulose includes nanofibers or fibrous nanostructures whose size range is on the nanometric scale (less than 100 nm) (Silva et al., 2020). In general, there are three kinds of nanocelluloses: (1) cellulose nanocrystals (CNC), (2) cellulose nanofibers (NFC), which include microfibrillated cellulose (MFC) and nanofibrillated cellulose (NFC), (3) bacterial cellulose (BC) (Curto, et al., 2021). Table 2.1 compares these types of nanocellulose based on how their sizes are distributed (Kostić, 2021).

In contrast to microcellulose, which is prevalent in many conventional materials like paper. Nanocellulose is distinguished by unique properties such as high crystallinity, a high degree of polymerization, high mechanical strength, low density, biodegradability, biocompatibility, and safety (Lin & Dufresne, 2014; Silva et al., 2020). For the same reasons, it has been adopted by numerous industries, including the food, biomedical, electronic, and construction sectors. (Zinge & Kandasubramanian, 2020) .

Table 2.1 - Terminology and nomenclature of cellulose nanomaterials, with the distribution of their dimensions (adapted from (Osong et al., 2016)).

Cellulose Nanomaterials	Width (nm)	Length (nm)	Aspect ratio (length/width)
Cellulose Nanocrystals (CNC)	2-20	100-600	10-100
Nanofibrillated Cellulose (CNF)	2-10	>10000	>1000
Microfibrillated cellulose (CMF)	10-100	500-10000	50 -100
Bacterial Cellulose (BC)	10-40	>1000	100 - 150

2.2.2.1. Nanofibrillated Cellulose

Nanofibrillated cellulose is composed of an entangled network structure with flexible nanofibers, which are longer and wider and less crystalline compared to CNC (Trache et al., 2020). However, as already mentioned, the typical characteristics such as crystallinity, morphology, physicochemical properties and yields depend a lot on the natural source, the isolation procedure and the pre- and post-treatments to which they are submitted. This versatility becomes advantageous for the development and optimization of a wide range of innovative fibrous materials (Trache et al., 2020).

The extraction of CNF is divided into two steps (Figure 2.5): In the first step, non-cellulosic components are removed, such as lignin, hemicellulose, and other compounds, through acidic or alkaline treatment. However, the use of solutions with acidic pH (such as sulfuric acid, hydrochloric acid, and phosphoric acid) to hydrolyze the biomass should be avoided due to its corrosive behavior and the need for a recovery step or pH neutralization by adding alkaline solutions to be economically viable (von Sivers & Zacchi, 1995). From another perspective, alkaline treatment using NaOH, KOH, $Ca(OH)_2$, hydrazine, and ammonium causes biomass swelling, disrupting the lignin structure, and destroying the bonds between lignin and other carbohydrate fractions. As lignin is removed, the activity of the remaining polysaccharides increases. Despite being considered a more environmentally friendly treatment, it has the disadvantage of not being as effective when applied in biomasses that have large amounts of lignin (Agbor et al., 2011).

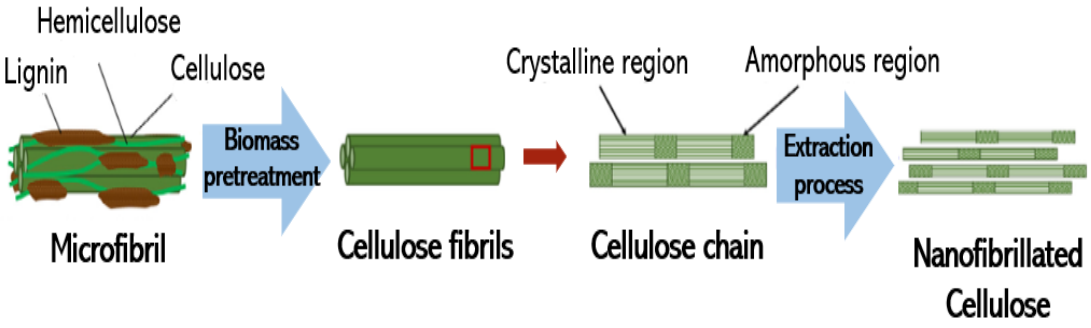

Figure 2.5 - Schematization of nanocellulose extraction from lignocellulosic plants (adapted from (Phanthong et al., 2018)).

The secondary step is composed of extraction processes that can be performed through four treatments: (1) mechanical treatment (such as homogenization, grinding, and milling), associated with high energy costs in the industry, (2) chemical treatment (e.g., TIME-mediated oxidation), (3) enzymatic treatment, (4) conjugation of treatments mentioned above (Abitbol et al., 2016; Zinge & Kandasubramanian, 2020). Mechanical treatment systematically separates the fibers by applying high shear forces to cleave the cellulose fibers along the longitudinal axis, resulting in nanofibrillated cellulose (Phanthong et al., 2018). The best-known and most used mechanical procedures are high-pressure homogenization, microfluidization, grinding, and high-intensity ultrasonication (Abdul Khalil et al., 2014).

For a better yield, it is common to combine a mechanical treatment with a chemical treatment, such as the oxidation measured by 2,2,6,6-tetramethylpiperidine-1-oxyl (TIME) (Figure 2.6). Through its selective oxidation of carbons, 6 of the primary hydroxyl groups of cellulose in an aqueous medium allows the binding of carboxylic functional groups and aldehyde groups with ionic charge, favoring the increase of electrostatic repulsions between the fibrils, consequently, their separation occurs (Morais, 2017; Zinge & Kandasubramanian, 2020).

Enzymatic hydrolysis is an excellent alternative to the above mentioned treatment due to its low energy consumption. It is considered a more ecological alternative combined with low emission of contaminants harmful to the environment. Enzymes such as cellulase, endoglucanase, xylanase, and ligninase react with cellulosic biomass and degrade lignin and hemicellulose regions (Zinge & Kandasubramanian, 2020). As mentioned earlier, combining these processes is quite common to benefit from larger quantities and achieve certain levels of optimization and product quality during the process.

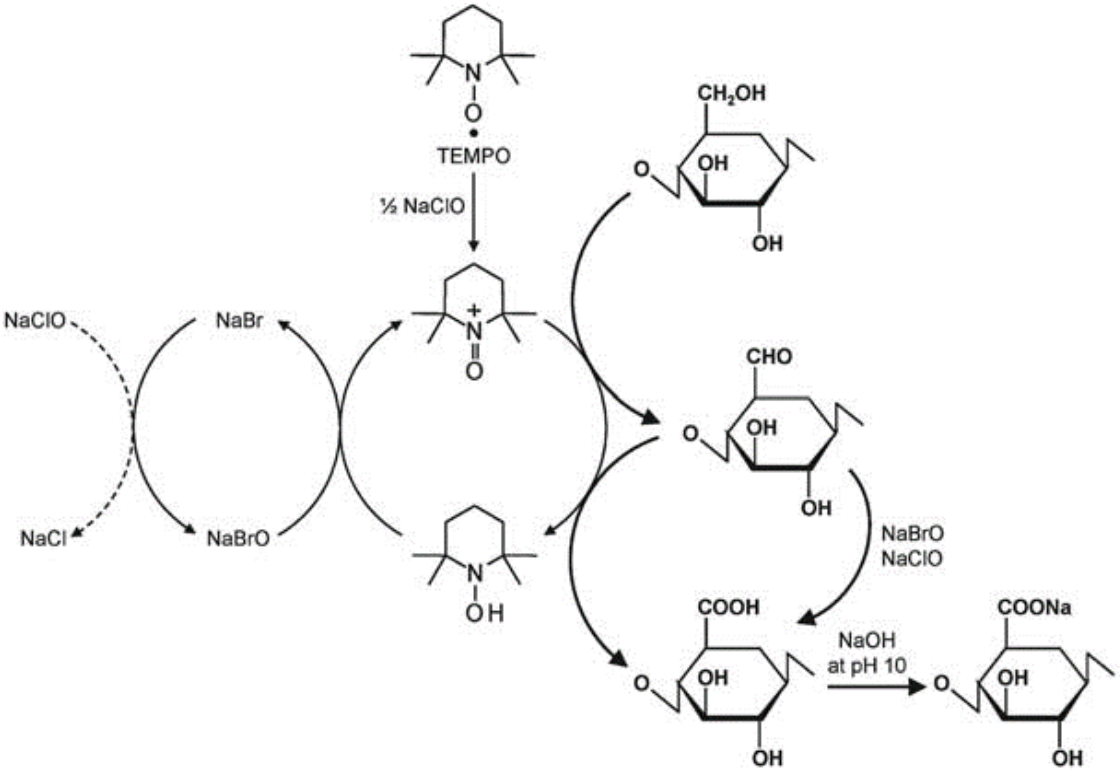

Figure 2.6 - Representation of the selective oxidation mechanism of C6 of the primary hydroxyl groups of cellulose measured by 2,2,6,6-tetramethylpiperidine-1-oxyl (TIME) (adapted from (Isogai et al., 2011)).

2.2.2.2. Additives

At first sight, paper is exclusively produced from vegetable fibers, being, therefore, a renewable and recyclable material. Two types of fibers are mainly used: (1) short fibers from hardwoods, such as E*ucalyptus* globulus, and (2) long fibers from softwoods. The first one are important to confer structural properties and the second one mechanical strength (Sousa, 2012). Currently, the paper industry works with fibrous mixtures, for example with a proportion of 75% hardwood and 25% softwood (Morais et al., 2021). However, it should be noted that the industrial paper produced also has non-fibrous materials in its composition, as with chemical additives. Without them, the paper would be a low-resistant material with a brownish color, unable to serve many purposes (Ginebreda et al., 2012; Sousa, 2012). In addition, industrial and economic points of view contribute to reducing water consumption, increased use of wastepaper, and reduced paper basis weight, saving raw materials. In the market, it is possible to find a variety of chemical additives for paper finishing, such as (1) retention aids, (2) sizing agents, (3) strength agents (wet and dry), among others (Ginebreda et al., 2012; Morais et al., 2021).

The retention aids increase the retention in the cellulosic fibers by decreasing fiber polarity and the specific surface area, allowing a better attachment of the fillers. In addition to improving the quality of the paper, it has operational and economic advantages, as it allows for higher production speeds, decreases the amount of freshwater used, and allows the use of more recycled paper in the mixture. At the environmental level, it contributes to an improvement in effluent quality. This factor is crucial given that it is one of the problems in this industry. In general, retention aids can be classified into three categories: (1) Inorganic compounds, such as aluminum sulfate (alum) and polyaluminium chloride (PAC), (2) modified natural materials, including cationic starch, (3) synthetic organic polymers, namely polyacrylamides (PAM) and polyethylenimine (PEI) the most retention aids used in the industries (Ginebreda et al., 2012).

When talking about sizing agents, it is important to understand the term "sizing" i.e., in the paper industry, "sizing" refers to the process of adding chemical additives to the papermaking suspension (internal sizing) or the final paper (surface sizing) (Chauhan & Bhardwaj, 2013; Seppänen, 2007).

The internal sizing has the advantage of preventing the penetration and spreading of the liquids through the pore system of the fibrous structures. On the other hand, surface sizing through spreading on fiber and filler surfaces is better considering sizing efficiency. Because it allows the size to be anchored to a greater extent to the fiber and filler, consequently, it reaches the desired sizing level using fewer sizing agents. Examples of sizing additives are rosin, alkyl ketene dimer (AKD), and alkenyl succinic anhydrides (ASA) (Seppänen, 2007; Sousa, 2012). AKD is a low-cost, non-toxic, and biodegradable agent capable of reacting with the hydroxyl groups of cellulose to improve the strength and hydrophilicity of fibers and paper (Nguyen & Lee, 2022; Oshani Nayanathara et al., 2023). It was concluded (Han, 2022) that using AKD as a water-proofing agent in nanocellulose mixture can significantly modify and improve the surface morphology of pulp molded lunch boxes.

Some currently used papers require wet strength agents to fulfill their purposes, such as filter papers, toilet papers, label papers, and packaging papers. These agents allow that when a sheet is exposed to a humid environment, it maintains part of its dry resistance and structural integrity. Wet strength additives consist of synthetic resins and other compounds suitable for paper products. Most synthetic resins are composed of formaldehyde-derived polymers, with urea formaldehyde (UF) and melamine formaldehyde (MF) being the most popular (Ginebreda et al., 2012; Sousa, 2012).

The choice of additives and how they interact with other substances should be carefully considered depending on the paper's purpose, especially when discussing paper for food packaging since they can impact consumer health. For example, a variety of perfluorochemicals (PFCs) are utilized to add oil and water resistance properties to paper that is used in the packaging of high-fat content and convenience food products, which potentially expose customers to oral toxins (Begley et al., 2008; Xu et al., 2013). Some alarming data from recent epidemiological studies report the presence of two specific perfluorochemicals, perfluorooctane sulfonate (PFOS) and perfluorooctanoic acid (PFOA), in human serum at very low part per billion levels. In comparison, PFOA is a manufacturing additive used to produce polytetrafluoroethylene (PTFE), for various items, including non-stick cookware. PFOS is a residual impurity in some paper coatings intended for food contact.

A possible solution to the problem above is using more biocompatible additives, such as micro/nanofibrillated cellulose (MFC/NFC), renewable and biodegradable cellulose-based material, as already mentioned. With the help of an appropriate retention aid, MFC/NFC can be deposited on the fiber surface before forming the sheets, which increases the bonding area similar to dry-strength polymers and makes the surface fiber softer. On the other way, MFC/NFC acts like a filler because the surface of nanocellulose is rich with free hydroxyl groups (see subchapter 2.2.1.). Allowing filling the voids between the fibers when added to the pulp or on the fiber surface promoting fiber-to-fiber adhesions and consequently improving the strength of the paper, figure 2.7 (A. Li et al., 2021). In recent years, some approaches and suggestions have emerged in the literature for producing and optimizing this additive as a possible alternative agent to reinforce these fibrous structures (Morais et al., 2021; Moreira et al., 2023; Medeiros et al., 2023)

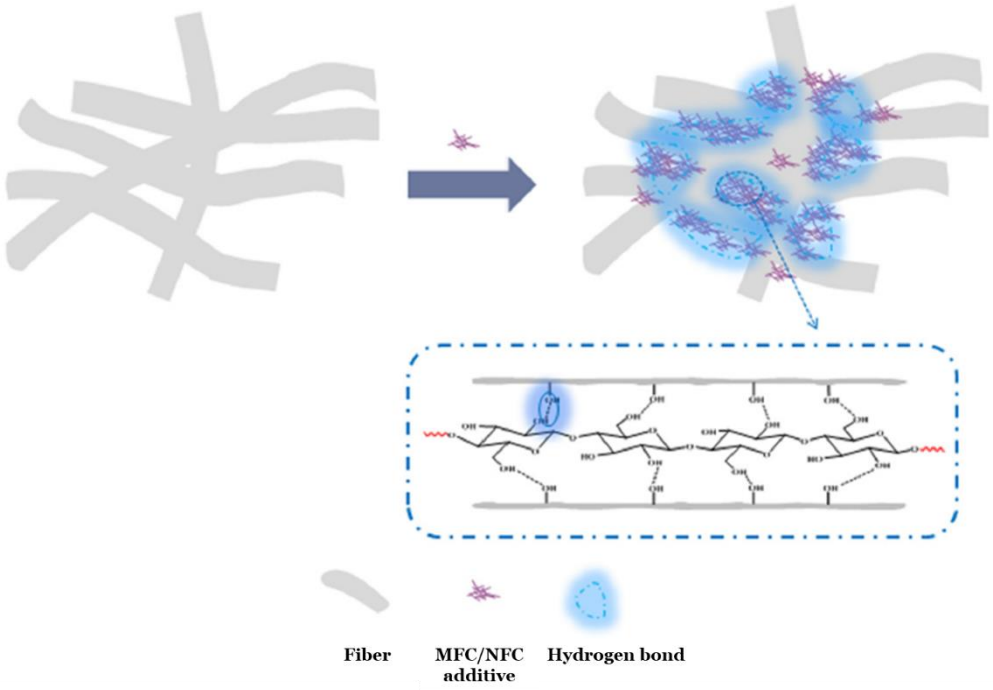

Figure 2.7 -The effect on the combination of MFC/NFC additive with pulp fibers (adapted from (A. Li et al., 2021)).

2.3. The Emerging of Eco-Friendly Packaging

The development of plastic packaging resulted from humans' need to create a material that could contain and preserve their food for either a short- or long term. Because of its low cost, lightweight, high performance, and simplicity of production, plastic is, in certain ways, a logical material option (Zhang et al., 2022). However, due to the dramatic increase in single-use plastic (SUP) manufacturing and the recognition that many of these fossil-derived materials are not biodegradable. Plastic pollution has emerged as one of the most critical environmental issues, affecting marine life and public health (Schenker et al., 2021; Semple et al., 2022; Zhang et al., 2022). The concerns about using fossil-based packaging materials, the benefits and drawbacks of eco-friendly packaging, the current manufacturing technologies, and the environmental sustainability through the analysis of a life cycle assessment of molded pulp products will be discussed in this chapter.

2.3.1. Concerns Regarding Packaging based on Fossil Resources

Plastics have increased exponentially more than almost all other manufactured materials, from 2 million metric tons (MT) produced annually in 1950 to 322 million MT in 2015. Food packaging and wrapping account for over 40% of all commercial packaging, with 40% of food packages made from plastics (Semple et al., 2022). Analyzing Figure 2.8, waste generated from plastic packaging grew by 23% (+6,5 kg) per resident between 2010 and 2020.

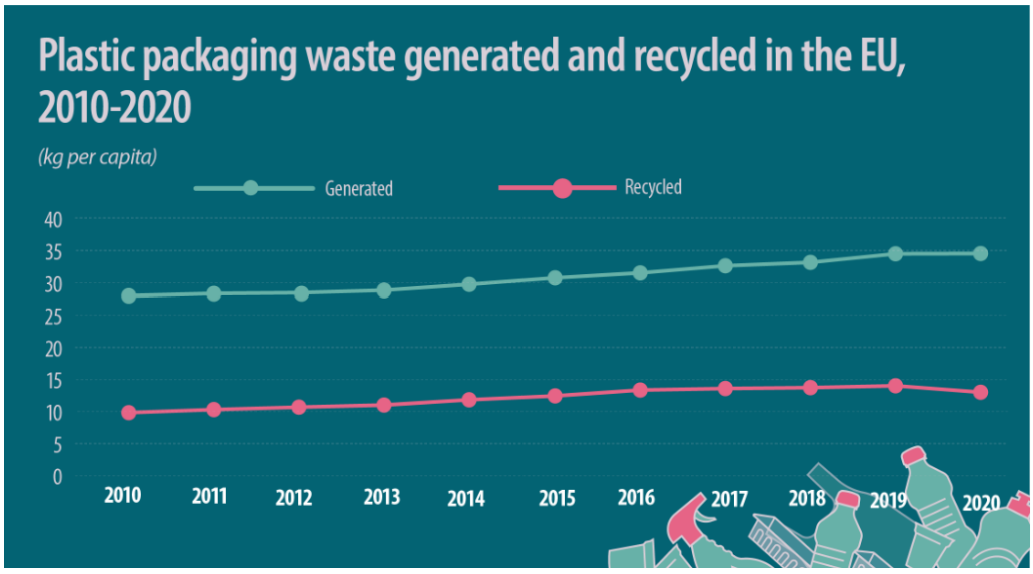

Figure 2.8 - Statistics on packaging waste generated and recycled in the 27 of European Union (EU) Member States and some non-member countries (adapted from(Eurostat, 2022)).

Over the same period, the volume of recycled plastic packaging grew by 32% (+3,2 kg). Despite this progress, since 2010, there has been a 3,4 kg per person increase in plastic packaging waste that was not recycled because the amount of plastic packaging waste produced overall has grown more rapidly (Eurostat, 2022). This may occur because most plastics are discarded for various reasons, including poor management systems, high costs, and misconceptions (Zhang et al., 2022).

The term "green plastics" emerged to address this issue, made from recycled plastic, but may not be the most reasonable solution. These plastics are filled with various polymers, co-additives, fillers, coatings and reinforcements, dyes, and plasticizers (Semple et al., 2022). For example, oxo-degradable plastics, which present co-additives to allow degradation under ultraviolet (UV) light as well as oxygen, complicate waste management and encourage consumers to waste more since they believe these materials quickly degrade over time (Hann et al., 2017).

As mentioned earlier, in response to concerns about the sustainability and consequences of plastic pollution on our ecosystem, major corporations have begun replacing non-recyclable packaging with fiber-based solutions. Since most cellulosic fiber materials are typically recyclable, many countries have developed recycling facilities and methodologies, making this material a good eco-friendly option (Schenker et al., 2021).

2.3.2. Sources of Cellulose Fibers

As stated in subsection 2.2 of the present study, vegetable fibers can be obtained from various plant sources, including wood fibers, recycled fibers, and even agricultural biomass residues such as hemp fibers, rice and wheat straw, and bamboo fibers, among others (Semple et al., 2022; Zhang et al., 2022). Various well-established industrial methods—mechanical, chemical, enzymatic mechanisms, and even their combinations—can extract virgin fibers today. These methods were already discussed in subsection 2.2.2.1. The chemical compositions and morphologies of the fibers differ based on the treatment used and the purpose for which they will be employed (Zhang et al., 2022). In summary, fiber-based packaging materials can be split into two categories: flexible (paper) and rigid (paperboard, molded pulp, corrugated board), with additional categories based on application and previous usage (Figure 2.9) (Schenker et al., 2021).

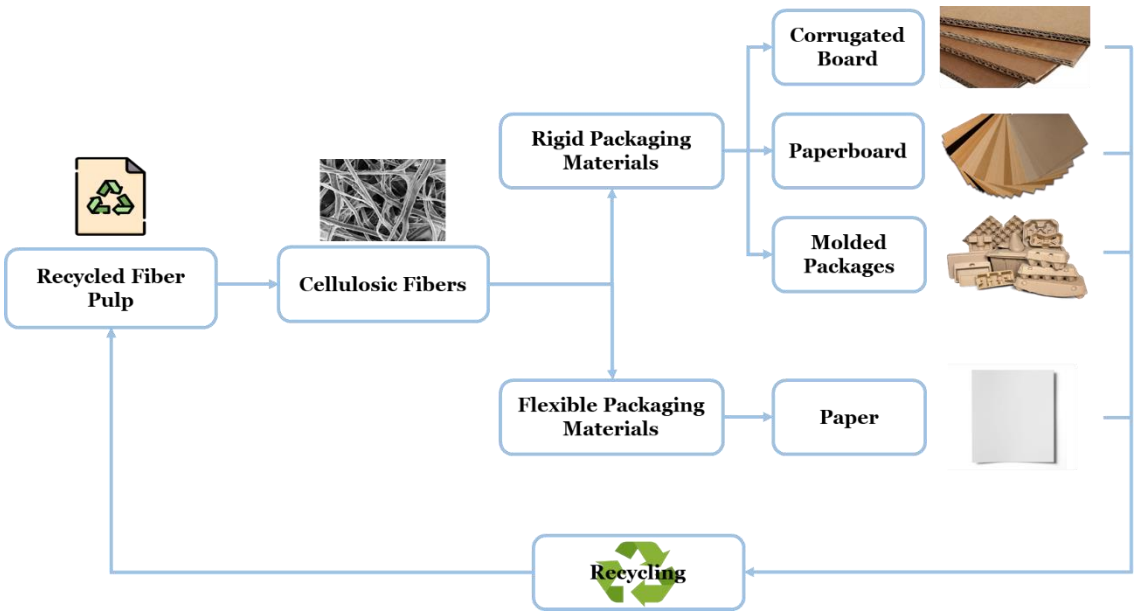

Figure 2.9 - Schematic overview of novel cellulose fiber-based packaging materials (adapted from (Schenker et al., 2021; Semple et al., 2022)).

Any of these techniques mentioned are suitable for producing great molded packages. In an even more environmentally friendly manner that supports the circular economy, companies could use recycled fibers. Which are fibers of unbleached or colored pulp with relatively low fiber strength and interfiber bonding because of higher fiber hornification during the multiple drying methods (Schenker et al., 2021; Zhang et al., 2022). Lastly, in line with the green chemistry philosophy, we can use agricultural biomass wastes, such as hemp fibers, rice and wheat straw, and bamboo fibers, for molded fiber products (Semple et al., 2022; Zhang et al., 2022). Certain companies can benefit from implementing this approach to promote economic development by increasing the consumption of their resources while decreasing waste and residues. Furthermore, this strategy considers the new guidelines and funding from the European Union. A set of policies and investments that will be implemented over the next decade to push the countries toward recovery, sustained economic growth, and convergence with Europe, led by a concept of sustainability influenced by the United Nations (United Nations, 2021).

2.3.3. The New Generation of Biodegradable and Biobased Materials for Food Packaging

2.3.3.1. The Modernization of Food Packaging

Food packaging has great relevance for the food industry since it makes it possible to maintain and prolong the quality and safety of food products (Ghaani et al., 2016). The current food packaging that reaches the consumer resulted from a whole evolution due to the improvement of these parameters mentioned above and the needs of the industry and the consumer. Traditional packaging was produced taking into account only four basic parameters: (1) protection, (2) containment, (3) communication, and (4) marketing (Biji et al., 2015). At the level of protection and containment, the industry was concerned with reducing the interaction between food and packaging material. The other two parameters, the use of the brand logo and informative texts (such as the list of ingredients, nutritional information, and expiration dates), clarified the consumer. However, the consumer's lifestyle overlapped in the selection of packaging, developing practical, fast (such as ready-to-eat foods) and easy-to-handle approaches, i.e., "easy to open", reusable and microwave-friendly (Vanderroost et al., 2014).

A new generation of food packaging materials is emerging due to consumers' new interests and environmental awareness. The fact that the population continues to grow exponentially forces companies to have better approaches to food production and conservation to ensure this global demand. Although the current society is in a fast-paced lifestyle, demarcated by a need for more time to purchase fresh food and prepare meals. However, they continue looking for alternatives that provide them with food safely and healthily, also considering their environmental impact (Salgado et al., 2021). The role of biotechnology and nanotechnology becomes crucial in developing or improving solutions capable of keeping and supervising their innocuousness and food quality (Enescu et al., 2019).

2.3.3.2. Benchmarking

Benchmarking is a term used in the industry as a point of reference to understand how it is positioned in the market compared to other companies. In other words, comparing products that are already on the market and may be considered to be the best clarify the strengths and weaknesses of each company's product (Andersson & Djeflat, 2013).

In the present work, it was important to conduct a preliminary analysis of the literature on new trends in food packaging and then, in a laboratory environment. Employing methods and tools that allow us to explore further and obtain more conclusions about this approach. As is the case, for example, of chemical characterization using infrared spectroscopy by FTIR-ATR technique and evaluation of the liquid spreading area using an optical system (Mendes et al., 2013; Curto et al., 2015; Morais et al., 2023) specifically developed to investigate the interaction over time of liquid droplets on different web fibrous structures.

2.3.3.3. New Trends in Food Packaging

A subdivision was conducted to elucidate some of the current sustainable and biodegradable solutions that are being studied or interested by companies in the food sector (Figure 2.10). Note that factors like the fiber sources (virgin fiber or recycled fibers), production process, and various post-treatments significantly impact the mechanical properties and value of this product group.

In the first analysis, the solutions presented in types 1 and 2 are similar, but their fibrous formulation and applicability differ. Type 1 only considers using a single type of vegetable fiber source (HW paper or SW paper). In contrast, type 2 fibers use the morphological and mechanical properties of heterogeneous fibers to produce a final product with pre-established parameters and are considered optimal in the industry (75% HW + 25% SW, for example) (Giordano et al., 2021; Morai et al., 2021).

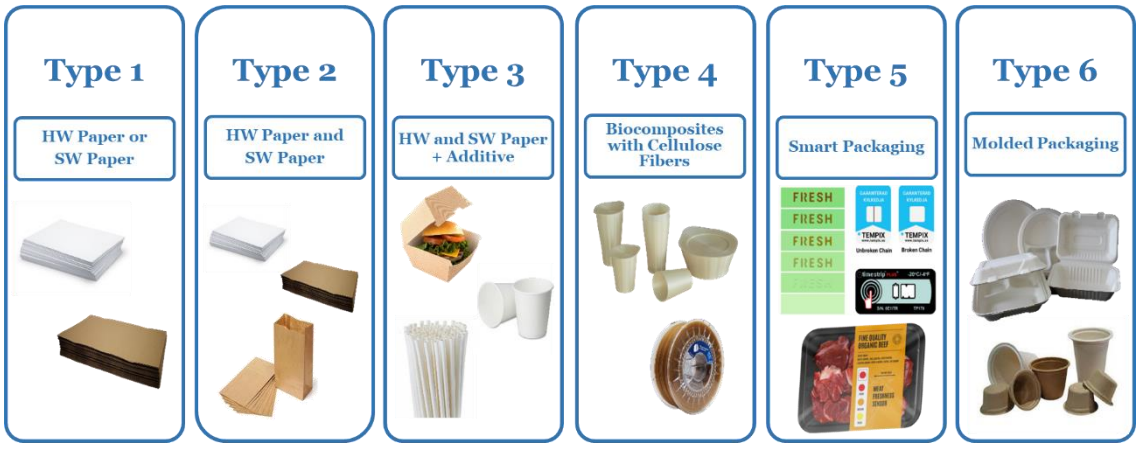

Figure 2.10 – Subdivision of different materials and packaging with current economic value for companies.

However, from a conservation and containment perspective, we found ourselves at a lower level. The associated production processes are also simple and cheap. Type 3, which also uses heterogenous fibers but improves their mechanical and morphological properties (permeability, retention, volume, stiffness) with the aid of additives, as is the case of those mentioned in subdivision 2.2.2.2 (Martins et al., 2018; Michelin et al., 2020; Morais et al. 2021). This approach allows an average level of containment and retention of food.

More technologically and recently, packaging 3D printing is represented in type 4 (Nida et al., 2021; Zhou et al., 2021). In (García-Guzmán et al., 2022), the preparation, modification, and processing of starch-based materials for food packaging applications are explored. Systematically, starch is not thermoplastic material; however, with the help of plasticizers (water or polyols), heat and pressure can behave as one. The starch undergoes an extrusion process leading to its rupture and diffusion of the plasticizer. Starch can be inserted in granules or gelatinized form in synthetic or biodegradable polymers such as Poly Lactic Acid (PLA) or chemically modified. Although the solution is promising and inserted as an environmentally friendly solution, it still needs a lot of research and optimization and more studies to scale up production on an industrial scale.

About type 5 packages differ from the others because they interact with the food, allowing better communication with the consumer about the state of freshness and quality of the food in real-time. They are called smart packaging (Figure 2.11) (Salgado et al., 2021). Within this category, we can divide into (1) active packaging and (2) intelligent packaging. The term “active package” refers to the ones where active components have been purposefully added. These components release or absorb substances to extend the shelf life and preserve the quality and freshness of food (Bento et al., 2020; Yildirim et al., 2018). There are two main types of active packaging: (1) active purification systems (absorbents) and (2) active discharge systems (emitters). Where antioxidant releasers, CO2 emitters, and antimicrobial packaging systems are examples of active delivery systems. In contrast, active scavenging systems use ethylene, moisture, and oxygen scavengers (Bento et al., 2020; Yildirim et al., 2018).

Intelligent packaging can detect, monitor, document, trace, and provide data about food quality. It can help with shelf-life, safety, and quality decisions (Salgado et al., 2021).

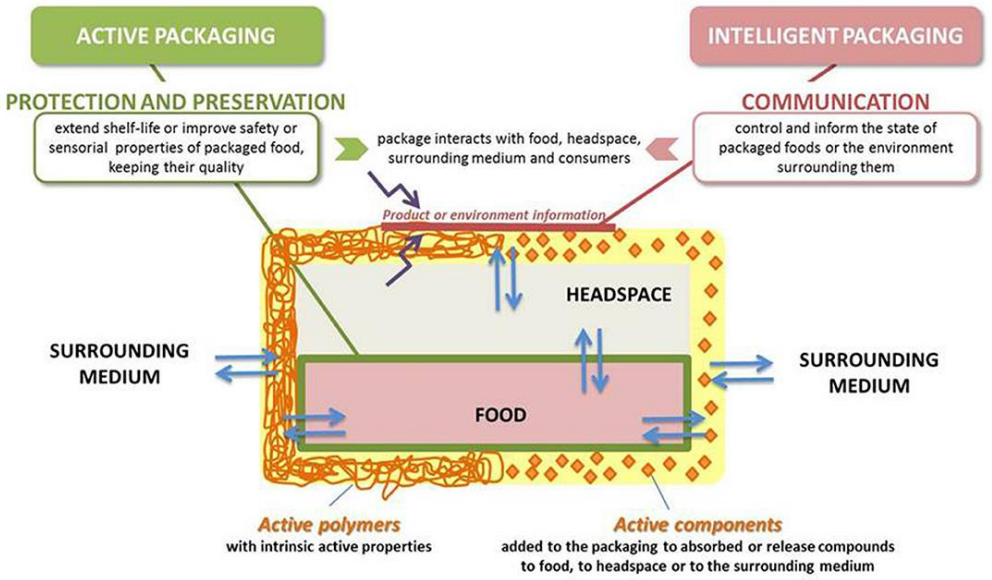

Figure 2.11 – Schematic diagram of a smart packaging, highlighting the differences between active packaging and intelligent packaging (adapted from (Salgado et al., 2021)).

The intelligent packaging systems can be divided into: (1) indicators through a color (or color intensity) change or dye diffusion. They help provide quick, visual, qualitative, or semi-quantitative information about food. Visible changes, such as time-temperature indicators (TTI), oxygen indicators, and freshness indicators, help provide information about changes in the food or its environment (like temperature or pH)(Salgado et al., 2021), (2) biosensor is a system that uses a recognition molecule and a target to detect potential changes in the surrounding environment. It includes a receptor that converts a chemical or physical signal into an electrical signal, which further goes through a transducer, converting an electrical signal to an analytical signal, which the consumer can easily and quickly understand, although this type of approach is more complex than indicators (Bao et al., 2022; Salgado et al., 2021), (3) data carriers, applied for forgery security, automation, traceability, anti-theft, and identification. Bar codes, QR codes, and radio-frequency identification (RFID) labels are some examples of data carriers (Salgado et al., 2021).

Lastly, and the focus of the present work, molded packages (Type 6) have also gained popularity due to their renewability, recyclability, sustainability, and biodegradability (Oliaei et al., 2021). Because those can be produced from photosynthetically renewable or recyclable materials, they can also be easily recycled (Debnath et al., 2022). Furthermore, such products can assume three-dimensional shapes by dewatering cellulosic pulp suspensions.

Molded pulp products are now used in four distinct markets: (1) food related (e.g., cups, bowls, egg cartons, and containers); (2) industrial packaging (e.g., electronics, household items, and vehicle parts); (3) single use medical (e.g., bedpans, urine bottles, and bows); (4) horticultural (e.g., trays and Pots) (Oliaei et al., 2021). The product density, production technique, and fabrication method used to be the foundation for classification, which made cataloging more challenging (Debnath et al., 2022; Didone et al., 2017). However, following the International Molded Fiber Association (IMFA) standards, they are now eligible to be classified as (1) type 1 - thick wall; (2) type 2 - transfer molded; (3) type 3 - thermoformed or thin walled and (4) type 4 – processed.

When discussing "thick wall", the packages are produced with an open mold, then oven dried. Walls usually present a thickness of 5 to 10 mm. While the other side is extremely rough, the surface in touch with the mold is relatively smooth. Traditionally, kraft paper and recycled paper are used as raw materials. Support packaging for bulky, non-fragile items (like furniture and auto parts) is the usual application.

Regarding "transfer molding", they present better dimensional accuracy, comparatively smooth surfaces on both sides and thinner walls between 3 and 5 mm. These are commonly used as packaging for electronic devices and egg cartons.

The "thermoformed mold" is formed using various heated molds, with a final wall thickness ranging from 2 to 4 mm (thin walled). Shapes are well-detailed, with smooth surfaces and very few draft angles. Without the use of a furnace, products are dried inside the mold. The walls are slightly dense due to the hot mold pressing procedure. Thermoformed fiber has the benefit of closely resembling thermoformed plastic material.

Finally, we have "processed mold", and this category covers products that need additional processing or specific treatment. The manufacturing process, grade, and quality, as well as the production cost, increase from type 1 (thick wall) to type 3 (thin wall), with type 4 (processed) having the highest value because of the incorporation of additives to achieve desirable properties.

Regarding the forming-drying process of molded products, there are two types of manufacturing methodology: (1) wet-press process and (2) dry-press process (Zhang et al., 2022). In the following section, these two aspects and their advantages and disadvantages will be explored.

2.3.3.4. Molded Packaging Manufacturing Methodology

Figure 2.12 demonstrates the approach to manufacturing a variety of different molded products. It can be separated into two stages: (1) pulp preparation (figure 2.12a) and (2) molding process (Figure 2.12b).

The pulp preparation of fibers (Figure 2.12a) starts with collecting and separating various waste papers, such as those mentioned in section 2.3.2. These sorted waste papers are then pulped in a pulper employing a hydrodynamic disintegration process. In which large quantities of raw fiber materials are combined with hot water to detach and separate the fibers from the others. Since we are working with recycled materials containing contaminants/impurities such as metals and plastics, a deinking, cleaning, and screening process is required. A benefit of working with recycled fibers is that they are more likely to undergo a moderate or non-refining treatment in the pulp system once they have been processed to a certain extent before recycling. On the other hand, in a premium view, virgin fibers in the furnishing system are essential for quality in terms of strength and product appearance.

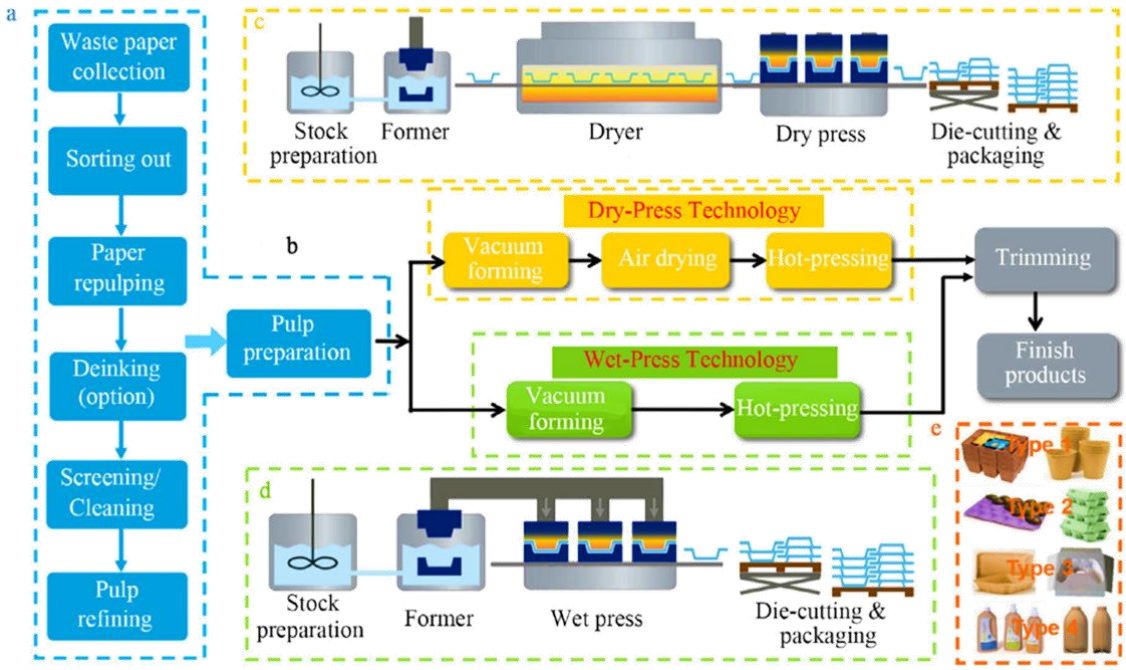

Figure 2.12 - Illustration of the typical production procedure for various kinds of molded pulp products (adapted from (Zhang et al., 2022)).

In this context, an independent fiber line is installed in the molded mill, where virgin fibers are repulped and refined before being integrated into the recycled pulp (Zhang et al., 2022).

During the molding process (Figure 2.12 c and d), two common steps are involved: the vacuum forming step and the drying step, respectively. During the vacuum forming process, the custom-designed die, which is the negative geometry to be made, is submerged in a tank filled with pulp. Where the pulp is sucked onto the mold via a vacuum-assisted process. The deposition of the wet pulp on the forming tool is a form of wet pressing, where 35% - 50% volume of water is removed to form a desired shape. The drying process follows the forming process to remove the residual water (44% - 55%). The dry-press method (plain molding, Figure 2.12c) and wet-press method (thermoforming, Figure 2.12d) are two types of drying process. Typically, oven drying is chosen as the dry-press method for plain modeling. Plain molding products fall into two categories: thick wall and transfer molded. Typically, the production systems for such items are designed for high-volume production with a high degree of automation. In contrast, heat is applied between the opposing sides of the mold for the dry-press process, also known as thermoforming.

During the drying process, the material is compressed, making the products denser, smoother, and more precise than those that have been air-dried. Additionally, the pressing improves the mechanical properties by strengthening the bond between the fibers (Didone et al., 2017; Zhang et al., 2022).

One thing to have in mind is the impact of specific parameters on the final product quality, such as hydropulping, vacuum forming, and dewatering. Excessive fiber refining (beating) and hydropulping, for example, can damage the fine fibers needed to fill the fiber network's void space and interact with the moisture and oil-resistant additives required in food packaging. Furthermore, changes in web porosity and permeability during vacuum forming and pressing, as well as its drainage rate and moisture retention, significantly affect the economics of molded pulp manufacturing. The drying schedule and time determine the homogeneity of wall thickness in molded pulp, which is important in avoiding cast deformation and friability (Semple et al., 2022).

This approach emphasizes the necessity for tools able to predict and select the parameters that affect the production of these materials in today's research to be applied by the industry. The use of advanced computational tools, such is the case of 3D molecular and fiber modeling (Curto et al., 2015; Morais & Curto, 2022c) in the present work intends to make a contribution to this goal.

2.3.4. Life Cycle Assessment

When discussing a product's life cycle, a Life Cycle Assessment (LCA) searches, quantifies, and assesses sources of environmental impact. In other words, investigate all the processes involved in producing, using, and disposing of the product (Figure 2.13). This approach aids in determining the environmental impact of various packaging solutions, for example, the use of virgin or recycled fibers and if mechanical or chemical pulping is applied, and then deciding which solution makes the most sense (Das et al., 2023; Didone et al., 2017). Some LCA studies on molded pulp products were collected and compared in (Didone et al., 2017) review, showing a wide range of goals and scopes.

In general, the studies of LCA covered forestry and other stages agree that the forestry stage has a small impact on the environment regardless of the wood, machinery, or fuel used. The same does not apply to the pulp and paper production stages, where there is a consensus that these two steps have the highest environmental impact in the life cycle.

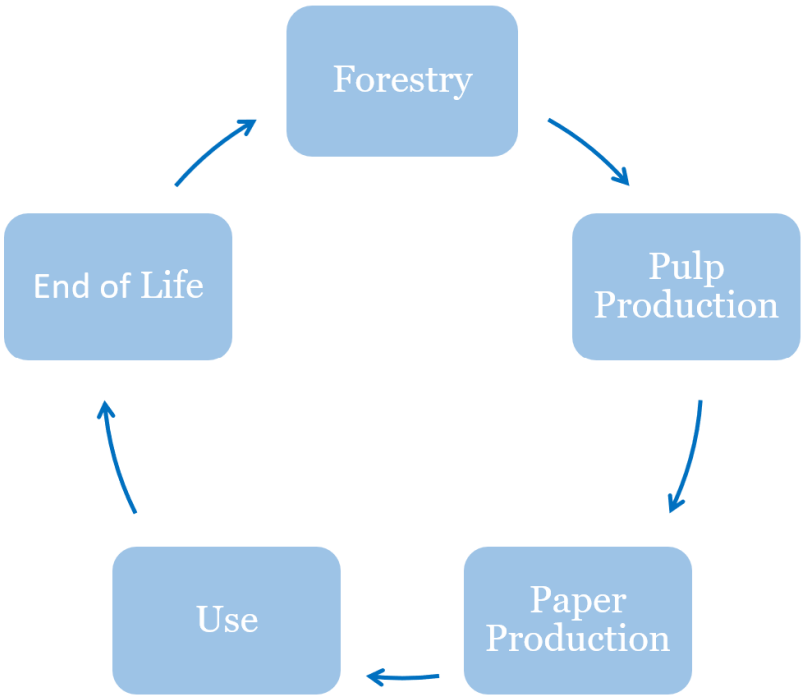

Figure 2.13 -Life Cycle Assessment of molded cellulose packaging (adapted from (Didone et al., 2017)).

For instance, producing 1 ton of tissue paper from recycled paper has a lower environmental impact than using virgin fibers. Also, recycled paper reduces the pressure on forests and the required energy consumption up to 27% less than virgin fiber pulp.

However, the quality of fibers is affected negatively every time they are recycled. Based on practical experience, fibers can be recycled five to seven times (Bajpai, 2014). Regarding paper production, pulp molding includes a drying process described in subsection 2.3.3.4, which can demand more energy and costs. In that view, the environmental impact is affected by the heat source used; for example, steam had a smaller impact than heated air. At the end-of-life stage, there are several options for molded pulp products, such as recycling, biodegrading, and landfilling. As mentioned in the previous subsection, the preparation of the recycling pulp involves a pulping, screening, refining, washing, drying, and finishing step. This could be a disadvantage when choosing recycling paper due to the use of various chemicals such as colophony, paraffin emulsion, sizing wax resin, and bauxite. Depending on the additives employed, biodegrading is a viable choice for paper products, being a good alternative for businesses as an economically viable by-product in the form of compost. For the same reason, the biodegradation of this type of cellulosic material will be studied in this work to provide important information not only to the scientific committee but also to the companies of the Beira Interior region. Landfilling could not be the best alternative because methane emissions are a primary contributor to the global warming potential of paper products. In conclusion, depending on the steps chosen in the production process, molded cellulose packaging has the potential to be environmentally sustainable. Because of this, the LCA substantially influences this decision-making process, yet the available data is limited, demanding more studies in this field.

2.4. Optimization using Advanced Computational tools

2.4.1. Molecular Modeling

Materials are nothing more than a set of molecules that interact through intramolecular and intermolecular forces. In the case of cellulose, as mentioned previously, OH-O hydrogen bonds cause most of the cellulose's intramolecular interactions. However, intermolecular interactions are also influenced by the weaker CH-O hydrogen bonds and Van der Waals interactions. These interactions interfere with the physical and chemical properties of the material, such as stiffness, resistance, and flexibility. Advanced computational tools such as molecular modeling has been present in several lines of investigation within the FibEnTech research group, such as: (1) modeling of molecules of various essential oils for the design and engineering of innovative protective masks (Mendes & Curto, 2021), (2) modeling of *Cochlospermum* angolense Welw molecules. ex Oli essential oil with antioxidant activity (Samba et al., 2023), and (3) modeling of

essential oil molecules from *Cannabis* sativa L. and *Ageratum* conyzoides L. in a DDS for dermal application (Medeiros et al., 2023). The results from this works indicate that molecular modeling is a good tool during an investigation to understand the 3D molecular organization of molecules and how they interact with other molecules.

2.4.2. The Evolution of Models to Simulate and Optimize Fiber Materials

Within a highly competitive industry, it is essential to use tools capable of improving production processes by reducing manufacturing times and resources, resulting in considerable cost savings. Computational modeling of fiber structures and data-driven modeling methods have been used progressively over the past few decades to improve the design of both materials and their products (Simon, 2021).

When working with a complex material, which is the case, it is crucial to understand the role of fibers in the paper properties, mainly transverse fiber dimensions and mechanical behavior (flexibility and collapsibility). Because when raw material is changed, several fiber dimensions vary simultaneously. Furthermore, both the fiber flexibility and collapse mechanisms co-occur during the refining. As a result, it becomes a challenge to quantify each cause's impact separately in experiments. From that point of view, mathematical paper models can be helpful tools for overcoming experimental limitations (Curto, 2012).

In 1960, Corte and Kallmes suggested a 2D geometric model of several rigid fiber networks, where the fibers were placed uniformly and randomly or even with different flocculation parameters in a rectangular or square area, with a distribution adjusted by a sample of known distributions (Bronkhorst, 2003; Kallmes & Corte, 1960; Lavrykov et al., 2012). Continuing their investigations in 1962, Cortes and Kallmes developed the modeling of fibrous materials for the first time through the superposition of several 2D layers forming a multi-planar structure made from rigid fibers (Kallmes & Corte, 1962). These models, however, only explored the fiber's position in the plane (xy direction). Leaving out its arrangement in the z direction, i.e., the thickness of the material.

Figure 2.14 illustrates a timeline of different models of porous materials that have been presented and implemented, allowing computational 3D models of porous cellulosic materials to be studied.

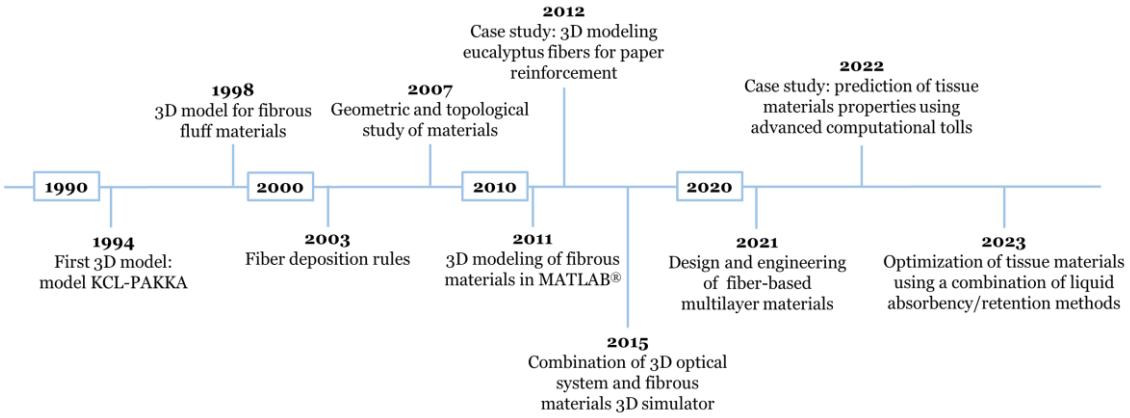

Figure 2.14 - A timeline of the different approaches that have been introduced and implemented for fibrous materials over time (adapted from (Morais, 2017)).

This approach allowed the development of the initial 3D model, the KCL-PAKKA model, presented in 1994 by Niskanen and Alava. This model recreates the 3D geometry of structures using a random arrangement of fibers in the xy plane. Through fiber flexibility, this model allowed the fiber to occupy the z dimension uniformly, i.e., the fibers conform to each other based on the input value for their flexibility, thereby innovatively producing 3D structures (Alava & Niskanen, 2006; K. Niskanen et al., 1997; K. J. Niskanen & Alava, 1994). In 1998, Heyden and Gustafsson proposed another 3D model for fluff materials. In this model, each fiber is represented by a single circle arc and put in a box to make a periodic network. Despite this, when added to the structure, the fibers' bending was not specified (Heyden, 2000).

In 2011, (Conceição et al., 2010; Curto et al., 2011) taking into consideration the KCL-PAKKA model, introduced and validated the voxelfiber, a 3D fibrous materials model developed and implemented in MATLAB®. More recently, the use of advanced computational tools for 3D fiber simulation has been applied to study cellulose-based materials in our research team (Curto, 2012; Curto et al., 2015; Mendes & Curto et al., 2021; Morais et al., 2022; Morais et al, 2023). In the subsequent subchapter, this same model will be explored because it is essential to understand the crucial processes step by step and parameters to obtain a realistic model.

2.4.3. Simulation of Fiber and Structures

In the 3D computational simulation fibers are modeled according to their dimensions, flexibility, and collapsibility. It is essential to select inputs from the experimental design and to determine the outcomes of a computational experience and process the data using optimization tools, to achieve specific goals.

The input parameters are (1) length/width ratio, (2) wall thickness, (3) lumen thickness, (4) fiber flexibility and (5) resolution, i.e., number of layers in the thickness direction. Additionally, length values might be expressed as distributions or averages. Also, fines and fillers can be added.

The implementation of the computational fiber flexibility is based on cellular automata (Figure 2.15), which uses a cell cartesian division to represent the simulation region, where fibers represent a sequence of voxels and occupy a user-defined pre-established volume (Curto et al., 2011). The highest allowed vertical deflection for the fiber is determined by a "bending" flexibility or dimension less computational flexibility (K. J. Niskanen & Alava, 1994). Therefore, any two close neighboring cells on the fiber can reach the maximum fiber flexibility. On top of that, the model is detailed up to a point to include the fiber's internal structure and the ability to adjust it, as well as the material's z-direction collapsibility.

One fiber at a time is deposited to form the simulated paper structure, each occupying its own space. The fiber conforms to the underlying structure depending on its position, dimension, and flexibility (Figure 2.15). Also, to simulate the formation of isotropic handsheets (those utilized for model validation), fibers are oriented in the xy plane and randomly positioned.

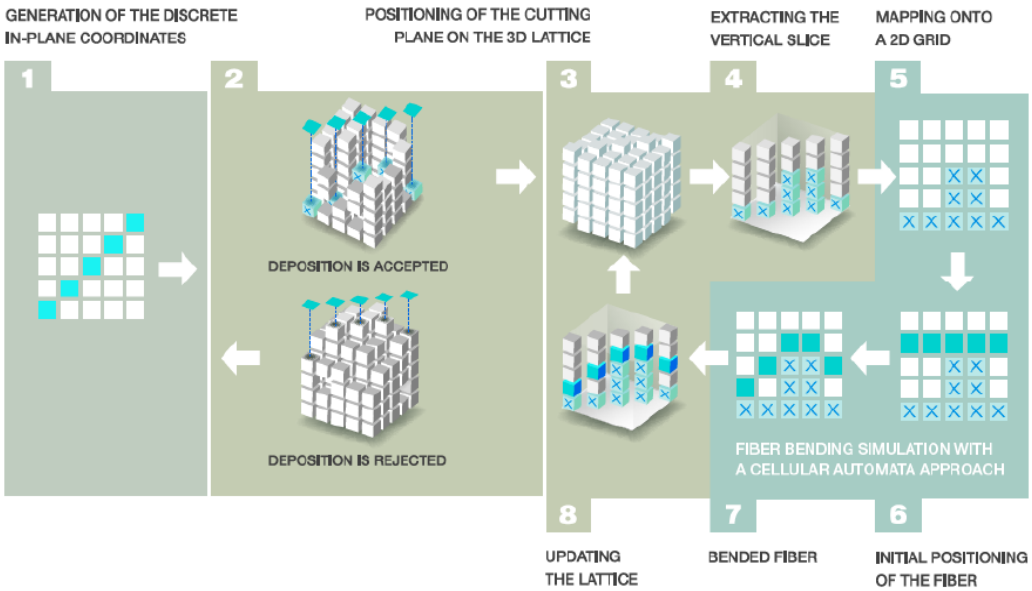

Figure 2.15 – An illustration that demonstrates the fibers' sequential deposition in a 3D matrix, followed by plain extraction and fiber bending to conform to the underlying structure (adapted from (Curto et al., 2011)).

The step-by-step process of deposition of fibers in the computational simulator is described below (Curto, 2012; Curto et al., 2011).

1) Generation of fiber in the in-plane direction.
2) Testing particle deposition rule. If the fiber is not accepted, the generation trial is repeated.
3) Extraction of the out-of-plane slice from the 3D network where the bending procedure occurs.
4) Fiber deposition according to fiber flexibility and conformation to the underlying surface.
5) Updating of the 3D network.

One thing to have in mind, the voxelfiber model is also based on designs extrapolated from Latin Hypercube Sampling. In other words, this method (which can be applied to tree dimension) involves dividing the space formed by two variables into a subdivided n x n square and selecting the n points in each subframe, so that no two points occupy the same line or column.

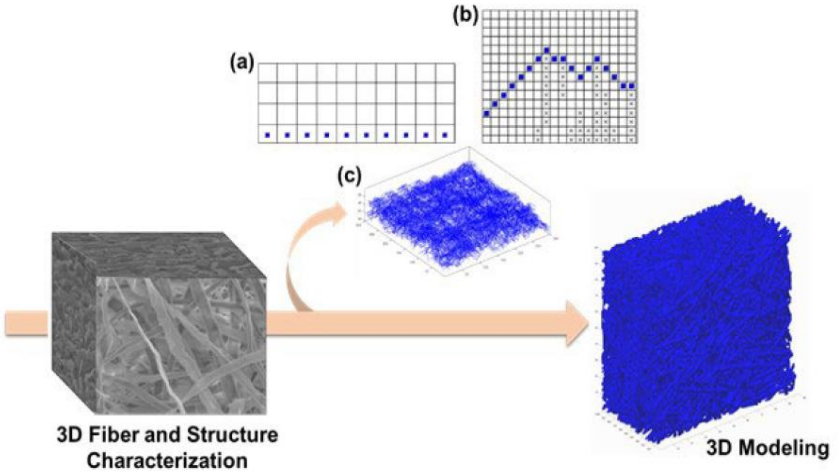

Figure 2.16 – A 3D fiber and structural characterization is given in the first section (left), and a 3D modeling approach is described in the second (right). The fibers are modeled with realistic parameters based on experimental analysis to perform these computational simulation investigations. The fibers are randomly deposited, (a) one at a time, (b) without depositing on others because the fibers' space will not be overlaid, and (c) inside a spatial arrangement (indicated by the user) in the 3D matrix to create the 3D computational structure (adapted from (Morais & Curto, 2022a)).

Lately, the model output is a 3D fiber network structure (Figure 2.16) formed with occupied and empty voxels, where the information concerning each fiber is kept. This formed structure can help predict several structural properties, including thickness (local and average), porosity (interfiber and global), RBA, coverage, and the number of crossings per fiber.

2.4.4. Data Mining Techniques

The optimization of fibrous materials requires a multiple-input multiple-output (MIMO) approach since using a complex material involves different fibers and structure properties along with the influence of several process operations. For this same reason, alternative techniques based on data mining for forecasting and optimizing advanced processes have been studied. This is especially relevant for analyzing large, complex, and highly nonlinear situations (Kerekes et al., 2020). These data mining techniques, for instance, can be decision/regression trees, multiple linear regressions (MLR), and artificial neural networks (ANN).

2.4.4.1. Decision/Regression Trees

One of the most effective and powerful techniques for data mining is decision trees. Its advantage is that it can handle various input data types, such as nominal, numerical, and alphabetical data. The decision tree's purpose is to create a model and then, using multiple inputs, predict the value of the target variable. It is considered an excellent support tool that uses a tree-like graph or model of decisions and their possible outcomes (Gupta et al., 2017; Somvanshi et al., 2016). In a summarized way, the decisions are made from the root node to the leaf node, while the leaves (terminal node) contain the responses. Each internal node, a node containing outgoing edges, divides the instance space into two or more sub-spaces based on a discrete function of the input attribute values (Rokach & Maimon, 2005). Decision trees offer a simple, straightforward, and visually appealing technique in this context.

2.4.4.2. Multiple Linear Regressions (MLR)

Multiple Linear Regression (MLR) modeling is used to predict the functional properties of structures made from the isotropic laboratory structures data. Using various statistical methods, MLR allows the development of different empirical models to produce a response surface methodology. These models often associate multiple independent factors with a dependent variable to formulate a linear equation for the experimental data (Morais & Curto, 2022b). Considering a set of independent variables, namely x_1, x_2, ..., x_n, associated with a value of the dependent variable y, the linear regression model that describes this relationship can be seen below:

$$y = \beta_0 + \beta_1 x_1 + \beta_2 x_2 + \cdots + \beta_n x_n + \varepsilon \qquad \textbf{(Equation 2.1)}$$

Where the parameters $\beta_j, j = 0, 1, \ldots, n$, are the regression coefficients, and ε is a random error. The n-dimensional space of the regressor variables (x_j) is described as a hyperplane. When the remaining independent variables x_i ($i \neq j$) are held constant, the parameter β_j represents the expected change in response y per unit change in x_j (Myers et al., 2016).

2.4.4.3. Artificial Neural Networks (ANN)

Artificial Neural Networks (ANN) models perform a nonlinear transformation on the input data to approximate the output data. This model learns from experimental data examples and has some generalizability outside the training data. The most frequently employed ANN is a multilayer feedforward network. Each variable in a layer, also called "nodes", is made up of three layers (Figure 2.17): (1) the input layer: includes the initial predictors, (2) the hidden layer: a set of constructed variables, (3) the output layer: contains the responses. Additionally, each node's output value is achieved by an activation or transfer function that can be presented as a sigmoid, a hyperbolic tangent, or an exponential. However, the predictive properties of ANN are not superior to those obtained from MLR studies.

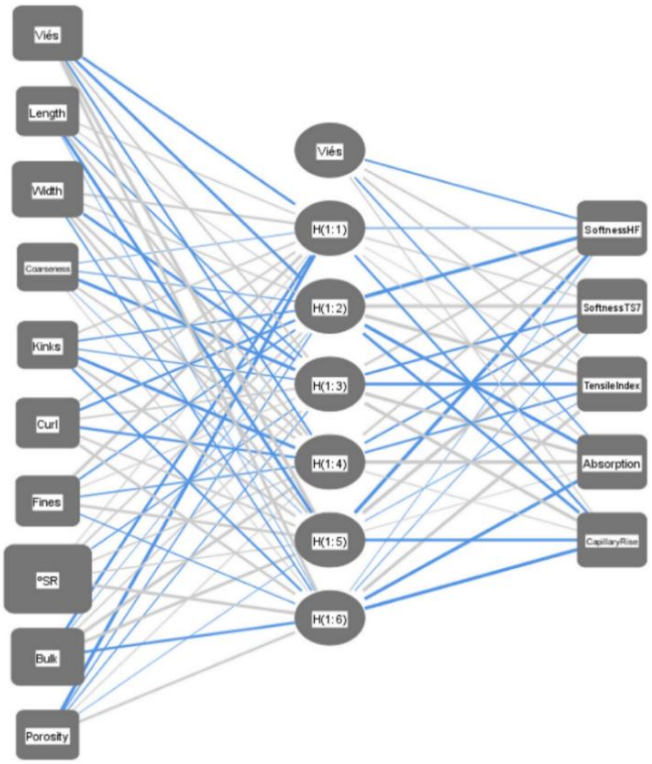

Figure 2.17 – Example of an architecture of ANN analysis (adapted from (Morais & Curto, 2022b)).

Despite being, at best, a predictive instrument, the underlying process mechanism that produced the data needs to be clarified (Myers et al., 2016). In that view, neural networks can supplement statistical procedures such as regression analysis to model the impacts of fibers on the 3D fibrous structure properties (Monga et al., 2017a, 2017b).

2.4.5. Simulation using Finite Element Method (FEM)

The simulation using Finite Element Method (FEM) analysis has been explored in our research team to predict, for example, key mechanical properties of the embossing process in tissue paper (Vieira et al., 2022) or even thermomechanical properties of printed circuit board (PCB) materials (Velosa et al., 2023). Using the last example made, the multi-layer PCB are made up of multiple layers of woven glass fiber reinforced epoxy resin (glass fiber/epoxy) substrates sandwiched between copper foils (L. Li et al., 2008). The new research group approach, however, is to replace glass fibers with cellulose fibers in the production of PCB (Figure 2.18). In this regard, the FEM will help predict and quantify in terms of deformation, the influence of natural cellulose fibers on replacing conventional glass fibers, particularly. Furthermore, the 3D simulator of fibrous structures mentioned before will be great for predicting the behavior of these materials and their optimization. This type of research demands the cooperation of a highly qualified and multidisciplinary team, considering that there should be an interconnection between multiple areas of engineering, chemistry, electronics, among others.

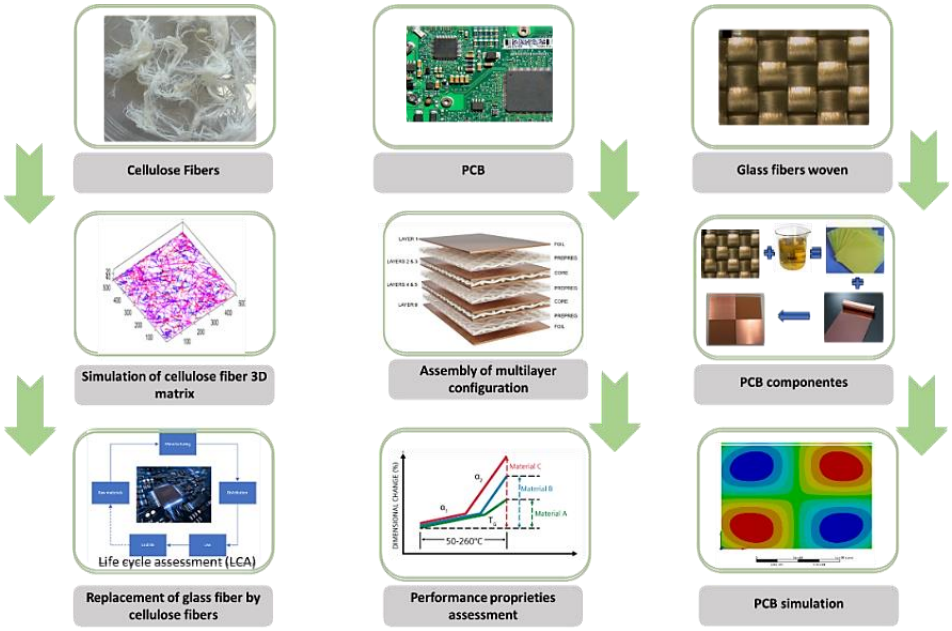

Figure 2.18 – Schematic of the methodology used to study the replacement of natural fibers in PCB, using experimental methods and computational tools (adapted from (Velosa et al., 2023)).

Chapter III
Materials and Methods

3. Materials and Methods

The materials and equipment used during the development of this project, as well as the methodology adopted to use them, will be addressed in this chapter. In summary, methods to produce fibrous structures in the laboratory and characterize their structural, mechanical, chemical, and optical properties for future 3D fiber simulation using a validated 3D model to compare actual data with simulated data. Considering the new European directives, a first study was conducted in laboratory on the biodegradation of these fibrous materials will also be described.

3.1. Materials

3.1.1. Cellulose Fiber

3.1.1.1. Cellulose Fiber Reference

Three cellulosic industrial materials from kraft processing were chosen as our fiber references in this study. An (1) E*ucalyptus* globulus, also known as hardwood (HW), which had been under a bleaching process; (2) *Picea* abies, also known as softwood (SW), which had not been breached and lastly an (3) industrial tissue paper (IT). It should be noted that both are entirely chlorine-free and have not received any drying operations.

3.1.1.2. Micro/nanofibrillated Cellulose Fiber Additive

The Micro/nanofibrillated Cellulose was produced by the FibEnTech research unit team resulting from the contribution of several studies (Martins et al., 2018; Morais et al.,2022).

3.1.1.3. Hemp Fibers

Hemp fibers (HF) were acquired from a hemp company and were extracted from the wood of the plant's stem by applying a cooking step followed by a bleaching step.

3.1.2. Biodegradability Studies

3.1.2.1. Cellulose Fiber Reference

A paper filter with the reference number 83211090 from Filtresrs® was used as a positive control. On the other hand, a silicone coated paper from a known industry served as a negative control.

3.1.2.2. Cellulose Fiber under Investigation

All other cellulose samples in this study were obtained from laboratory handsheets produced according to the respective ISO standards.

3.1.2.3. Laboratory Scale Composting

Compost soils were obtained from the University of Beira Interior (UBI) gardens (latitude: 40.277927, longitude: -7.554752) and a laboratory-scale composting apparatus, which included a plastic container with holes and a seed tray with 40 cells.

3.1.3. Benchmarking

For this evaluation the infrared spectroscopy by FTIR-ATR method where was used to evaluate: (1) plastics nonwoven fabric (material with fossil origins); (2) bamboo nonwoven fabric (semi-synthetic material made from (natural) bamboo fibers); (3) a commercial paper coffee cup (inner layer and outer layer); (4) silicone coated paper (the coated side). They will be compared with the web structures produced and optimized in the laboratory with the reference fibers.

In the other study, the liquid retention was analyzed using an optical prototype system, and three samples were selected: (1) handsheets structures with a basis weight of 60 g/m^2; (2) handsheets structures with a basis weight of 120 g/m^2 and (3) commercial sample, made from materials of fossil fuel.

3.2. Equipments

The types of equipment used throughout the present research are listed in Table 3.1. Also, the software used can be found in Table 3.2. It should be noted that the use of this equipment will be addressed in the following chapter.

Table 3.1 - List of equipments.

Equipment	Specifications & Manufacturer	Country
Analytical Balance	AG104, Mettler Toledo	Switzerland
Infrared Balance	LJ16, Mettler Infrared Scale	Switzerland
Sheet Press	App. 40 Type 5-1, L&W	Germany
ºSP	App. 14W Type 95041, L&W	Germany
Former	App. 32 Type 4_1, L&W	Germany
Morfi	Pilot, Techpap	France
Lab Desintegrator	95 568, Karl Frank GMBH	Germany
PFI-mill	Mark VI, Hamjern Maskin A/S	Norway
Tensile Test	733K, Thwing-Albert	Germany
Color Analyzer	Color Touch 2 (Model ISO), Technidyne Corporation	United States
Micrometer	M120, Adamel Lhomargy	France
FTIR-ATR	iS10 FTIR + Smart Diamond ATR, Thermo Nicolet	United States
Optical Microscope	Labophot-2, Nikon Instruments Inc.	Japan
SEM	S-2700, Hitachi	Japan
Sputter Coater	Q150R S, Quaorum	United Kingdom
Optical System	Prototype, University of Beira Interior	Portugal

Table 3.2 - List of software.

Software	Version
ACD/ChemSketch	2022
MATLAB	9.6 (R2019a)
Microsoft Office Excel	2016
Microsoft Office PowerPoint	2016
Adobe Photoshop	2023

3.3. Methods

The scheme below (Figure 3.1) describes the experimental and computational methodologies to produce and characterize the structures and their 3D simulation (green color). In addition, the processes required to extract hemp fiber from the plant are shown (orange color). The method used for the compost assays can also be seen in blue.

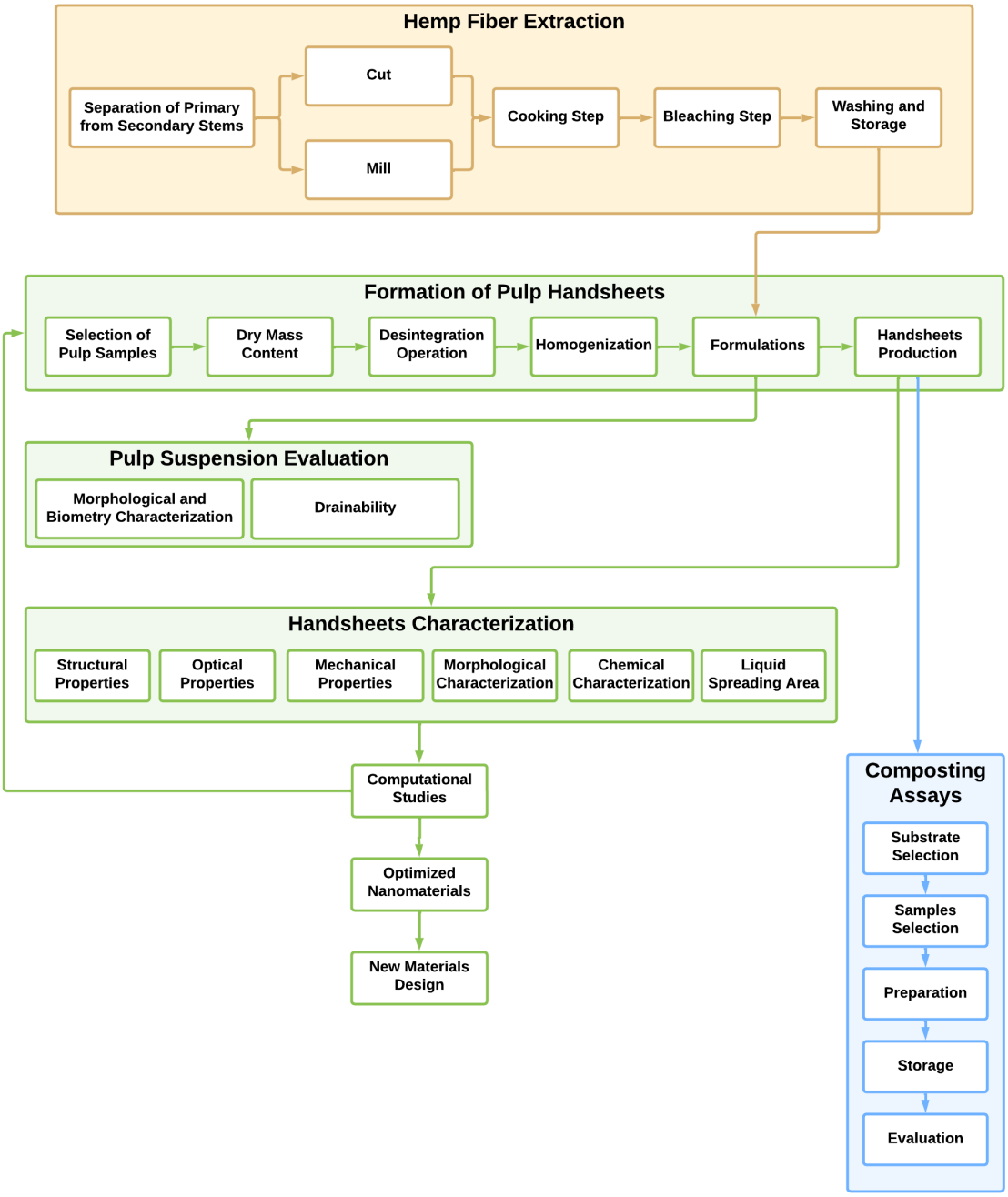

Figure 3.1 - Experimental and computational methodology developed throughout the study.

3.3.1. Forming Handsheets for Physical Tests of Pulp

3.3.1.1. Selection of Pulp Samples

In the development of this project, three types of cellulosic industrial materials were used as reference: bleached *Eucalyptus* globulus (designated as hardwood (HW)), unbleached *Picea* abies (referred to as softwood (SW)) and lastly an industrial tissue paper (IT). It should be emphasized that they are entirely free of total chlorine and have not received any drying operation.

3.3.1.2. Dry Mass Content

Before weighing our wet samples, we must determine their Dry Mass Content (DMC). In other words, heating is applied in a controlled laboratory environment to promote evaporation of the sample's water, resulting in a dry sample. This method allows us to weigh the matter content of a sample obtained much more precisely because the extra water weight is no longer considered.

As the **ISO 5263/1**, a laboratory-wet disintegration of chemical pulps method specified, a sample was placed on a Mettler LJ16 moisture analyzer infrared balance to measure the DMC of various materials. The sample was dried at 105 ºC under controlled conditions until the complete removal of the water present in the sample. Table 3.3 provides the percentage of DMC values since they differ according to the material.

Table 3.3 - DMC obtained for different materials used, as well as the time used for each one.

Materials	Time (min)	Temperature (ºC)	DMC (%)
Hardwood (HW)	20	105	92,71
Softwood (SW)			93,11
Tissue Industrial (IT)			100,0

3.3.1.3. Desintegration Operation

Since the fibers are presented as dry pulp sheets, they must be disintegrated after being chosen. The purpose of the disintegration process is to separate the fibers; for that, **ISO 5263/1**, was applied using a laboratory disintegrator.

Using 2 liters of deionized water containing 30 grams of dry pulp that have been soaked for at least 24 hours. Depending on the pulp consistency, the suspension disintegrates at 30000 or 10000 revolutions, as mentioned in the previous ISO.

3.3.1.4. Pulp Samples Homogenization

Following the disintegration operation, 4 liters of deionized water were added to the fibrous suspension obtained after disintegration. The fibrous suspension was then agitated with a paddle stirrer at 3000 rpm to prepare laboratory sheets for physical tests, as mentioned at the **ISO 5269/1.**

3.3.1.5. Production of Cellulose Fiber Structures

Considering the physical tests of fibrous cellulose sheets, structures were produced following **ISO 5269/1**, using a conventional sheet former method. It results in 60 g/m^2 discs subjected to a pressing process to remove as much water as possible. The structures were then moved to a conditioned room, where the temperature (22 ºC) and humidity (50%) remain constant over time to dry under tension following **ISO 5269/1**.

3.3.1.6. Pulp Samples Modification Process

For the laboratory refining of pulp, under **ISO 5264/2**, was use a PFI-mill. The HW and SW pulps were PFI-refined at different revolutions to evaluate the mechanical treatment (MT) behavior and morphology of the fibers as an additive in mesh structures.

The material was refined in a PFI-mill refiner at an intensity of 3.33 N/mm at distinct number of revolution (rev). Finally, both previously resuspended cellulosic pulps were disintegrated at 10000 revolutions following **ISO 5269/1**. Along with the previously described PFI-refining process, a pre-chemical process was made to increase the degree of fibrillation of the E*ucalyptus* globulus fibers. The sample was prepared by soaking the fibers for 24 hours in a NaOH solution at pH=12. After that was refined at 12000 revolutions. Considering the study of micro/nanofibrillated cellulose as an additive, an optimized combination of 90% HW_MT_1 and 10% HW_MT_12 sample was considered, which was referred to as additive. The number of essays, their designations, and the number of revolutions performed on a single type of fiber pulp (HW or SW) in the laboratory can be seen in Table 3.4.

Table 3.4 – List of fibrous structures PFI-refined in the laboratory.

Assay Number	Assay Designation	Assay Description
1	HW_MT_1	100% Hardwood Fiber PFI-refined at 1000 rev
2	HW_MT_3	100% Hardwood PFI-refined at 3000 rev
3	HW_MT_6	100% Hardwood PFI-refined at 6000 rev
4	HW_MT_12	100% Hardwood PFI-refined at 12000 rev at pH=12
5	Additive	90% Hardwood PFI-refined at 1000 rev + 10% Hardwood Fiber PFI-refined at 12000 rev at pH=12
6	SW_MT_1	100% Softwood Fiber PFI-refined at 1000 rev
7	SW_MT_3	100% Softwood Fiber PFI-refined at 3000 rev
8	SW_MT_6	100% Softwood Fiber PFI-refined at 6000 rev

This method aims to conduct a prior, comparative, and isolated study of the mesh structures regarding a specific PFI-refinement and how it influences our fibers. Once the research has been completed, we will be better positioned to decide on the ideal fiber formulations.

3.3.1.7. Pulp Samples Formulations

Considering these previous and isolated studies of the fibers, it was proposed to produce suspension formulations of refined or unrefined fibers to investigate the influence of fiber mixture in a fibrous porous structure. Structures were produced with these pulp formulations, with the method mentioned in subchapter 3.3.1.5. The formulations can be seen in Table 3.5.

Table 3.5 – List of fibrous formulation of the structures produced in the laboratory.

Formulation Number	Designation	Assay Description
1	50_HW_50_SW	50% Hardwood Fiber + 50% Softwood Fiber
2	80_HW_20_SW	80% Hardwood Fiber + 20% Softwood Fiber
3	90_HW _10_SW	90% Hardwood Fiber + 10% Softwood Fiber

3.3.2. Pulp Suspension Evaluation

3.3.2.1. Morfi Analyzer

Considering the morphology and biometry of fibers can affect their structure and mechanical behavior, Morfi®, a fiber analysis system based on image analysis developed by Techpap in Grenoble, France, was used. It allows valuable information to be extrapolated to analyze the previously mentioned parameters, such as weighted length in length (μm), width (μm), thickness (mg/100m), and fiber distribution (percentage of length (μm) to width (μm)).

Depending on the type of fiber, a minor pulp sample suspension (— for example, 0,2 g of oven dry pulp for HW pulp or 0,3 g of oven dry pulp for SW pulp) is placed inside the equipment, and the image analysis software is used to analyze the fibers. A computer screen attached to the equipment allows us to observe and evaluate the results.

The results presented in this work were taken with the July 2022 version of the software and calibrated Morfi®.

3.3.2.2. Optical Microscope

A LAS X program, coupled with the Nikon Labophot-2 optical microscope with a Leica MC190HD camera, is another straightforward and practical method for the morphological characterization of the fibers under investigation.

After the correct preparation of the fiber suspensions, as mentioned in subsection 3.3.1.4., a small sample of fibers in suspension is collected, placed between a slide and a coverslip, providing attachment, and then taken to the microscope. A picture of the fibers is taken using the equipment's software using a specific magnification chosen by the user. Consequently, it is possible to calculate the length and width of the fibers directly.

3.3.2.3. Evaluation of Pulp Drainability using ^{0}SR method

One of the problems in industrial paper production, especially when working with nanoscale fibers, is the long time required to drain the water from the suspension. The characterization of pulps measuring the freeness or drainage capacity was conducted using the **ISO 5267/1** for the determination of drainability using Schopper-Riegler method, using 2g of each fibrous suspension with deionized water at 20^{0}C.

3.3.3. Hemp Fiber Extraction

3.3.3.1. Sample Preparation

The research team applied two different methodologies (Figure 3.2b) to treat our primary sample, i.e., the plant stems consisting of: primary and secondary stems. Previously it was separated manually, the primary stems from the secondary ones (Figure 3.2a). Then, the two types of stems were (1) cut 2–3 cm in length using scissors (Figure 3.2c), as described in (Moonart & Utara, 2019), and (2) milled the stems with a mill until they reached dimensions between 0.5-2 cm (Figure 3.2d). These two distinct cutting approaches aim to understand their advantages and disadvantages regarding fiber morphology, costs, and production times.

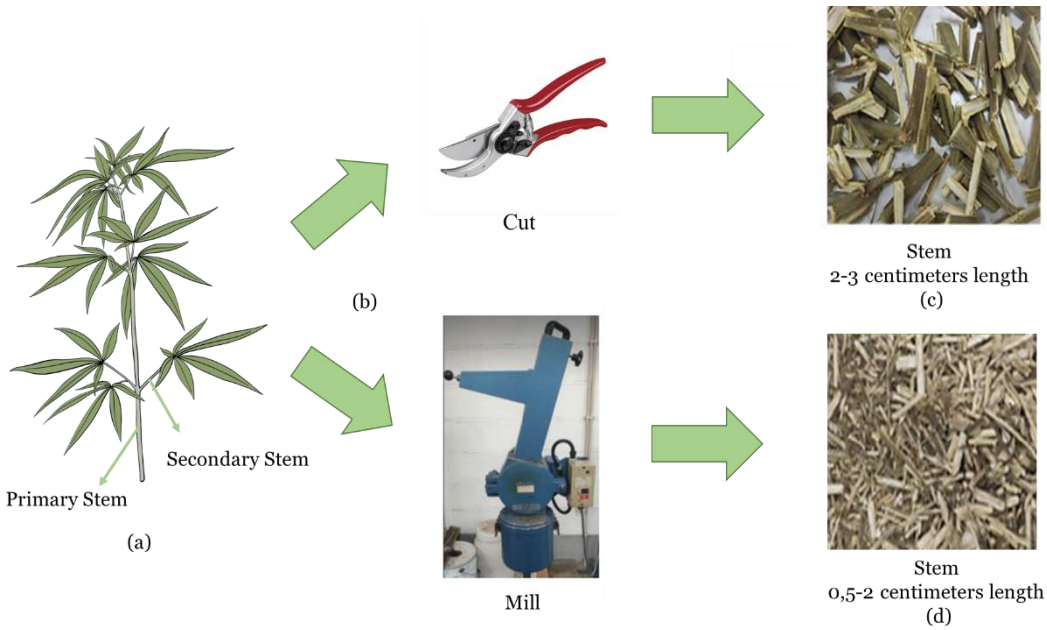

Figure 3.2 – Methodology applied in the laboratory for hemp fiber extraction (a) after separating the main stems from the secondary ones, (b) two types of cutting were applied, one with scissors and the other using a mill, resulting in (c) stems with 2-3 cm length and (d) stems with 0.5-2 cm length.

3.3.3.2. Cooking Step

The first step to obtain the hemp fibers was cooking them. This process was divided into two steps, according to the methodology developed by (Barbash et al., 2022): (1) impregnation or cooking ramp, lasting 90 minutes, characterized by increasing the temperature until reaching the reaction temperature (140°C), then step (2) cooking begins, which remains constant for 180 minutes, totaling a residence time of 270 minutes.

Temperature stability over time makes it possible to increase the degree of fibrillation of the stems, thus reducing the non-fibrillated fraction in cooking, commonly known as uncooked. In addition to the temperature factor, the research team studied the influence of different NaOH concentrations on hemp fibers, respectively, with 0,5 M, 1M, and 2M NaOH concentrations (Table 3.6).

Table 3.6 - Reaction conditions and composition of the cooking liquor.

Parameters	Cooking		
Proportions	1:10*		
Alkaline Load (%)	20	40	80
Concentration (M)	0,5	1	2
Mass of NaOH(g)	1,871	3,742	7,485

* Solid:Liquid ratio (stems:NaOH solution)

3.3.3.3. Bleaching Step

The bleaching process promotes the removal of residual lignin that was not eliminated during cooking. The hemp fibers were bleached using a 12% hydrogen peroxide solution for 2 hours at 50°C. After the bleaching reaction, the fibers were washed and stored in a refrigerated place until their characterization.

3.3.4. Characterization of Hemp Fibers

The morphologic and biometric characterization of the hemp fiber was carried out identically to the HW fibers and SW fibers (subchapter 3.3.2.). In this sense, the HF fibrous suspension was analyzed under an optical microscope and with Morfi® analyzer.

3.3.4.1. Production of Cellulose Fiber Structures with Hemp Fiber Incorporation

Aiming to study the reinforcing behavior of hemp fibers in 3D cellulosic matrix, the research team incorporated 1% and 10% milled hemp fibers into their known fibrous structure's final composition (basis weight 60 g/m²). Furthermore, it was considered reasonable to study the same behavior in the fibers after undergoing a PFI-refining step. In this sense, 10% of milled hemp fiber PFI-refined at 1000 revolutions was also incorporated.

Table 3.7 - Composition and designation of structures produced containing hemp fibers.

Assay Number	Designation	Assay Description
1	99_IP_1_HF	99% Industrial tissue paper + 1% milled hemp fiber
2	90_IP_10_HF	90% Industrial tissue paper + 10% milled hemp fiber
3	90_IP_10_HF_1	90% Industrial tissue paper + 10% of milled hemp fiber with an extra PFI-refining at 1000 rev

3.3.5. Fibers Structures Characterization

3.3.5.1. Structural Properties

For the structural characterization of the handsheets produced in the laboratory, the thickness and bulk were determined using **ISO 12625/3**. Also, the grammage of the structures was determined according to **ISO 12625/6**. The Microsoft Office Excel 2016 software was used to extrapolate and organize these numerical values. The grammage was determined by dividing each structure's weight by its surface area (0.02138 m^2).

The thickness was measured with a paper micrometer. By dividing the thickness by their weight, the volume of the structures was determined. Additionally, the apparent theoretical porosity was calculated using the following formula:

$$\text{porosity}(\%) = 100 \times \left(1 - \frac{\rho\text{structures}}{\rho\text{cellulose}}\right) \quad \textbf{(Equation 3.2)}$$

It is important to note that $\rho_{cellulose}$ refers to the known value of cellulose density (1,5 g/cm^3), where $\rho_{structures}$ is the apparent density of the structures (g/cm^3).

3.3.5.2. Optical Properties

When light reaches the surface of a sheet of paper, some of it is reflected, and the remainder is absorbed and released as energy (heat). Within this fibrous structure, light spreads in many different directions. Figure 3.3 illustrates the behavior of a beam of light once it hits the paper's surface. Color, opacity, whiteness, brightness, and fluorescence are examples of optical properties (Sousa, 2012).

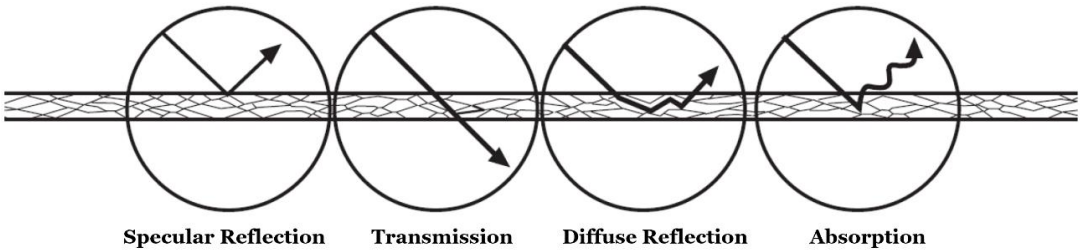

Figure 3.3 - Interactions of a beam of light when it hits a paper surface (adapted from (Sousa, 2012)).

3.3.5.2.1. Whiteness

The whiteness and color of paper was quantified according to **ISO 2470/1,** method for measuring the diffuse blue reflectance factor (ISO brightness) of papers, performed using the equipment Color Touch 2 from the Technidyne brand.

3.3.5.2.2. Opacity

The opacity of paper was quantified according to **ISO 2471,** method for the determination of the opacity of paper by diffuse reflectance, performed using the equipment Color Touch 2 from the Technidyne brand.

3.3.5.3. Mechanical Properties

Fibrous structures tensile index (Nm/g) was determined, following the **ISO 1924**, using the tensile test, translating the maximum tensile strength to the permanent deformation of a given material. Young's modulus or modulus of elasticity expressed in MegaPascals (MPa) was also determined for all types of sheets, a mechanical property that measures the rigidity of a material.

3.3.5.4. Morphological Characterization using Scanning Electron Microscopy (SEM)

Complementary to the optical microscope, the Scanning Electron Microscopy (SEM) method was used, Hitachi S-2700, in the Faculty of Sciences of Health of the University of Beira Interior (FCS – UBI) optical laboratory.

Using only a tiny sample, SEM makes it possible to view images with high definition and depth, not only in the xy plane (i.e., surface) but also in the z plane (i.e., thickness). However, the samples to be visualized must be electrically conductive and connected to a support to prevent the accumulation of electrostatic charges on the surface. Previously, the samples were prepared for the SEM, where they were cut in a rectangular format. With the help of a double-sided glue, the samples were affixed to the sample holder, and the samples in the xy plane were attached at an angle of zero degrees and the samples in the z plane, at an angle of 90 degrees, to the surface. The samples were then covered in gold using the Sputter Coater to become electrically conductive. After coating, the samples were analyzed with a Bruker detector operating at 20kV and different magnifications. The image analysis methodology includes, in the first stage, exploring the sample as a whole and, in the second stage, enlarging and selecting the fractions of interest.

3.3.5.5. Chemical Characterization using Infrared Spectroscopy by FTIR-ATR

Fourier Transform Infrared Spectroscopy (FTIR) is a non-destructive and direct method that allows characterizing and identifying substances in the solid, liquid, or gaseous state. The equipment used was a FTIR-ATR Thermo-Nicolet IS10. The Attenuated Total Reflection (ATR) technique coupled with FTIR enables the analysis of solid and liquid samples (Figure 3.4a). This technique measures changes when an infrared ray (IR) falls on the sample's surface (Figure 3.4b). The selected structures were inserted into the equipment without the need for pre-treatment. The spectra were obtained according to the conditions shown in Table 3.8.

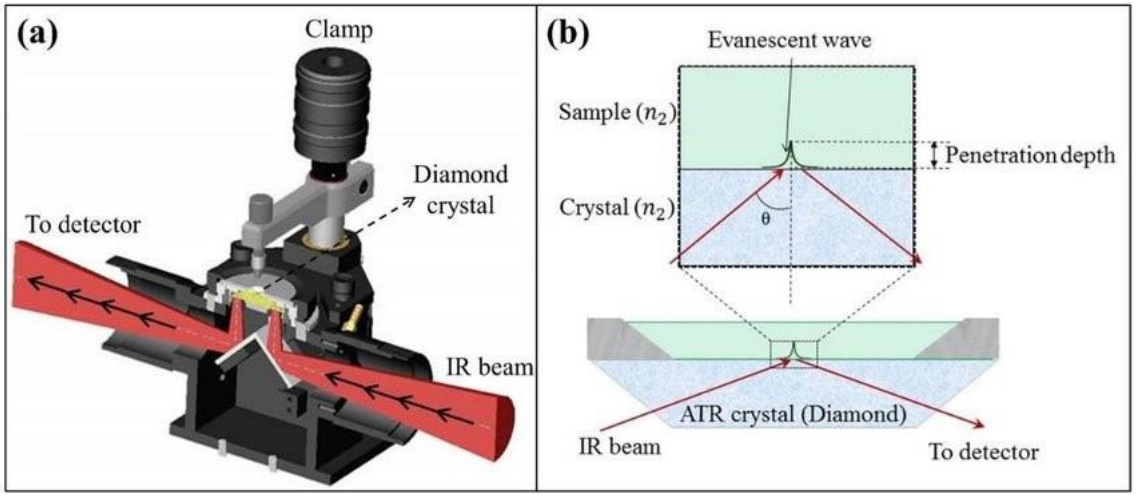

Figure 3.4 - Illustration of an (a) ATR accessory for FTIR spectrometer and (b) schematization of the evanescent wave at the interface of an ATR crystal (into (a)) (adapted from (Jafari, 2017)).

Table 3.8 -Operating conditions for the FTIR-ATR method.

Operation conditions FTIR-ATR	
Collect No. Scans	32
Resolution	4 cm^{-1}
Wavelength	600 – 4000 cm^{-1}

3.3.5.6. Evaluation of Liquid Spreading Area

The liquid spreading area was studied using an optical system specifically developed to study the interaction of different liquids on the surface of various paper structures (Mendes et al., 2013; Fiadeiro et al., 2013; Sousa et al., 2014; Curto et al., 2015; Morais et al., 2023). The optical system works by ejecting microliter droplets toward the sample surface, whereas images of the droplets are being captured for a given time. We were able to quantify the time of deposition and spreading area along time. During the event, three image detectors (Figure 3.5), ID1, ID2, and ID3, provide image registration of the liquid droplet's interaction with the study's paper sample. The images are then stored in a computer for their corresponding processing to determine specific parameters for evaluating the liquid-paper interaction.

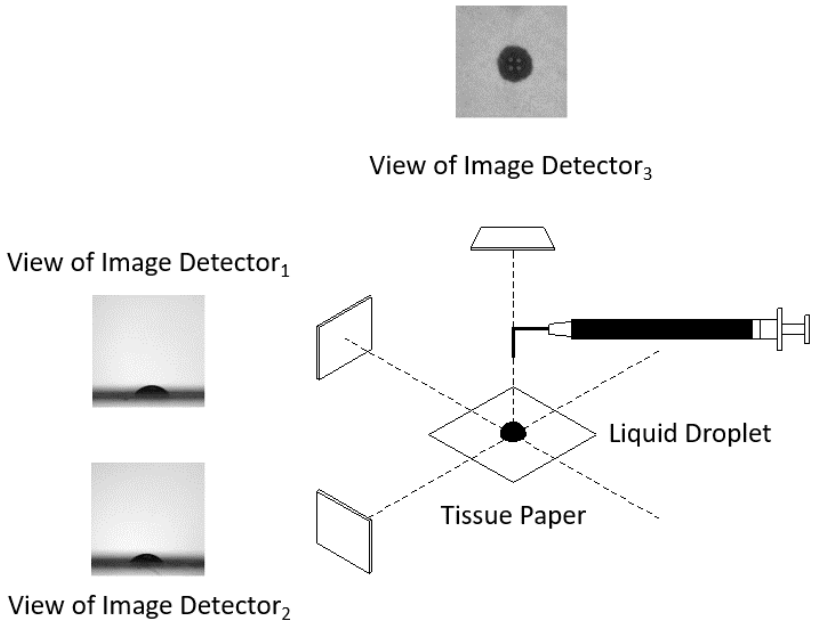

Figure 3.5 – Scheme of the optical system used for analysis over time of the interaction of liquid droplets on web fiber structures (adapted from (Mendes et al., 2013)).

3.3.6. Laboratory Scale Composting Assays

There are different methodologies to assess the degree and rate of biodegradation. Materials can be degraded by enzymes or microbes in laboratory culture or biodegraded in soil, activated sludge, or compost. Composting, an aerobic biodegradation type, is one of the most widely used methods.

The composting test was selected to evaluate the biodegradability of samples produced in the laboratory. Based on the **ISO 17556**, the method for determination of the ultimate aerobic biodegradability of natural polymers materials under controlled composting conditions in soil with adaptations, the methodology (Figure 3.6) was suggested for this study.

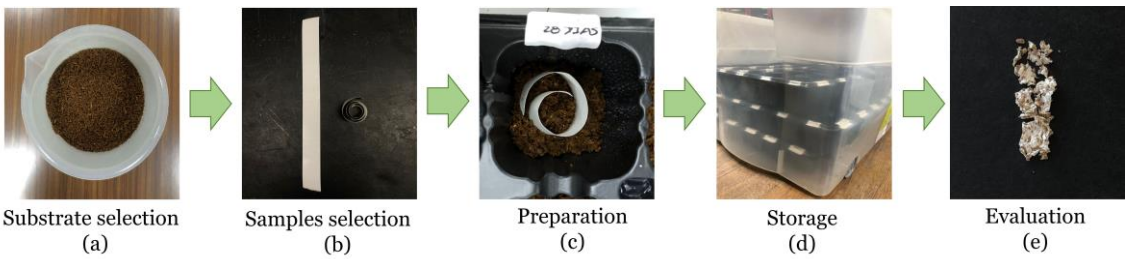

Figure 3.6 – Methodology used to evaluate the biodegradability of structures produced in the laboratory.

The compost soil (Figure 3.6a) was collected from the University of Beira Interior (UBI) gardens (latitude: 40.277927, longitude: -7.554752). The moisture content was measured 52,90%, a value similar to (Saha et al., 2019). Regarding the selection and weighing of the samples (Figure 3.6b), the filter paper was chosen as a positive control.

The remaining samples were obtained from handsheets, whose composition was made of: (1) silicone coated paper, (2) one type of fiber without mechanical treatment (HW or SW), (3) PFI-refined fibers of HW or SW at 3000 rev, (4) fiber mixture of 50% HW and 50% SW and (5) a fiber mixture containing micro/nanofibrillated cellulose additive. Table 3.9 shows the chosen samples and their description. When this test was carried out, samples containing hemp fibers were unavailable, so they were not considered.

As for the assay preparation (Figure 3.6c), in a seed tray (40 cells), 16 × 1.5 cm strips of the lab-made handsheets were placed in the middle of the compost medium to ensure maximum surface contact between the compost and the sample (Saha et al., 2019).

Each cell had the same amount of compost soil, and three samples were buried for each type of sample. Knowing that pure cellulose readily degrades into a good compost in approximately 47 days, which may take longer in the case of materials containing lignocellulose (Erdal & Hakkarainen, 2022), it was decided to collect samples 28 days and 60 days after the beginning of the experiment.

Since the humidity of the composting soil is essential to keep its ecosystem alive, every seven days, the seed trays were humidified with a spray bottle containing distilled water. After this, the sets were stored inside a plastic container with holes to allow air circulation (Figure 3.6d). After 28 and 60 days of biodegradation, the samples were collected, dried naturally (24h), carefully cleaned with a brush, then weighed on a scale.

Table 3.9 – Selected samples with their designation and detailed description. For each sample type, three samples were buried and removed after 28 days and 60 days, respectively.

Assay	Designation	Assay Description	Collect Day	
A	ISO_Control	Filter paper	28 After	60 After
B	Conted_Paper	Silicone coated paper		
C	50_HW_50_SW	50% Hardwood Fiber + 50% Softwood Fiber		
D	HW_MT_3	100% Hardwood Fiber PFI-refined at 3000 rev		
E	SW_MT_3	100% Softwood Fiber PFI-refined at 3000 rev		
F	MFC/NFC Additive	90% Hardwood Fiber PFI-refined at 1000 rev + 10% Hardwood Fiber PFI-refined at 12000 rev at pH=12		
G	HW	100% Industrial Hardwood		
H	SW	100% Industrial Softwood		

Two types of evaluation were performed: (1) visual evaluation and (2) weight loss evaluation. The first evaluation was subjective (Figure 3.6e), intending to observe the samples' decomposition state and understand whether the selected compost soil was still viable. In the second evaluation, equation 3.2 (Wan et al., 2009) was used to evaluate the percentage of lost mass. W_i is the initial mass, and W_f is the remaining mass on the final day after the sample dry, 28 or 60 days later, respectively.

$$\text{Weight loss } (\%) = 100 \times \left(\frac{Wi - Wf}{Wi}\right) \qquad \textbf{(Equation 3. 3)}$$

3.3.7. Computational Studies

Computer simulations were one of the main steps studied in this work, an important link between engineering and biotechnology. In this sense, a simulator was used, the voxelfiber, developed and validated by (Conceição et al., 2010; Curto et al., 2011), capable of computationally simulating the 3D cellulosic network produced by the random and individual deposition of the fibers, using the MATLAB® language.

In the present work, different fibrous structures were modeled in a 3D fiber-based computational simulator, in which the code is available on GitHub (https://github.com/eduardotrincaoconceicao/voxelfiber). The simulated fibers were precisely those studied in the laboratory: hardwood fiber (HW), softwood fiber (SW), hemp fiber (HF), and micro/nanofibrillated cellulose additive (MFC/NFC). Individual and joint experimental sets were carried out to compare results, similar to the previously performed experimental methodology. Although the simulator can work with several inputs, it was decided to only work with two inputs in the first step: (1) fiber length and (2) fiber flexibility. The values obtained in the morphological characterization of our cellulosic structures in the laboratory were used in this step as inputs for the length of the fibers. As for the flexibility of the fiber, in the simulator, it varies between 1 (most rigid) and 4 (most flexible). It was determined that HW and SW would have a value of 3 for flexibility, HF would have 2 for flexibility, and the additive of MFC/NFC value 4 for flexibility.

Since the world and science are constantly changing and confronted with technological innovations, as is the current case of artificial intelligence. This tool becomes valuable in studying, quantifying, and optimizing the number of fibers to prepare our materials, reducing material and financial resources.

3.8. Statistical analysis

The data from the present study were processed using the Microsoft Office Excel 2016 software and MATLAB®.

Chapter IV
Results and Discussion

4. Results and Discussion

This chapter contains the results of the morphological, structural, mechanical, optical, and chemical characterization of the structures and their interpretation. Also, it was evaluated the liquid droplet spreading area over time. Initially, the structures of the reference fibers (HW and SW) were characterized with and without mechanical treatment. Then, the hemp fibers were evaluated according to different cooking approaches and later with and without mechanical treatment. The characterizations were completed by analyzing structures with a mixture of hemp fibers with industrial tissue paper fibers.

Also, it is shown a primary study on the biodegradation of structures previously produced through composting, considering the R&D lines of the research group. Being a pioneering attempt at biodegradation, the results of this research were highly encouraging and allowed for further development.

The 3D computational simulations of the laboratory structures are presented in the same order as mentioned above. Length and flexibility, in this case, were used as inputs to the simulator. The simulated structures were compared and validated with images of actual fibrous structures taken from the SEM images.

4.1. Evaluation of Reference Fibers using Characterization Methods

4.1.1. Fiber Suspension Characterization

4.1.1.1. Fiber Morphology

The optical microscope was used as a first step in evaluating the reference fibers to explore the fibers' morphology, dimensions, and fibrillations, among other features. Because of its visual presentation allows the researcher to understand how different treatments affect the fibers. Taking this into account, the bleached *Eucalyptus* globulus fibers (hardwood fibers) and the *Picea* abies fibers (softwood fibers) are represented in Figure 4.1 and Figure 4.2, respectively.

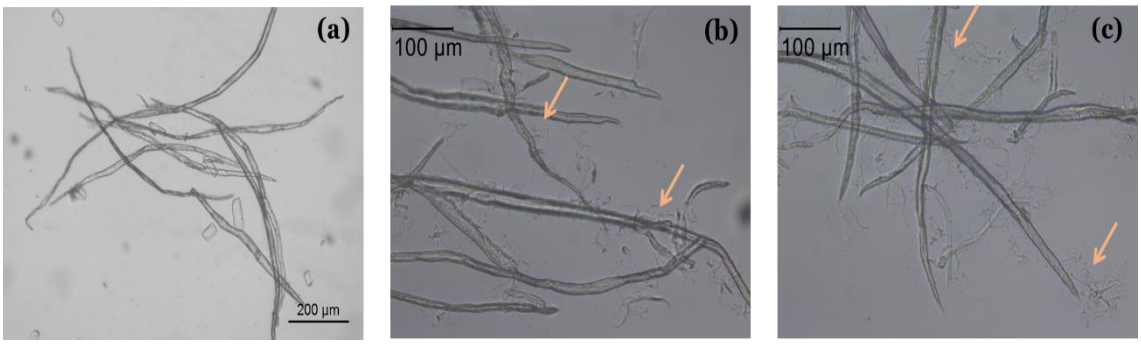

Figure 4.1 - Microscopic images of hardwood fibers, namely, (a) unrefined, with a magnification of 40x, (b) PFI-refined at 3000 revolutions, and (c) PFI-refined at 6000 revolutions, both with a magnification of 100x. The orange arrows show the fine elements on the surface of the fibers.

The above technique could help identify the vegetable fiber specie that is working on. Small pits can be seen along the softwood fibers (Figure 4.2a), which are almost nonexistent in the hardwood fibers (Figure 4.1a). These scores ensure the exchange of water, nutrients, and other substances between vessels in species known as resinous, the case of *Picea* abies fibers (softwood fibers).

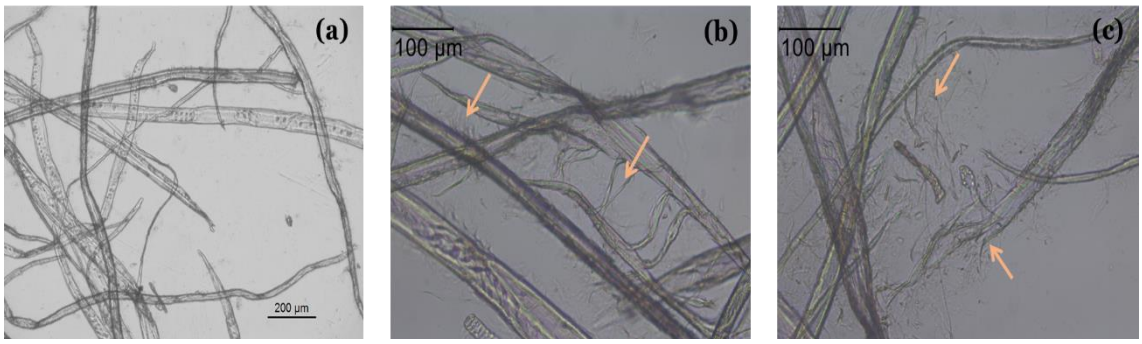

Figure 4.2 - Microscopic images of softwood fibers, namely, (a) unrefined, with a magnification of 40x, (b) PFI-refined at 3000 revolutions, and (c) PFI-refined at 6000 revolutions, both with a magnification of 100x. The orange arrows show the fine elements on the surface of the fibers.

Comparing both type of fibers, it is possible to say that the softwood fibers are longer than hardwood fibers. We were able to cover the entire length of the hardwood fibers at the same magnification (100x), but this was not the case for the softwood fibers. A longer fiber length allows for contact points between fibers, also known as interfiber bonds, that are important for the fibrous matrix's stability. The difference may be explained by the industrial pre-treatments given to the fibers, particularly the bleaching process that the hardwoods underwent. Promoting a higher level of polymerization and, as a result, a decrease in length in general.

The widths of softwood fibers are also bigger than those of hardwood fibers. Due to some fine elements on the fibers' surface, mechanical treatment's effects are more evident on hardwood fibers at 3000 and 6000 revolutions (Figure 4.1bc). However, softwood fibers, particularly those to which 6000 revolutions have been applied, have a substantial number of fine elements. The presence of a broken and fibrillated fiber end in Figure 4.2c (orange arrow) highlights the effects of this mechanical treatment on fibers. Therefore, the quantity of fine elements in the final sample increases with the amount of mechanical treatment used (i.e., the number of PFI-mill revolutions).

4.1.1.2. Fiber Morphology using a Fiber Analyzer, the Morfi®

Considering the need for input data for the computational simulations, that is, data obtained from the morphological characterization of the fibers, the fiber analyzer (Morfi®) became a valuable tool in the present work.

The reference fibers (HW or SW) and mixture (HW:SW), following ratios: 90:10, 80:20, and 50:50 were characterized. More details about the parameters collected during this characterization, including fiber population, length weighted by length, width, coarseness, fibrillation, broken ends, and kinked fibers, can be accessed in Appendix B1 (Table B1.1). Figure 4.3 validate the previous optical microscope observation about the softwood fibers being longer than hardwood fibers.

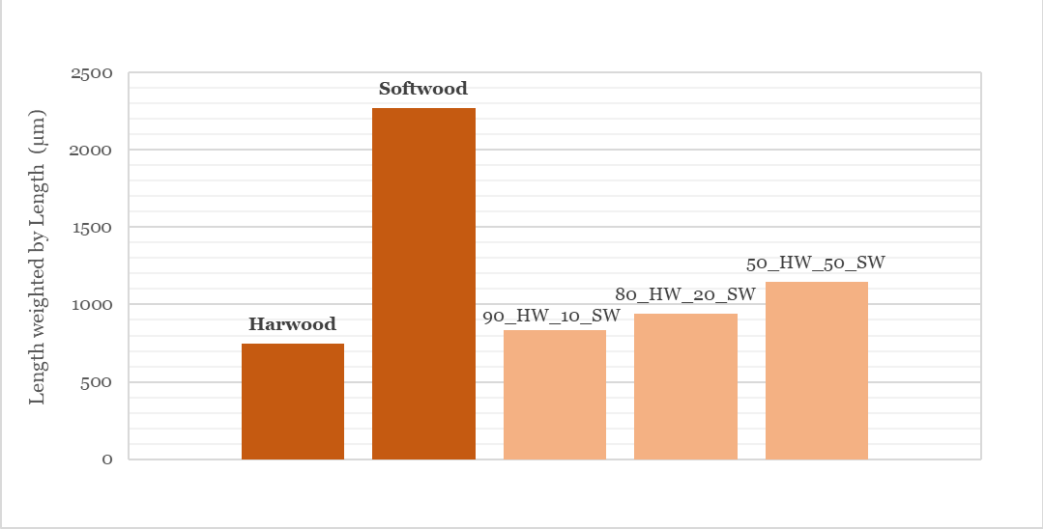

Figure 4.3 - Length weighted by length of reference fibers alone (hardwood or softwood) and mixture (90_HW_10_S, 80_HW_20_SW and 50HW_50SW).

Softwood fibers are up to three times longer than hardwood fibers. This difference directly influences the experimental sets with mixed fibers. As the softwood content increases in the sample (10% to 50%), the length of the fibers also increases (Figure 4.3, light orange bars).

In terms of fiber width, softwood fibers are approximately twice as wide as hardwood fibers, 27,2 µm and 15,4 µm, respectively (Figure 4.4, dark orange bars). The combination of the fibers also supports the direct relationship between the width of the fibers and the ratio of HW to SW fibers, i.e., the greater the proportion of SW fibers in the mixture, the wider the fibers detected in the sample.

These comparative studies have industrial relevance, as the value of hardwood fiber can be around 500 euros/ton, while softwood fiber is around 750 euros/ton. The ability to adjust these mixtures while preserving their desirable properties might benefit corporations economically.

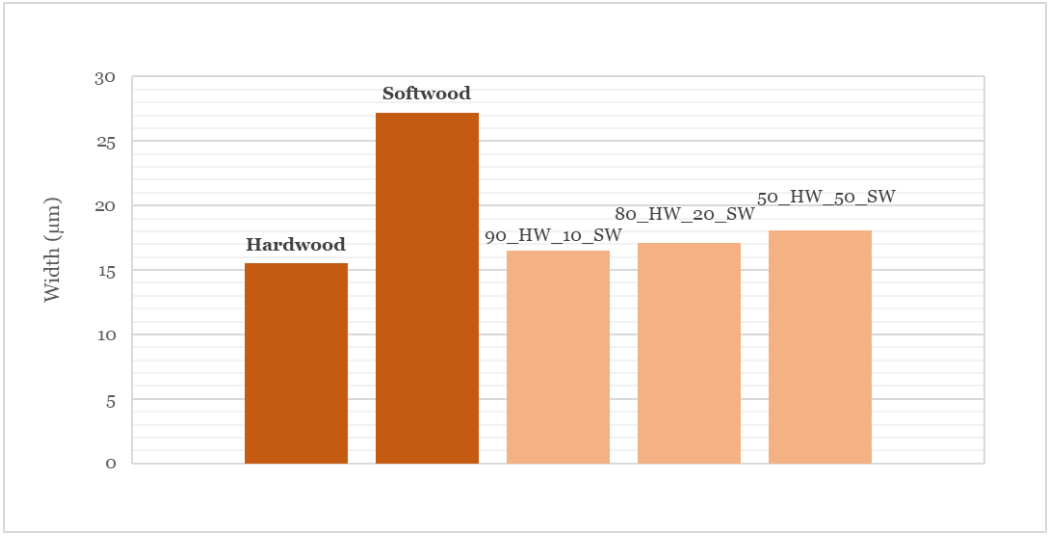

Figure 4.4 - Length weighted by length of reference fibers only (hardwood or softwood) and mixture (90_HW_10_S, 80_HW_20_SW and 50HW_50SW).

The next stage was the evaluation of the samples that underwent mechanical treatment, i.e., PFI-refinement. There were three different levels of refinement: 1000 revolutions, 3000 revolutions, and 6000 revolutions. Exceptionally, the research team proposed applying a chemical treatment to hardwood fibers at pH = 12, followed by 12000 revolutions in the PFI-refiner. Values that aim to test the fibers' resistance when subjected to a more severe treatment. Combining HW fibers PFI-refined at 1000 and 12000 revolutions (ratio 90:10) between them was also appealing to create a micro/nanofibrillated cellulose additive.

Figure 4.5 shows the length weighted by the length of HW and SW fibers before and after mechanical treatment (light orange bars) and the length of fibers without treatment (dark orange bars). It is possible to see that the mechanical treatment had a minor impact on the length of the HW fibers. Only the fibers PFI-refined at 12000 revolutions differ from the HW fibers without refining. The increase in pH may have contributed to more significant fiber fibrillation. The length of the fibers additive barely changed when PFI-refined HW fibers were combined. Values are similar to the length of HW fibers PFI-refined at 1000 revolutions.

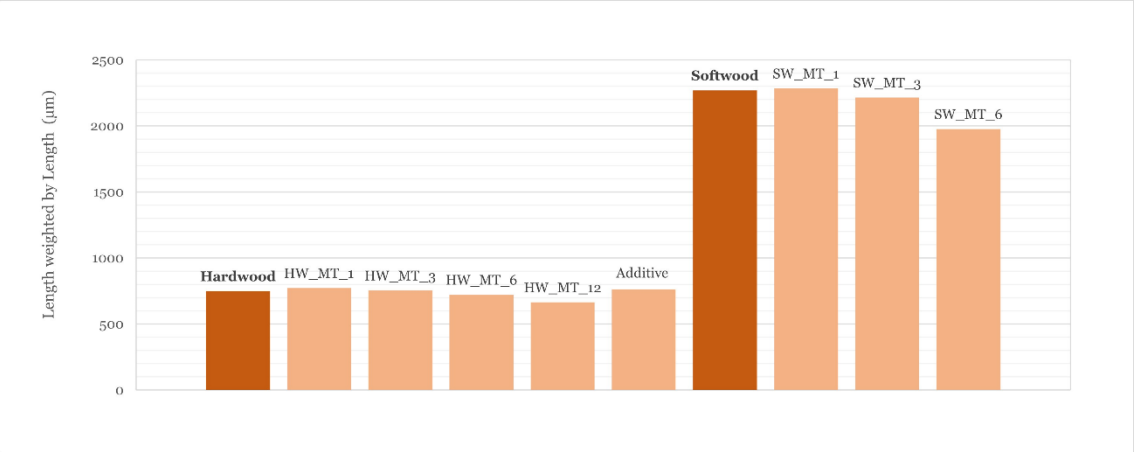

Figure 4.5 - Length weighted by length of unrefined reference fibers (hardwood or softwood) and with PFI-refinements of: (1) 1000 revolutions (HW_MT_1 and SW_MT_1), (2) 3000 revolutions (HW_MT_3 and SW_MT_3), (3) 6000 revolutions (HW_MT_6 and SW_MT_6), (4) 12000 revolutions (HW_MT_12 at pH=12) and lastly (5) additive of micro/nanofibrillated cellulose.

In contrast, the mechanical treatment was more successful for SW fibers. There was a 13% reduction in length between SW fibers that had undergone 6000 revolutions of refinement (SW_MT_6) and those that had not. PFI-refinement may have had a more impact on SW than HW because these fibers are longer than HW fibers. Even after the most extreme PFI-refining, the width of SW fibers remained bigger and constant than that of HW fibers (Appendix B1, Table B1.2).

The graphs illustrated in Figure 4.6 and Figure 4.7 intended to represent the distribution of fibers, considering their length and width. As mentioned, applying mechanical treatment to HW fibers did not cause significant morphological changes. The distribution of fibers in the graphs of Figure 4.6ab reflects this same stagnation with the increase of revolutions in PFI-refiner. The majority of the dimensions of HW fibers, both before and after 6000 revolutions on the PFI-refiner, remained within the range of 409 µm - 1196 µm in length and 12 µm - 26 µm in width, showing minimal variations in size.

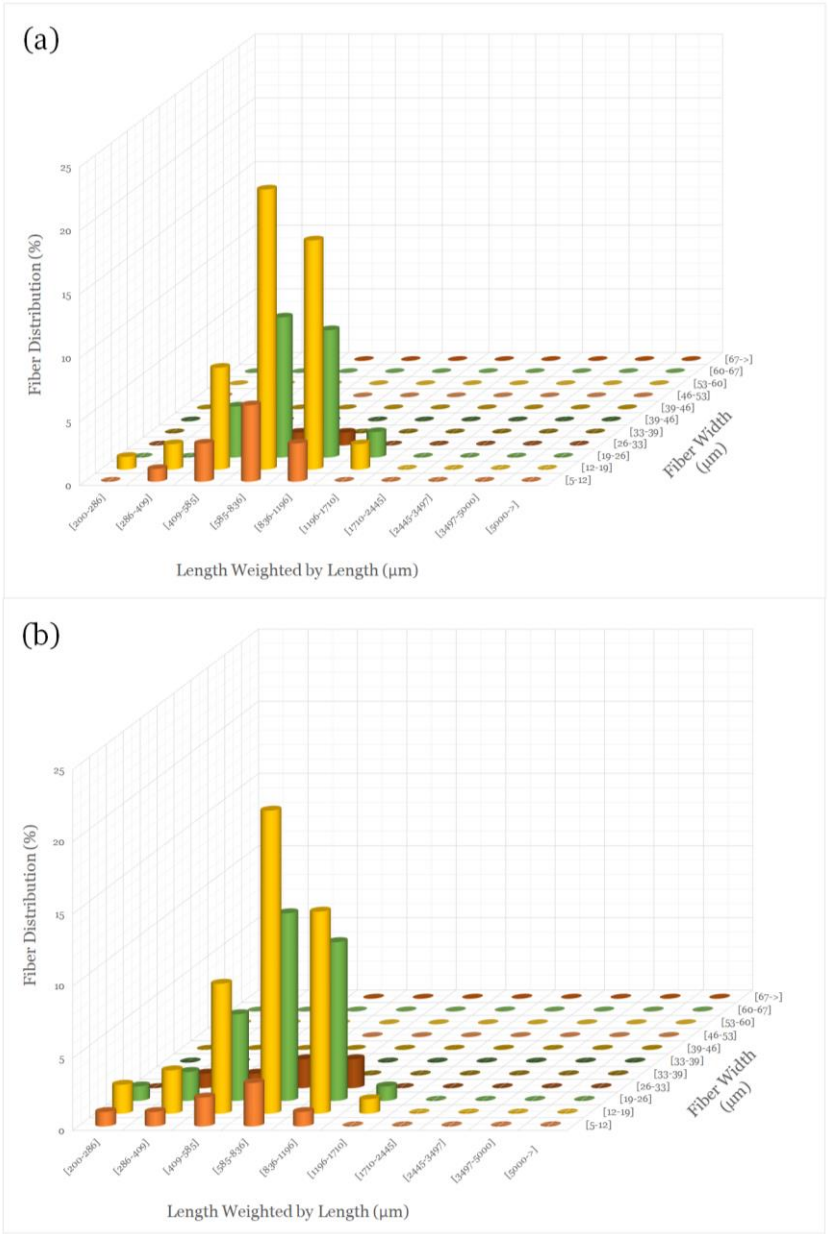

Figure 4.6 - Fiber length weighted by length and width distributions of (a) unrefined HW fibers and (b) HW fibers PFI-refined at 6000 revolutions.

Figure 4.7 shows that the distribution of softwood fibers during the mechanical treatment. The arrangement of the softwood fibers in relation to their length is altered by PFI-refiner, as shown by comparing the graphs of the softwood fibers, both before and after 6000 revolutions on the PFI-refiner (Figure 4.7a) and after (Figure 4.7b). This influence is especially noticeable in the length ranges of 585 µm - 1196 µm.

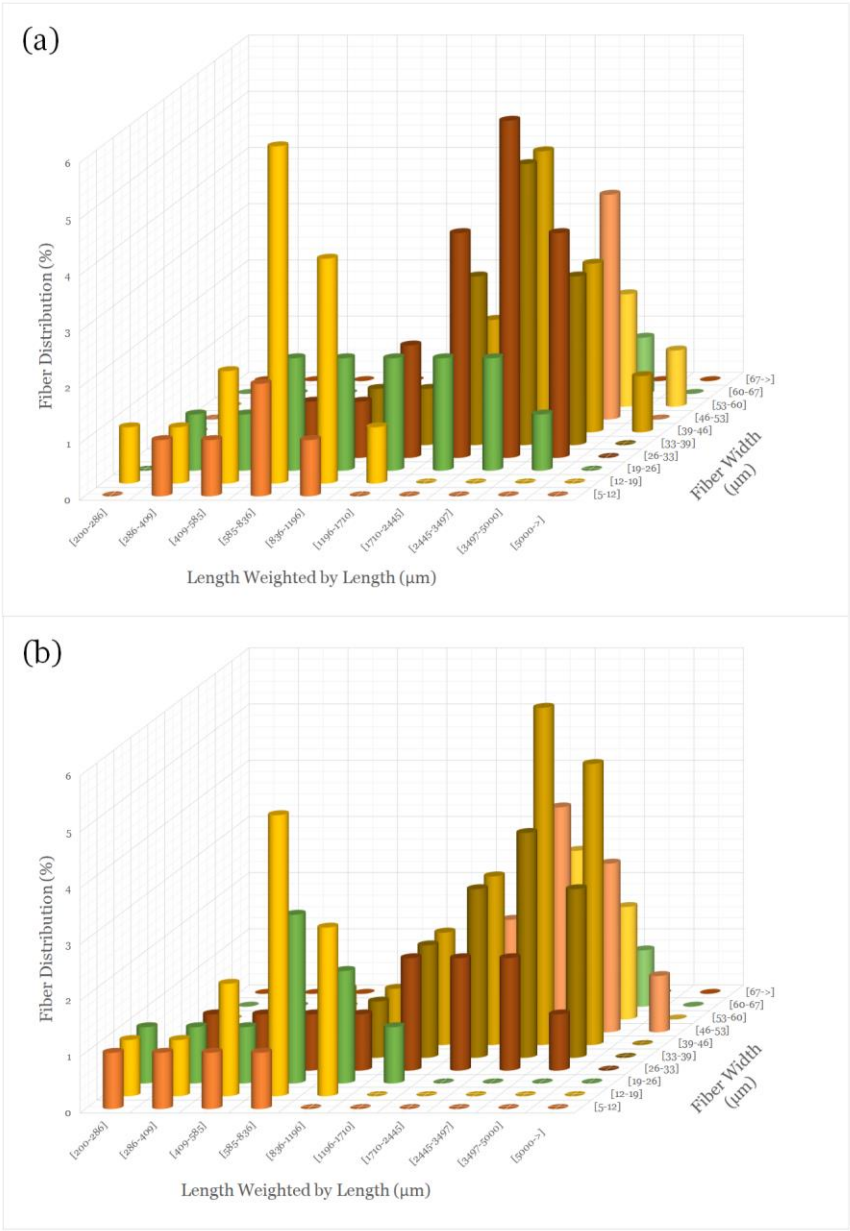

Figure 4.7 - Fiber length weighted by length and width distributions of (a) unrefined SW fibers and (b) SW fibers PFI-refined at 6000 revolutions.

The fiber fibrillation percentage increase can also explain these dimension variations. As shown in Figure 4.8, the percentage of fibrillation for hardwood fibers showed a slight increase as the PFI-refining revolutions were increased. The hardwood fibers PFI-refined at 12000 revolutions had the most significant increase, about 1,41%, compared to hardwood fibers. For softwood fibers, however, there is a noticeable rise in the percentage of fibrillation. Applying only half the revolutions to these fibers, it is possible to achieve higher fibrillation values compared to hardwood fibers.

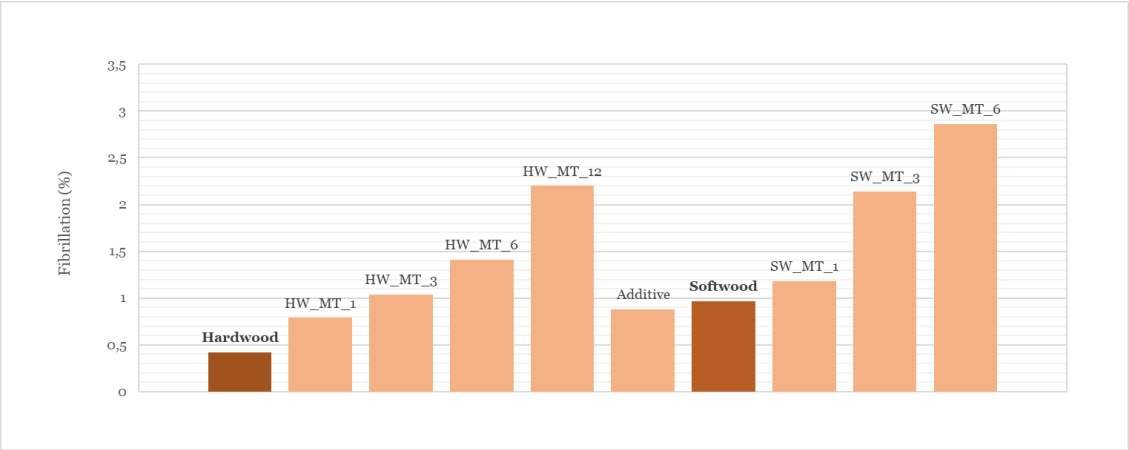

Figure 4.8 - Fibrillation percentage of unrefined reference fibers (hardwood and softwood) and with PFI-refinements of: (1) 1000 revolutions (HW_MT_1 and SW_MT_1), (2) 3000 revolutions (HW_MT_3 and SW_MT_3), (3) 6000 revolutions (HW_MT_6 and SW_MT_6), (4) 12000 revolutions (HW_MT_12 at pH=12) and (5) additive of micro/nanofibrillated cellulose.

The percentage of fibrillation of SW fibers at 6000 revolutions was approximately 2,86%, an increase of 1,68% compared to unrefined SW. Throughout this morphological evaluation, it is noticeable the influence that the combination of different types of fiber may have on the final product, whether they are or not under the influence of a mechanical treatment. Even though PFI-refining did not change the size of the HW fibers much, this could mean they don't need an extra fiber treatment. From an industrial standpoint, this translates to more efficient production requiring less processing and energy, reducing company costs.

While HW fibers PFI-refined at 12000 revolutions stands out from other HW fibers with different mechanical treatments. In this circumstance the processing time, cost of energy, and the increase in the temperature (friction inside the PFI-mill) could be disadvantages of such aggressive mechanical treatment. Nevertheless, these results indicate that the HW fibers PFI-refined at 12000 revolutions are highly fibrillated and should be considered as fibers to be used in mixtures, in small percentages, such the case of the micro/nano fibrillated cellulose additive. This approach would offer barrier properties to food packaging, keeping beverage contents and gases (humidity).

SW fibers generally displayed the best mechanical treatment outcomes even when low revolutions were used. The long fibers (SW) morphologies may increase the fibrous structure's stability, which is crucial when working with food packaging. Nevertheless, as previously stated, these fibers are more expensive, and adding this type of treatment can increase costs even further.

4.1.1.3. Evaluation of Pulp Drainability using the Schopper-Riegler Degree Method

The drainability of fiber pulps is very important to assess the fibers' quality and suitability for production on a larger scale. In the present work, the drainability of the PFI-refined fibers was measured using the Schopper-Riegler method (°SR), according to the ISO standard mentioned in section 3.3.3. The values can be analyzed in Table 4.1.

Table 4.1 - Schopper-Riegler degree of pulps subject to different PFI-refinements.

Fiber Type	Samples	°SR	Weight (g)
Hardwood	HW_MT_1	25	2,00
	HW_MT_3	40	2,04
	HW_MT_6	73	1,78
	HW_MT_12	100	2,08
Softwood	SW_MT_1	13	1,99
	SW_MT_3	22	2,10
	SW_MT_6	52	1,97

In the paper industry, the lower the °SR value, the greater is the efficiency of water drainage by the fibers, along with a more efficient paper production performance. As the refining level increased for both pulp types, the °SR increased progressively. However, there are limitations to this technique, as only values between 10 and 90 are considered reliable. As stated before, these results indicate that the HW fibers PFI-refined at 12000 revolutions are highly fibrillated and should be considered as fibers to be used in mixtures, in small percentages, with the function of being a micro/nanofibrillated cellulose additive. The of use of MFC/NFC as an additive in a mixture should be optimized, to accomplish the improvement of properties and avoid the economic and sustainable drawbacks.

4.1.2. Fiber Handsheets Characterization

4.1.2.1. Structural Properties

Appendix B2 (Table B2.1) has the complete data concerning the structural characterization of the laboratory handsheets with a basis weight of approximately 60 g/m² according to the ISO standard mentioned in section 3.3.1.5.

Fibrous structures were produced with HW fiber or SW fiber individually and together (HW:SW) in proportions 90:10, 80:20, and 50:50. Also no mechanical or chemical treatment was applied. The handsheets produced exclusively from SW fibers were thicker (0,211 mm ± 0.30) than those produced only from HW fibers (0,175 mm ± 0.15). As the proportions of HW and SW in handsheets with mixed fibers were equalized, the thickness increases proportionally. The bulk, which assesses the handsheet's volume in relation to its weight, is correlated to this parameter. For example, HW handsheets, are thinner and more compact, having lower bulk compared to SW handsheets. Also, HW handsheets showed higher density compared to SW handsheets. The porosity showed lower values for the HW handsheets, but a slight increase of 2% for the SW handsheets. As the SW fibers ratio increased in the HW:SW mixtures, the bulk and porosity increased until HW:SW ratio became equal.

Appendix B2 (Table B2.2) contains information about handsheets made from mechanical treatment fibers. This study did not consider HW handsheets PFI-refined at 12000 revolutions since it was not possible to produce the handsheets in the laboratory former. The graph (Figure 4.9) compares handsheet thicknesses before refining (dark orange bars) with handsheet thicknesses after PFI-refining under different levels of revolutions (light orange bars). For handsheets produced with PFI-refined HW fibers, their thickness decreases considerably. In the case of HW_MT_6, they achieved a reduction of about 62% in thickness, compared to the HW handsheet without PFI-refining. With an identical reduction in their thickness, the handsheets produced with PFI-refined SW had their thickness reduced by 60% compared to the original SW hansheets.

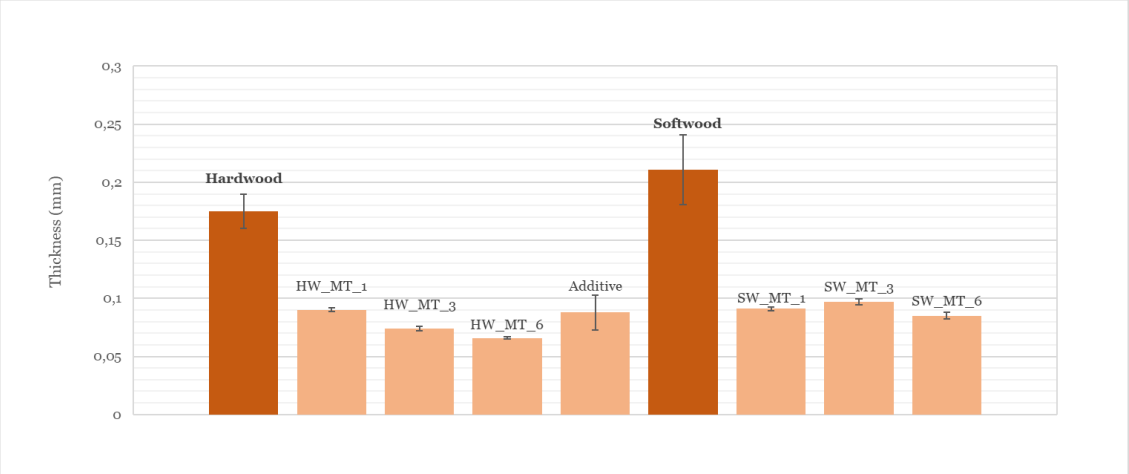

Figure 4.9 - Graph referring to the average thickness (mm) of HW and SW handsheets without PFI-refining (dark orange bars) and HW and SW handsheets PFI-refined at 1000 revolutions, 3000 revolutions and 6000 revolutions and the micro/nanofibrillated cellulose additive (light orange bars).

In general, mechanical treatment reduced the dimensions of both fibers, this factor may favor higher compactness when the fibers are superimposed. Making the thickness of the handsheet reduce and consequently the bulk as well. This behavior is supported by the progressive decrease in bulk as refinements increase for both fiber types (Figure 4.10a, light orange bars). Except for the additive, which has values similar to HW_MT_1.

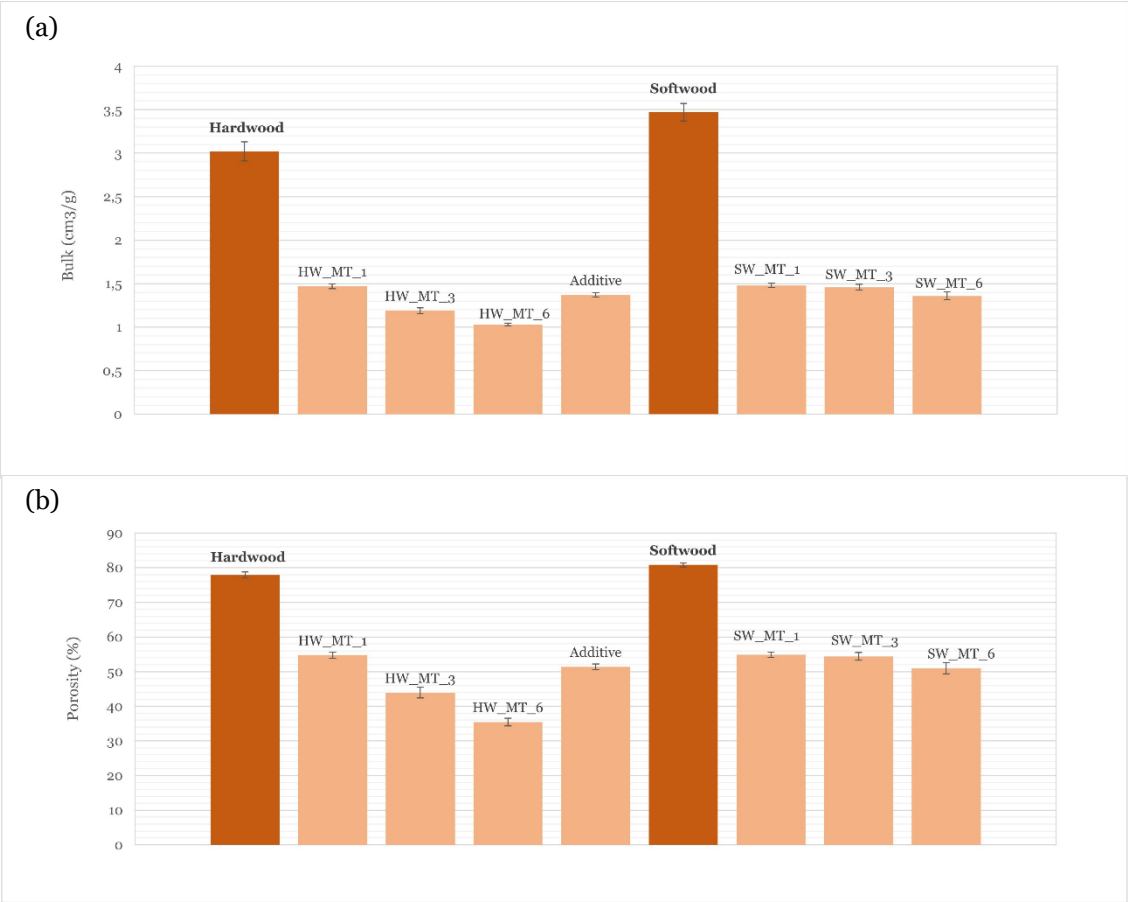

Figure 4.10 - Graph referring to the (a) bulk (cm^3/g) and (b) porosity (%) of HW and SW handsheets without PFI-refining (dark orange bars) and HW and SW handsheets PFI-refined at 1000 revolutions, 3000 revolutions and 6000 revolutions and the micro/nanofibrillated cellulose additive (light orange bars).

Porosity (Figure 4.10b) decreased significantly for both types of fibers when compared to structures that did not undergo any mechanical treatment. PFI-refining had a more significant impact on HW handsheets. Reaching the lowest porosity for HW handsheets PFI-refined at 6000 revolutions, a 42% reduction compared to HW handsheets without mechanical treatment. Although there was a noticeable reduction in porosity in the PFI-refined SW handsheets, however it remained constant over all revolutions stages. At 6000 revolutions, the SW handsheets PFI-refined had a 37% reduction, compared to SW handsheets without mechanical treatment.

Finally, changes in the structural properties of handsheets, particularly their thickness and porosity, are influenced by fiber mixing and refining. This fiber heterogeneity may be relevant in producing paper with specific thicknesses and grammages more economically and efficiently at the industrial level.

4.1.2.2. Mechanical Properties

In this stage, the mechanical properties of the handsheets were evaluated. In the present work, greater consideration was given to the tensile index and elastic modulus values of our structures. The tensile index measures the paper's capacity to withstand tensile forces without breaking or tearing. Two concepts must be considered in this logic: (1) "Fiber Breakage" refers to disruption at the molecular level, specifically, hydrogen forces and adhesion forces (see subchapter 2.2.1), and (2) "Fiber Bond Breakage" represents a break between the various layers that make up the paper's hierarchical structure. The force required to break bonds between fibers is much bigger than the force needed to break bonds between layers. The elastic modulus can calculate the paper's stiffness and elastic deformation capacity. Typically, there is a direct relationship between these two variables.

Analyzing the fibers without mechanical treatment and their mixtures (Appendix B3, Table B3.1), a low tensile index can generally be verified for all samples. The highest index attributed to handsheets with a proportion of 90% HW with 10% SW, 11,6 Nm/a. Since there are few fine elements, it reduces the formation of better molecular adhesion; consequently, these structures are vulnerable to tensile forces. Furthermore, these structures have a limited capacity for deformation, as all samples revealed low modulus of elasticity, all below 800 MPa.

On the other hand, as shown in Figure 4.11ab, the tensile index and elastic modulus values of the PFI-refined structures revealed relatively high values. Both HW and SW structures PFI-refined at 6000 revolutions had the highest and similar tensile index values, 85,6 MPa and 86,8 MPa, respectively. Large amounts of fine elements may have contributed to forming a more united structure at the molecular level. Because polymerization contributes to forming more hydrogen bonds, so it requires more force to break it. This behavior can also be seen a slight improvement in the tensile index of the additive structure after adding 10% HW PFI-refined at 12000 revolutions.

The elastic modulus also increased as the level of refinement increased, resulting in a greater resistance to deformation. The highest elasticity modulus value corresponds to HW handsheets PFI-refined at 6000 revolutions, approximately 5959,98 MPa.

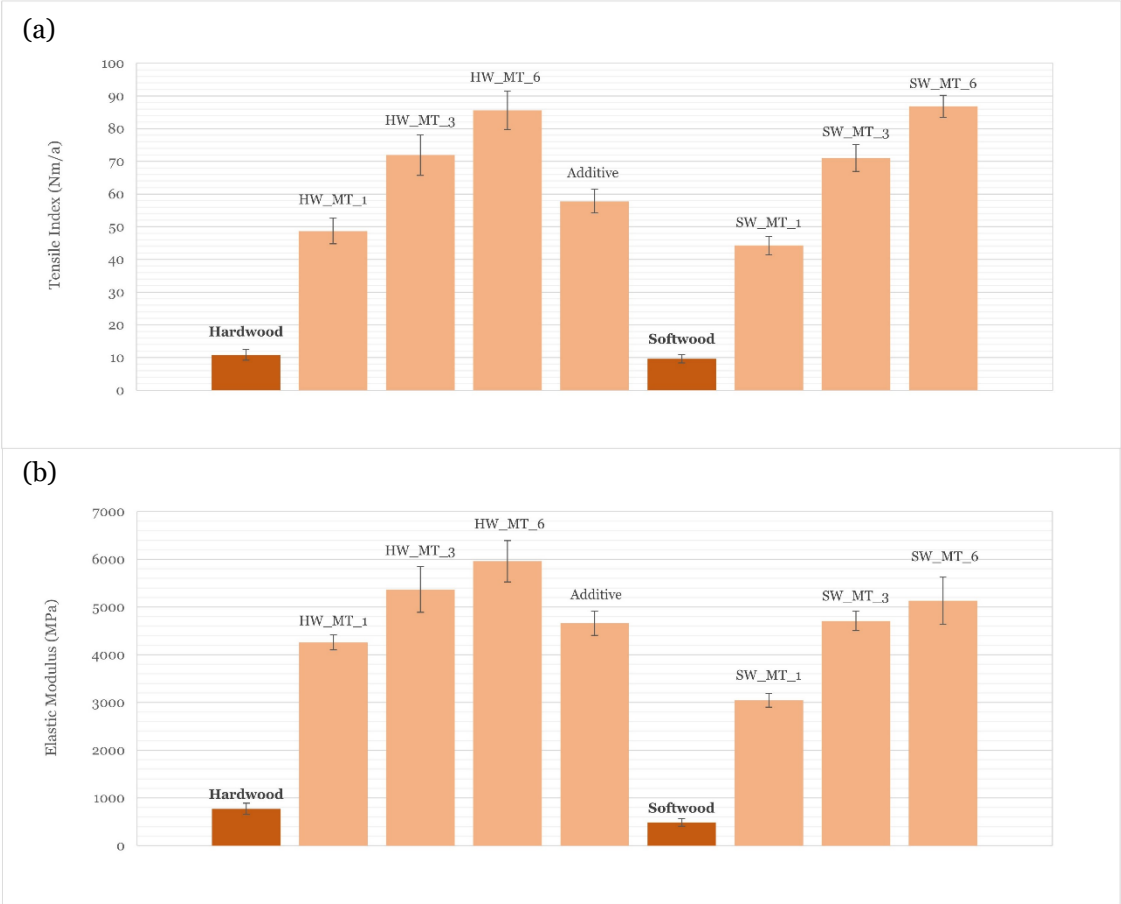

Figure 4.11 - Graph referring to the (a) tensile index (Nm/a) and (b) elastic modulus (MPa) of HW and SW handsheets without PFI-refining (dark orange bars) and HW and SW handsheets PFI-refined at 1000 revolutions, 3000 revolutions and 6000 revolutions and the Micro/nano-fibrillated cellulose additive (light orange bars).

4.1.2.3. Optical Properties

Bleaching the pulps, adding additives, or adding optical whitening agents influence the whiteness of the paper. From a social perspective, the brownish color of paper packaging is associated with a more environmentally friendly product, quality that consumers increasingly desire and so adds value to the company's product. Table 4.2 contains the whiteness and opacity values of structures that have not undergone any mechanical treatment. The HW fibers, because they have been subjected to a bleaching process, have the highest percentage value of whiteness (72,18%), in contrast to the SW fibers, which have not gone through any bleaching step, have the lowest value (24,76%). The whiteness decreased as the HW:SW ratios equalized. The presence of SW in the mixture compromised the whiteness.

Table 4.2 – Optical characterization of the structures produced in the laboratory individually (HW or SW) and their mixtures (heterogeneous fibers) in the proportions HW:SW (90:10, 80:20, 50:50), both without any type of mechanical treatment.

	Homogeneous Fibers		Heterogeneous Fibers		
	HW	SW	90_HW_10SW	80_HW_20SW	50_HW_50SW
Whiteness (%)	72,18 ± 1,44	24,76 ± 0,30	59,50 ± 0,25	51,71 ± 0,33	41,37 ± 0,85
Opacity	81,80 ± 1,75	96,90 ± 1,43	92,79 ± 0,23	94,77 ± 0,28	97,42 ±0,21

Table 4.3 shows the whiteness and opacity values of the PFI-refined structures for both structures. In both cases, the whiteness decreases as PFI-refining increases. However, the whiteness values of bleached HW fibers remained higher than those of unbleached SW fibers.

Table 4.3 - Optical characterization of structures produced individually in the laboratory, namely hardwood and softwood handsheets PFI-refined at 1000 revolutions, 3000 revolutions and 6000 revolutions.

	Hardwood			Softwood		
	HW_MT_1	HW_MT_3	HW_MT_6	SW_MT_1	SW_MT_3	SW_MT_6
Whiteness (%)	68,97 ± 0,17	63,74 ± 0,66	57,86 ± 0,52	22,9± 0,16	20,09 ±0,27	19,51 ± 0,17
Opacity	78,86 ± 0,45	70,01 ± 0,66	69,81 ± 0,67	96,45 ± 0,42	95,6 ± 0,37	93,44 ± 0,65

Comparing both samples, the unrefined HW handsheets have lower opacity (81,80) than the unrefined SW handsheets (96,90). Increasing the amount of non-bleached SW fibers in the mixture increases opacity in structures with mixed fibers. Furthermore, the mechanical treatments reduced the opacity of both fibers, with the bleached HW fibers losing 15% of their opacity compared to the unrefined HW fibers. The fact that PFI-refined HW structures have fibers with smaller dimensions in their composition favors their compaction during deposition, which ended in a finer and more uniform structure.

4.1.2.4. Morphological Characterization using Image Analysis by SEM

Figure 4.12 shows the structures observed by SEM technique in the XY plane, i.e., the structures' surfaces. They are composed exclusively of HW fibers, with no mechanical treatment. A random arrangement of fibers can be seen on the left side (Figure 4.12a). In general, the fibers appear to have very similar and small dimensions. The fiber walls are less collapsed, giving the fiber a bulky appearance. A HW fiber that supports other fibers is highlighted in orange on the right side (Figure 4.12b).

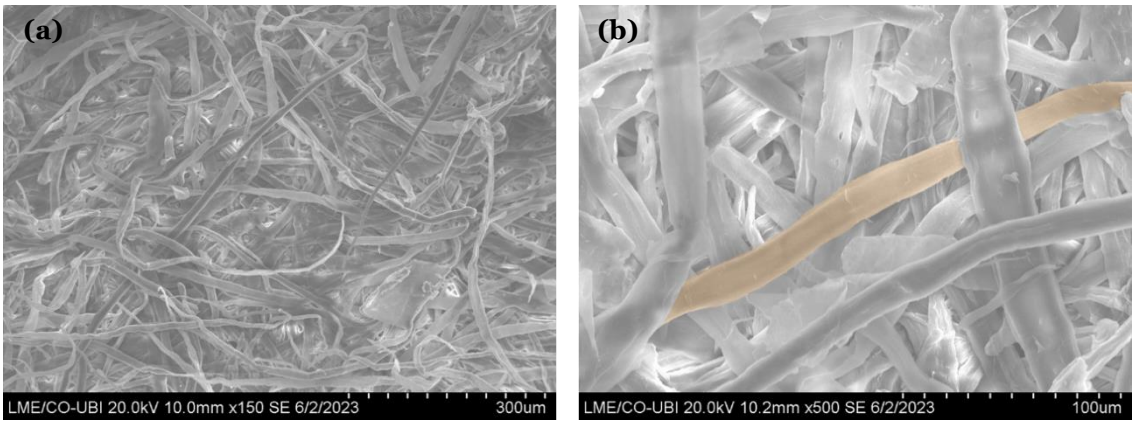

Figure 4.12 - SEM images of structures of 100% HW fibers without mechanical treatments (a) random arrangement of the fibers magnified at 150x in the XY axis and (b) overlapping of the fibers on top of each other, in this case, the orange fiber on top, magnified at 500x in the XY axis.

Figure 4.13 shows the structures observed in the XY plane, produced from SW fibers without mechanical treatment. Furthermore, these fibers present a greater degree of collapse, giving the fiber a ribbon aspect (Figure 4.13b). The presence of pores is reduced for the same reason. Figure 4.13a also shows the random arrangement and overlapping of fibers on top of each other.

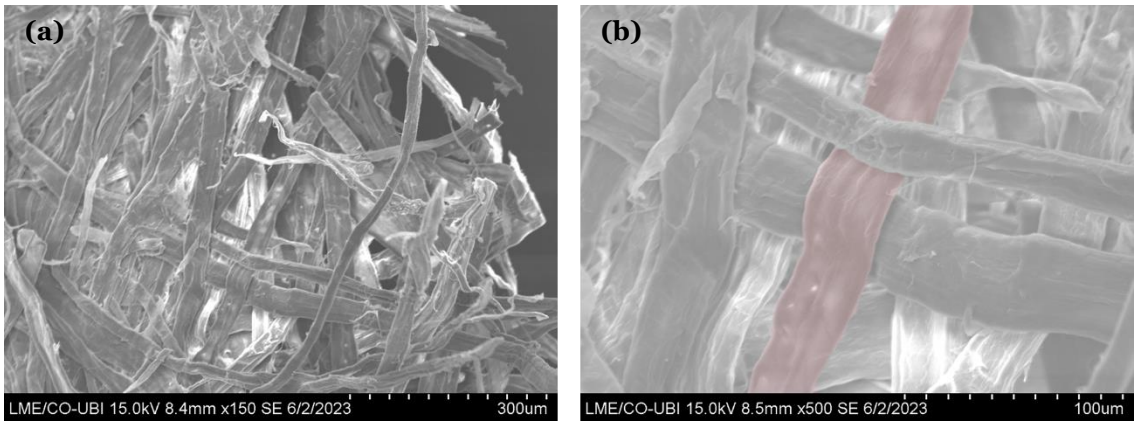

Figure 4.13 - SEM images of structures of 100% SW fibers without mechanical treatments (a) random arrangement of the fibers magnified at 150x in the XY axis and (b) overlapping of the fibers on top of each other, providing support, for example the fiber highlighted in red, magnified at 500x in the XY axis.

Figure 4.14a illustrates the concept of interfiber connections of the two types of fibers discussed previously, in the proportion of 50:50. The SW fibers (red) are larger (they even run through the image from end to end) and form the main structure of the mesh. Then there are the HW fibers (orange), which connect with each other, and the HW fibers develop resistance to the structures because of their reduced dimensions.

From another perspective, the handsheet sample was analyzed based on the Z plane, i.e., its thickness. The deposition of the fibers can be seen layer by layer, and there is no significant compaction due to the presence of unattached fibers on the handsheet surface.

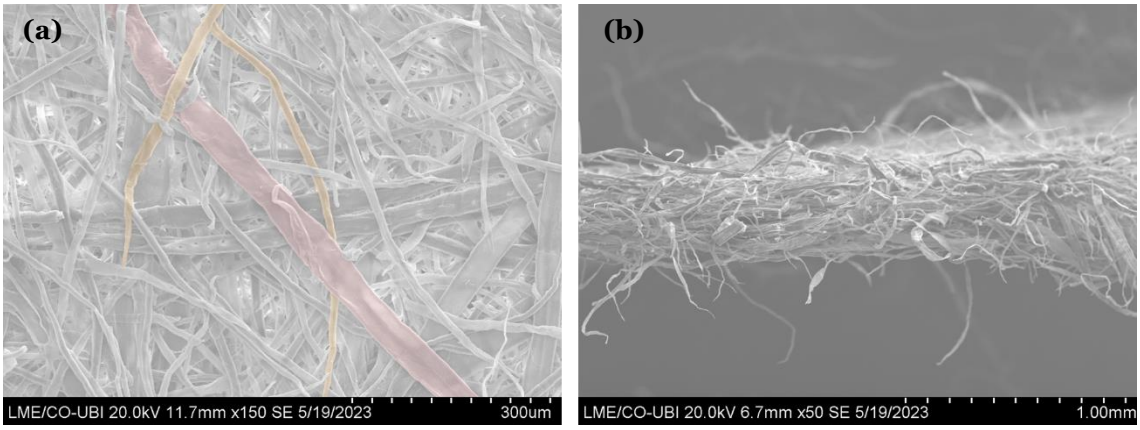

Figure 4.14 - SEM images of structures of 50% HW fibers and 50%SW fibers without mechanical treatments (a) random arrangement of fibers magnified at 150x in the XY axis and (b) thickness of structures, magnified at 50x in the Y axis.

Applying a severe mechanical treatment, such as PFI-refining at 12000 revolutions, can affect fiber conformation. High refining leads to excessive fiber polymerization, resulting in fragmentation into very small units. Eventually losing its three-dimensional structure and cohesion, having a jelly-like appearance (Figure 4.15a), and the porosity becomes extremely low. In Figure 4.14b, micro/nanofibrillated cellulose connects more significantly, with widths reaching the nanometer scale (198 nm and 534nm).

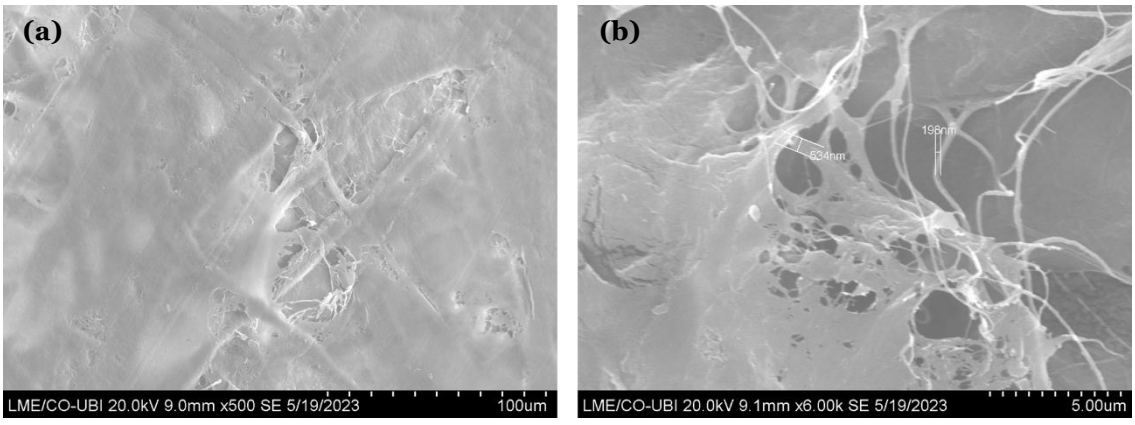

Figure 4.15 - SEM images of structures of 100% HW fibers refined at 12000 revolutions (a) jelly-like appearance of the fiber with a very uniform and smooth surface magnified at 500x in the XY axis and (b) measurement of the width of some micro/nanofibrillated cellulose magnified at 6.00kx in the XY axis.

4.1.2.5. Chemical Characterization using Infrared Spectroscopy by FTIR-ATR

Figure 4.16 explores the FTIR-ATR spectra of the handsheets obtained from the HW and SW fibers without any mechanical treatment. When analyzing the two spectra, it is important to consider two regions in the FTIR-ATR spectrum. On the left side, the region 4000-2700 cm^{-1} is called the “informative” zone and corresponds to the O-H and C-H bond stretching vibrations. This zone is not much explored due to the similarities in the chemical composition between cellulose, hemicellulose, and lignin, which means there are peaks with similar wavelengths. On the right side, the region referred to as the "fingerprint" ranges at 1800-800 cm^{-1}, which represents distinct stretching vibrations of diverse functional groups within wood (Carrillo et al., 2018). Like people, materials have unique and different “fingerprints” depending on their composition.

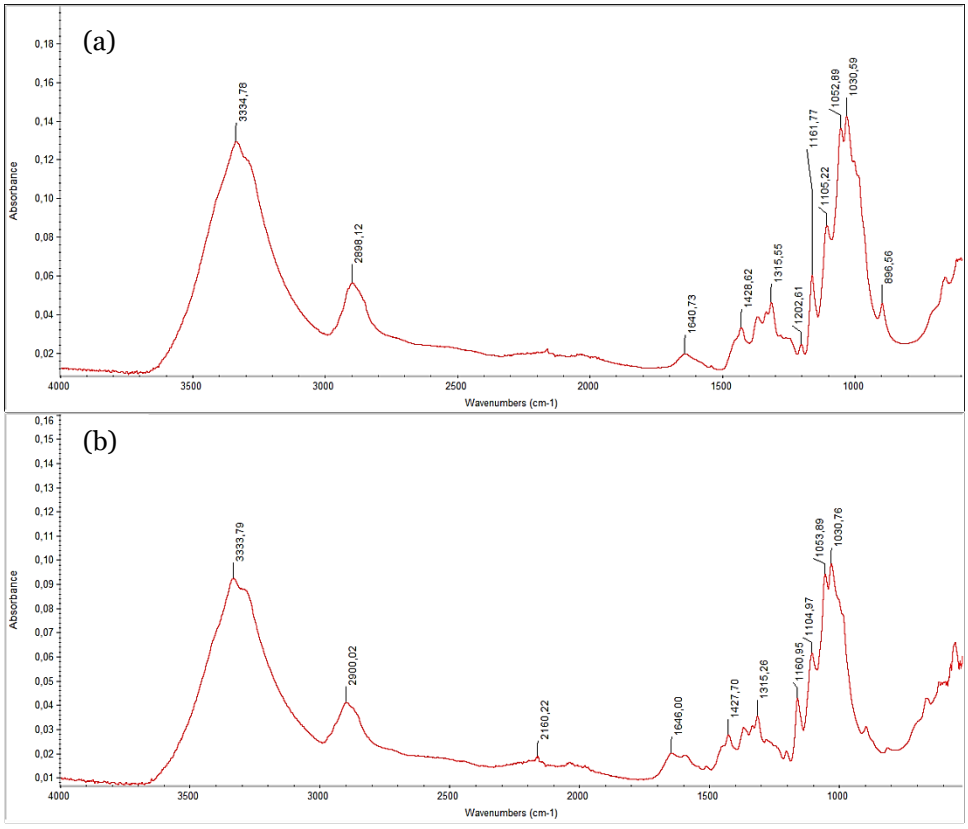

Figure 4.16 - FTIR-ATR spectra of the hansheets produced from (a) HW fibers and (b) SW fibers, both without any kind of additional mechanical treatment.

Starting the analysis on the left side of both spectra, the first peak at 3334 cm^{-1} for HW and 3333 cm^{-1} for SW correspond to the stretching of the O-H bond referring to the hydroxyl groups of cellulose, hemicellulose, and lignin and also of water.

Moving on to the second peak, we have for the HW sample the value of 2898 cm^{-1} and for the SW sample the value of 2900 cm^{-1}. In this case, it is correlated to the stretching of the C-H bond, also present in the cellulose, hemicellulose, and lignin molecules.

Moving to the right side of the spectrum, the peaks at 1640 cm^{-1} (HW) and 1646 cm^{-1} (SW) are in the stretching region of the C=C bond, corresponding to the aromatic rings present in lignin. Despite being a slight difference between values, it may be correlated due to the lower amount of lignin in the hardwood sample. Analyzing the “fingerprint” zone, the few differences between both spectra are noticeable. The 1428 cm^{-1} (HW) and 1427 cm^{-1} (SW) peaks are associated with the vibrations of the CH2 bonds of type I cellulose. At 1161 cm^{-1} (HW) and 1160 cm^{-1} (SW) is the stretching of the C-O-C bond typical of cellulose I and II. The 896 cm^{-1} band of both spectra is associated with C-H vibrations of type II and amorphous cellulose. Something to be considered, in a more discreet way, is the presence of a small peak at 1500 cm^{-1} (Figure 4.16b), also representative of the C=C stretching of the lignin aromatic ring in the SW sample. The presence of this band is the only distinguished element between spectra (a) and (b) in the "fingerprint" zone, but due to its low intensity, it cannot be considered conclusive.

In the present study, the infrared spectroscopy by FTIR-ATR method was mainly used to identify the functional groups and molecular characteristics of the materials produced in the laboratory and to identify the fingerprint section for the benchmarking materials.

This analysis is an important tool for assessing and comparing the different materials that constitutes the benchmarking study for the sustainable materials identified in the market and that are references according to ISO standards in this field.

According to ISO standards, the paper filter was identified as reference and used in this study. The silicon coated paper will be used as a sample to assess the coatings' chemical composition. Regarding the single use plastics available in the market a disposable coffee paper cups was studied. To identify any differences, we considered the evaluation of both the inner and outer surfaces. Finally, it was thought pertinent to analyze the chemical composition of a nonwoven cellulose-based derived from a different natural source, like bamboo. Figure 4.17 shows the FTIR-ATR spectrum of all these samples pointed before.

In general, the materials that presented very identical peaks along the spectrum were precisely the paper filter (black line), the outer layer of the coffee paper cup (red line), and the bamboo nonwoven (purple line). Peaks in the 3500 – 3200 cm^{-1} range correspond to the stretching of the O-H bond referring to the hydroxyl groups of cellulose, hemicellulose, and lignin. The 3000 – 2800 cm^{-1} range, stretching of the C-H bond, is also present in the molecules referred to before. On the right side, although some oscillations, it can be said there are some similarities between samples in the fingerprint zone. Concluding that we are working with materials with some similarity in terms of chemical composition.

Despite presenting certain peaks identical to previous samples, the surface of coated silicone paper is not so evident. However, these peaks do not exclude the possibility of being associated with cellulose, hemicellulose, and lignin chemical groups. However, these same molecules may be affected due to the coating process. A peak in the range 1300-1200 cm^{-1}, stretching of the C-N and C-O bond, could be related to the presence of coating polymers.

The differences are more noticeable for the sample of the inner layer of the coffee paper cup. With a considerable wavelength in the range 3000 – 2800 cm^{-1} range, it is stretching of the C-H bond, which could also be associated with organic compounds, such as polymers, related to the coatings of paper cups. Furthermore, it has a visible peak in the 1500-1400 cm^{-1} range, stretching of the C-H, which may indicate the presence of coating materials, polymers, or other compounds that are part of the cup coating.

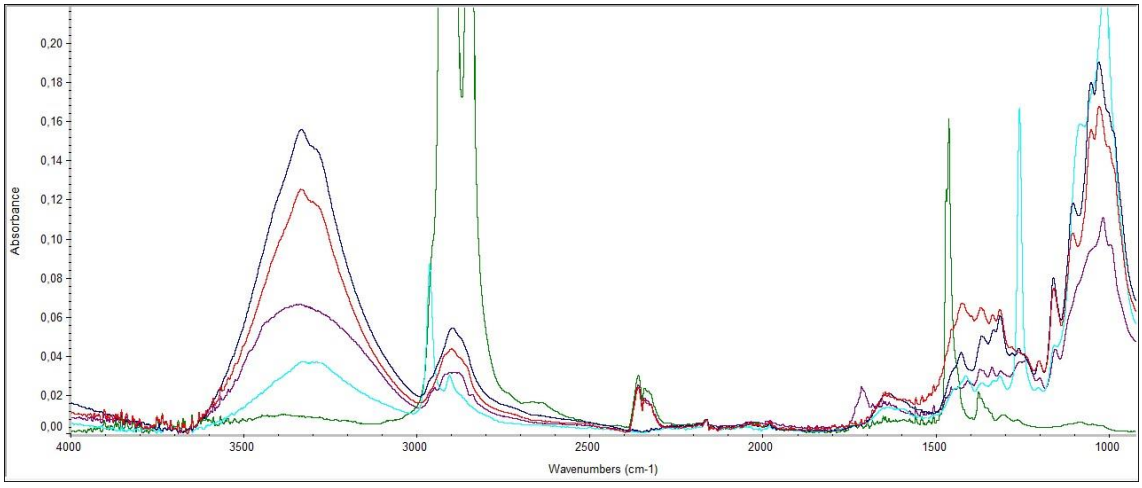

Figure 4.17 - FTIR-ATR spectrum comparison: (1) paper filter (black), (2) surface of coated of silicone paper (light blue), (3) coffee paper cup - outer layer (Red), (4) coffee paper cup (green) - inner layer and (5) nonwoven made of bamboo fibers (purple).

4.1.2.6. Optimization of Fibrous Materials on Liquid Retention/ Absorption

This study used an optical prototype system to evaluate the kinetics of the liquid droplet spreading area over time (Mendes & Curto, 2021). These results will be important to consider two behaviors: absorbency and retention of liquids. It is important to understand these behaviors in food packing, as they will serve to retain drinks (for example, coffee cups) or absorb undesirable liquids (for example, fats and oils). This component is also part of the benchmarking assessment.

The results showed that liquid droplet deposition into these fibrous structures had a smaller spreading area as the basis weight increased, corresponding to a less porous structure, resulting in a structure bulk decrease with the basis weight, as shown in Figure 4.18. It was also possible to confirm that the 60 g/m² laboratory made structures (Figure 4.18a) had a larger spreading area for liquid droplets than the structure with the double basis weight (Figure 4.18b). This could be due to fiber hornification in higher basis weights, as well as differences in structure bulk and porosity.

Comparing the commercial sample to the laboratory made structures, it can be seen that the spreading area changes very little over time, concluding that this material can retain liquids very effectively. The research team aims to achieve the following quality in food packaging lines.

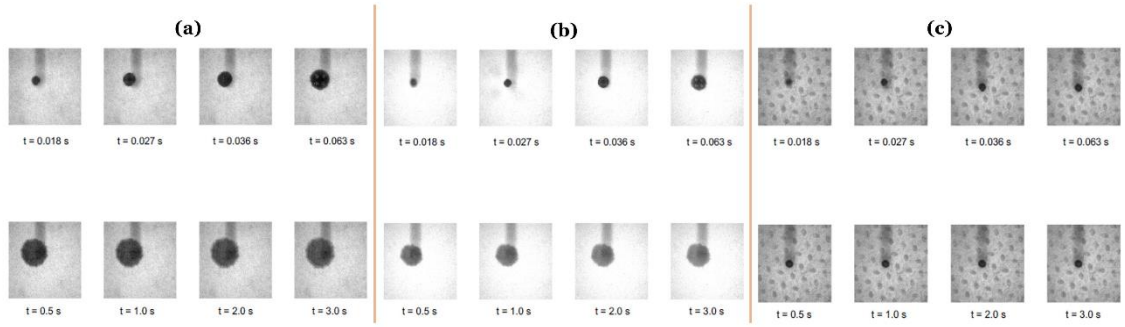

Figure 4.18 - Evolution of the liquid droplet spreading area over time in laboratory-made structures produced from industrial tissue paper (a) basis weight of 60 g/m², (b) basis weight of 120 g/m² and in a (c) commercial sample.

4.2. Evaluation of Hemp Fibers using Characterization Methods

This subsection will describe fibers extracted from hemp stem using different concentrations of NaOH. The cooking step and fibers evaluation were carried out with the assistance of members of the research team, considering the observation of microscope images and the fiber analyzer, Morfi®.

4.2.1. Fiber Suspension Characterization

4.2.1.1. Fiber Morphology

Following the extraction of the hemp fibers, their morphological evaluation was performed using an optical microscope, as was previously done for the reference fibers. In the first observation (Figure 4.19), hemp fibers were longer than reference fibers. They shared some similarities with SW fibers in terms of fiber width. Comparing hemp fibers with themselves showed that most fibers obtained from milled samples are shorter in length than those manually cut. With the increase of NaOH concentration, there was a certain degree of degradation and the presence of cut fibers and fine elements.

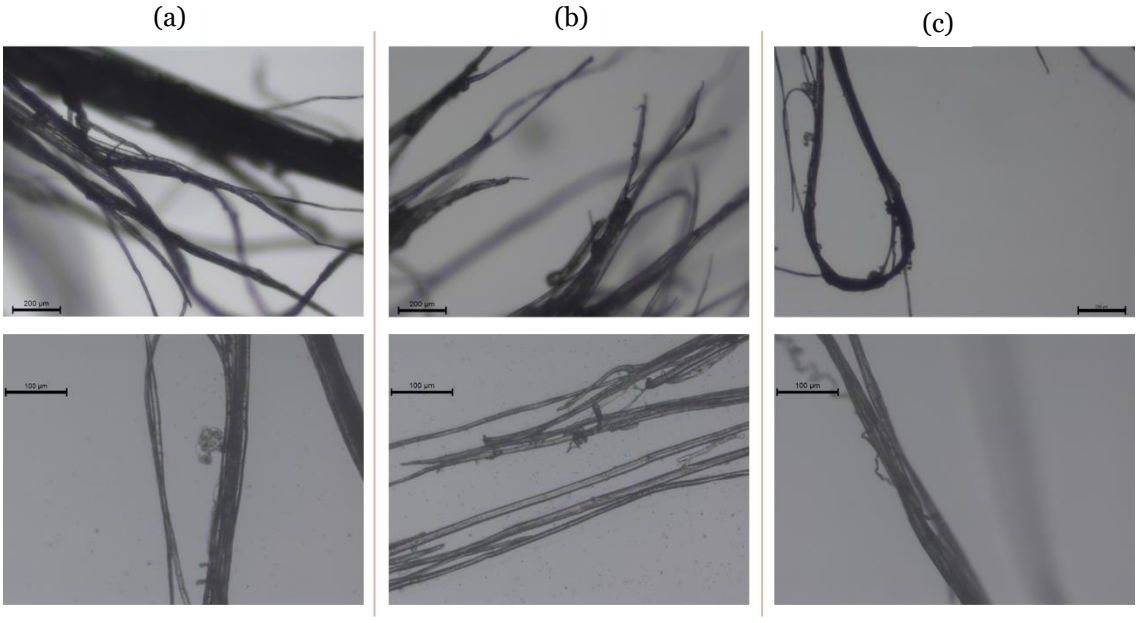

Figure 4.19 - Microscope images of hemp fibers with different separation methods and different concentrations of NaOH. Note that the top images have a 40x magnification and the bottom images a 100x magnification. In (a) cut hemp fibers subjected to a coking step at a 1M NaOH concentration, (b) milled hemp fibers and applied a coking step at a 1M NaOH concentration, and (c) milled hemp fibers with a coking step at a 2M NaOH concentration.

4.2.1.2. Fiber Morphology using a Fiber Analyzer, the Morfi®

Appendix C1 (Table C1.1) contains the values obtained in the morphological characterization using the Morfi® fiber analyzer. As done previously, the following parameters were considered: fiber population, length weighted by length, width, coarseness, fibrillation, broken ends, and kinked fibers. However, because it is a fiber of great economic interest with few characterization studies, the tests were performed in triplicate with the respective standard deviations to obtain more accurate results.

Figure 4.20 shows the length weighted by the length of cut and milled hemp fibers at different concentrations. Considering the data taken from Morfi®, these fibers had bigger length compared to SW fibers (see subchapter 4.1.1.2). Comparing the hemp fibers with each other, the length values are similar for both samples (cut and milled) when cooked in a lower concentration of NaOH.

However, fibers cut manually and exposed to 2M NaOH concentrations, have a similar length to those with lower concentrations. It can be due to the more difficult of NaOH to interact with the hemp fiber, because interfiber bonds are less accessible. Fibers manually cut with a NaOH concentration of 0,5M (2720 µm, HF_C_0,5M) had the longest length. While milled fibers with a NaOH concentration of 2M (1460 µm, HF_M_2M) had the shortest length. A 46% decrease in length indicates that the milled fibers were significantly degraded during cooking with high concentrations of NaOH.

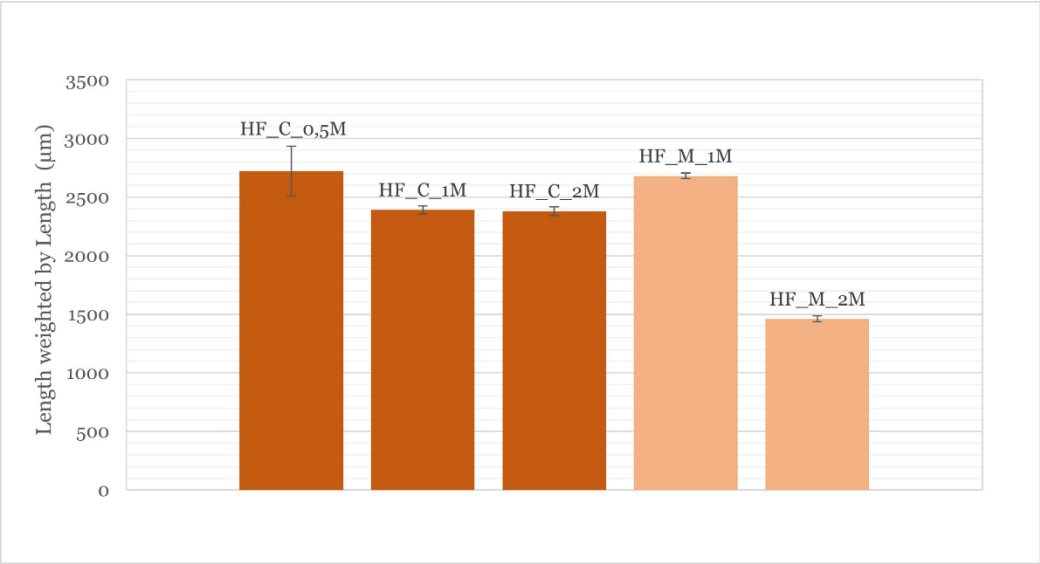

Figure 4.20 - Length weighted by length of hemp fibers. The dark orange bars represent fibers cut manually and with different concentrations of NaOH (0,5M, 1M, 2M). The light orange bars are milled fibers with different concentrations of NaOH (1M and 2M).

Unlike the length, using different concentrations of NaOH during cooking did not affect fiber width much. However, there was a slight reduction in width for cut fibers exposed to 2M NaOH concentrations.

So far, identical values for the lengths and widths of hemp fibers have been observed in small NaOH concentration. The highest level of fibrillation is found in milled fibers cooked with a 2M NaOH concentration (HF_M_2M), reaching 1,51%. Comparing this value with those obtained during the mechanical treatment of HW and SW fibers. It is evident that the HF_M_2M sample achieved higher fibrillation values than some PFI-refined HW and SW samples.

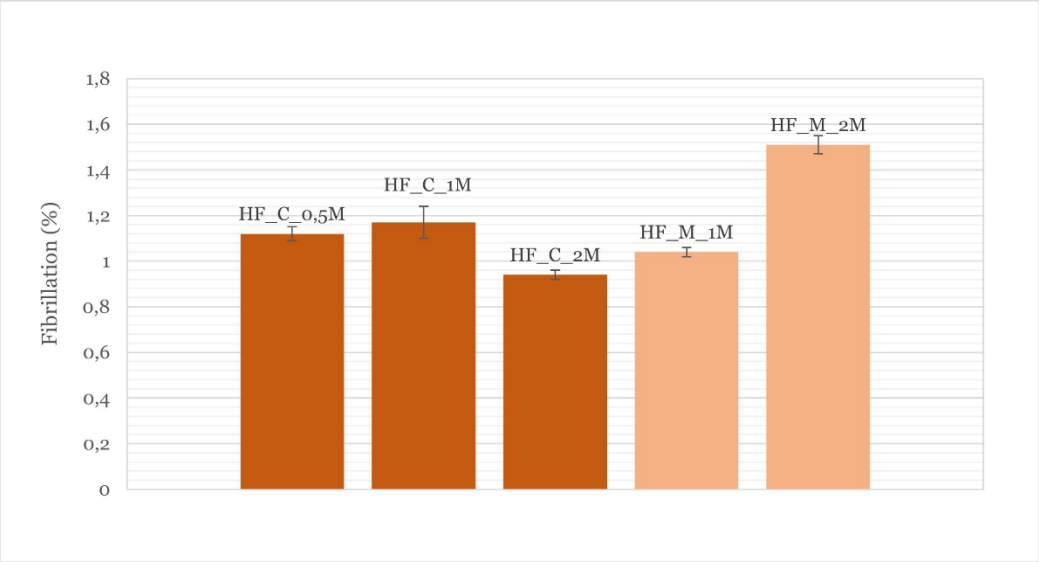

Figure 4.21 - Percentage of fibrillation of hemp fibers. The dark orange bars represent fibers cut manually and with different concentrations of NaOH (0,5M, 1M, 2M). The light orange bars are milled fibers with different concentrations of NaOH (1M and 2M).

Figure 4.22ab demonstrates the effect of cooking at different sample preparation conditions on fibers' length and width distribution. The fiber distribution barely changed for cut and milled hemp fiber samples cooked in a concentration of 1M NaOH. Even though the graph of milled fibers (Figure 4.22b) shows a slight increase in the shorter length range, both samples showed a higher percentage in the [3492 - 5000 µm] range. Additionally, independent of the type of cut applied, the fibers of both samples remained in the same width range [5 – 33 µm] for both samples.

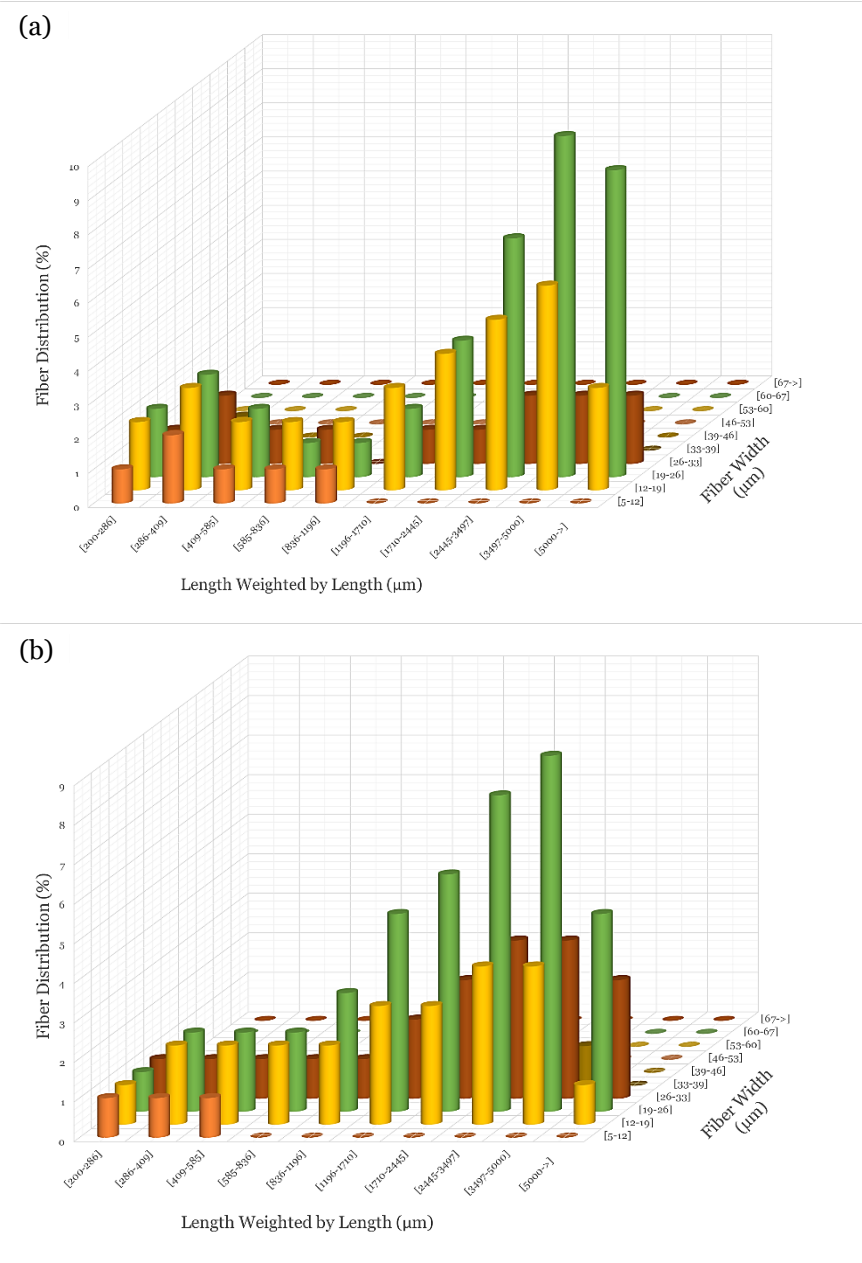

Figure 4.22 - Fiber length weighted by length and width distributions of (a) cut manually hemp fiber cooked to 1M NaOH concentration and (b) milled hemp fiber cooked to 1M NaOH concentration.

From an industrial standpoint, using this method to obtain micro/nanofibrillated cellulose at a lower cost may be advantageous. When the fibers have reduced dimensions, as with milled fibers, the penetration and effectiveness of cooking with NaOH are enhanced. It is possible to increase the percentage of fiber fibrillation by using a higher concentration of NaOH, achieving more positive results than those achieved with the refinement methodologies developed for this purpose (Morais et al., 2019). Also investing in milling machines is more economically viable than human labor, revealing the economic advantages of obtaining this type of fiber.

4.3. Evaluation of Hemp Fibers Mixture

After carrying out the research to characterize the reference structures and the hemp fibers isolated, we arrived at the phase of investigating and assessing how these fibers behave when they are mixed with others. In this sense, this subchapter describes the characterization of the fibers and handsheets produced by combining reference fibers (industrial tissue paper) with hemp fibers extracted in laboratory.

4.3.1. Fiber Suspension Characterization

4.3.1.1. Fiber Morphology

Figure 4.23 shows microscopic images of industrial tissue paper (IT) fibers used as reference samples. Some morphological similarities between these and unrefined HW fibers can be seen (see subchapter 4.1.1.1.). Compared to the hemp fibers previously characterized, the IT fibers have extremely small dimensions. These differences could provide properties similar to those of handsheets made from a mixture of short fibers (HW) and long fibers (SW) (refer to section 4.1.1.2).

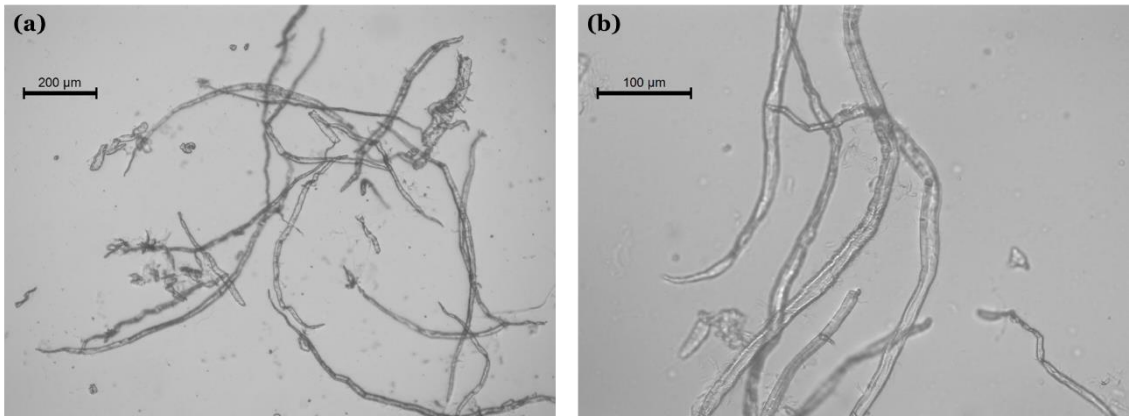

Figure 4.23 - Microscope images of industrial tissue paper fibers at (a) 40x magnification and (b) 100x magnification.

4.3.1.2. Fiber Morphology using a Fiber Analyzer, the Morfi®

In Morfi®, samples of industrial tissue paper and samples with the following mixtures were analyzed: (1) 99% industrial tissue paper + 1% hemp fiber (99_IT_1_HF), (2) 90% industrial tissue paper + 10% hemp fiber (90_IT_1_HF) and (3) 90% industrial tissue paper + 10 % hemp fiber PFI-refined at 1000 revolutions (90_IT_10_HF_1).

The respective values of fiber population, length weighted by length, width, coarseness, fibrillation, broken ends, and kinked fibers were extrapolated. All of them can be consulted in Appendix D1 (Table D1.1). These inputs will be important during the computational 3D simulations of these fibrous handsheets.

Figure 4.24 illustrates the length weight by length of the reference fibers (HW and IT) and the mixture fibers (99_IT_1_HF, 90_IT_1_HF, 90_IT_10_HF_1). Comparing the lengths of the reference fibers, it concludes that the IT fibers are 7% shorter than the HW fibers.

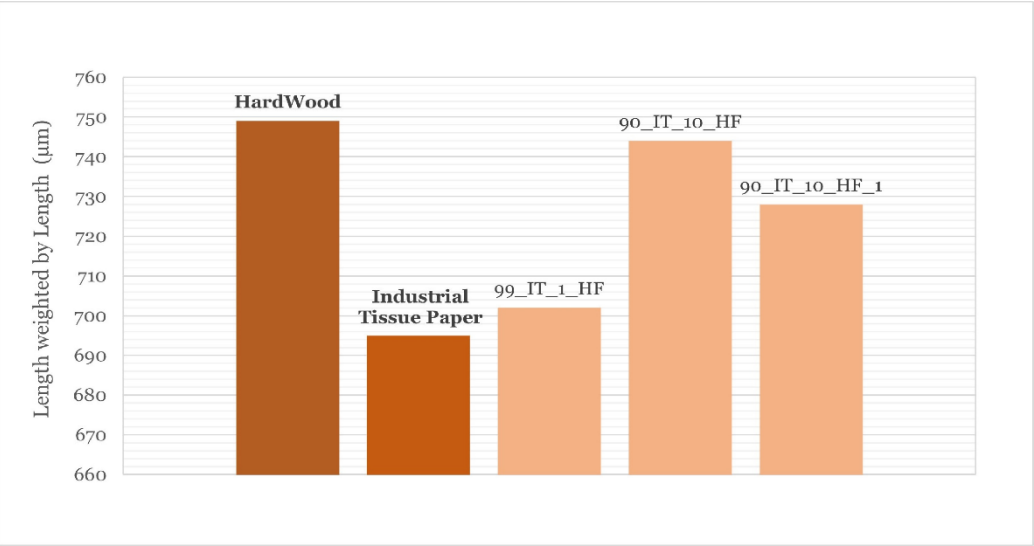

Figure 4.24 - Length weighted by length of the reference fibers, namely HW and IT exclusively (dark orange bars) and mixture fibers 99_IT_1_HF, 90_IT_10_HF and 90_IT_10_HF_1 (light orange bars).

Evaluating samples with a mixture of fibers, the length increased as the proportion of hemp fiber increased, reaching a peak at 744 µm (90_IT_10_HF). In contrast, the length of the 90_IT_10_HF_1 sample is reduced by 2% compared to the previously mentioned sample. In terms of width, IT fibers were larger than HW fibers. In contrast, as the proportion of HF increased in the mixed samples, there was an increase in sample width, due to the broader width of HF fibers.

Figure 4.25 shows four graphs that represent the distribution of fibers in samples of IT fibers and their mixtures with HF, taking into account their length and width (99_IT_1_HF, 90_IT_10_HF, 90_IT_10_HF_1).

They all showed a similar fiber distribution, with the fiber distribution peak centered in the interval [585 - 836] μm in length and [12 - 39] μm in width. It is possible to confirm similarities in fiber distribution by looking to Figure 4.6a (unrefined HW fibers), with their fiber distribution peak percentage being the same for all the graphs below. When looking closely at graphs 4.25bc, it is noticeable how the fiber distribution has been moved to ranges with smaller lengths (figures 4.25b to 4.25c). Which makes sense given that the proportion of PFI-refined HF has increased to 10%. This same distribution declines to a shorter length range in graph 4.25d, considering that this sample contained HF PFI-refined at 1000 revolutions.

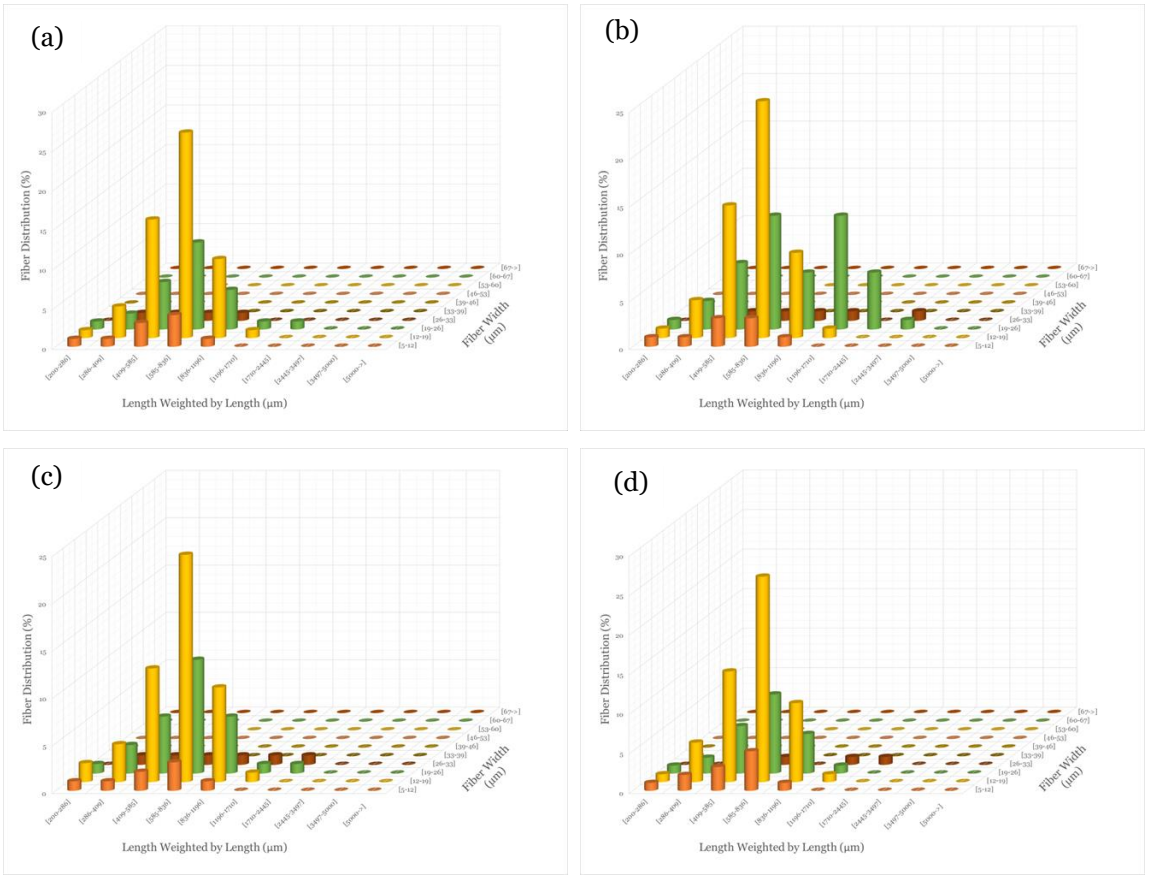

Figure 4.25 - Fiber length weighted by length and width distributions of (a) only IT, (b) 99_IT_1_HF, (c) 90_IT_10_HF and (d) 90 _IT_10_HF_1, respectively.

The remaining parameters such as coarseness, fibrillation, broken ends, and kinked fibers, generally showed identical values and were within the expected ranges for the IT fibers samples and mixtures. The highest degree of fibrillation (1,12%) was found in the 90_IT_1_HF_1 sample, indicating that mechanical treatment affected fiber morphology and the fiber structure in general. In light of these results, developing new and innovative tools for optimizing fibrous structures is necessary, and the relationships between different parameters can impact the final material.

4.3.2. Fiber Handsheets Characterization

4.3.2.1. Structural Properties

For the structural characterization, handsheets were produced in the laboratory with industrial tissue paper fibers and also with the mixtures previously studied (99% industrial tissue paper + 1% hemp fiber, 90% industrial tissue paper + 10% hemp fiber, and 90% industrial tissue paper + 10% hemp fiber refined at 1000 revolutions) (Figure 4.26). Also, Appendix D2 (Table D2.1) shows all parameters evaluated in this characterization. All handsheets were produced with a basis weight of approximately 60 g/m².

Comparing the characterization results of handsheets made exclusively with HW fibers and those made with IT fibers shows a general similarity. The differences become more evident when we contrast the results with the fiber mix hansheets. The presence of 10% hemp fiber in the composition of the 90_IT_10_HF handsheets results in a slight increase in thickness. As mentioned, the HF were differentiated by their larger dimensions compared to the reference samples. This percentage variation between these two samples also revealed that an increase in the proportion of hemp fibers in the sample corresponds to a rise in bulk and a decrease in density. Even though the fibers take up much space, they also increase porosity, which results in a larger air-to-solid interface and lower density.

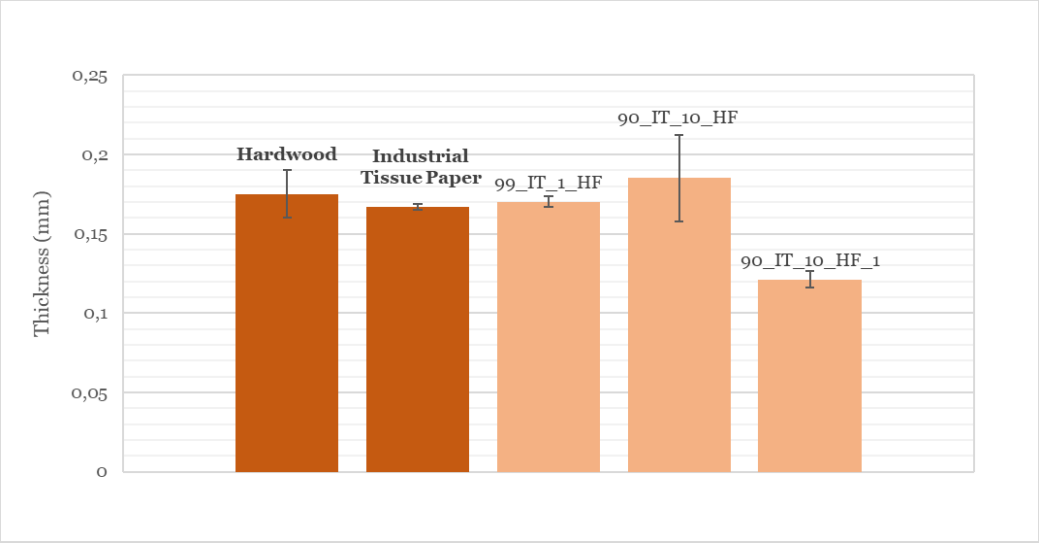

Figure 4.26 - Graphs referring to the thickness (mm) of the HW and IT handsheets (dark orange bars) and handsheets 99_IT_1_HF, 90_IT_10_HF and 90_IT_10_HF_1 (light orange bars).

Figure 4.27 shows that the 90_IT_10_HF sample has the highest percentage of porosity compared to the others. In contrast, the thickness of the 90_IT_10_HF_1 handsheets was reduced by approximately 30% compared to the reference IT handsheet (Figure 4.26). Furthermore, when compared to the IT structures, the composition of the 90_IT_10_HF_1 sample presented a significant decrease in bulk (22%), as well as an increase in density (28%). This is a consequence of higher compaction and interconnection between the different fibrous layers of the structure, as observed in hansheets made from PFI-refined fibers. Compared to those made with HW, the porosity of IT handsheets decreased by approximately 4%.

Increasing the percentage of hemp fiber in the mixture by 10% increased the structure's porosity by 2% compared to the IT samples. The sample 90_IT_10_HF_1 revealed the lowest level of porosity, approximately 67,83%, compared to the others.

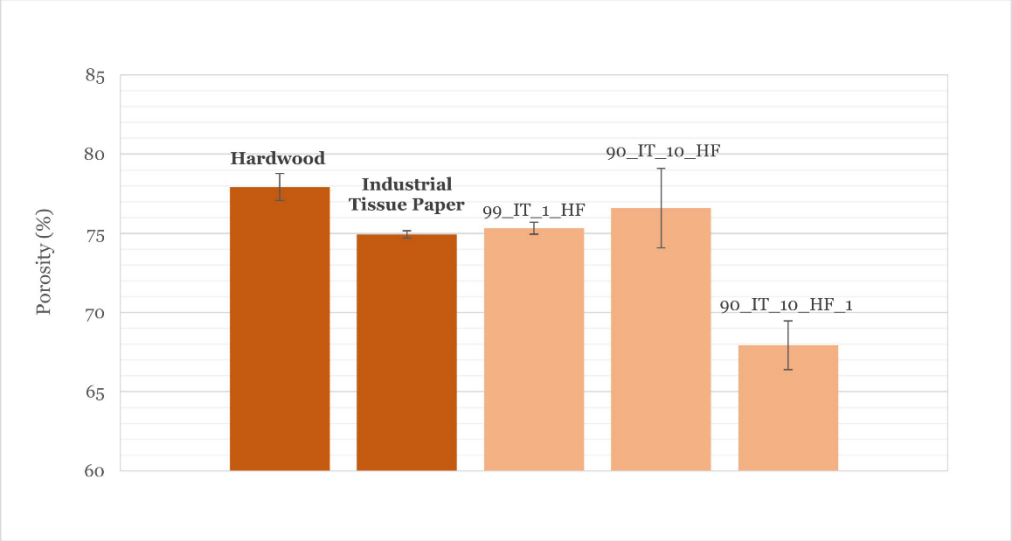

Figure 4.27 - Graphs referring to the porosity (%) of the HW and IT handsheets (dark orange bars) and handsheets 99_IT_1_HF, 90_IT_10_HF and 90_IT_10_HF_1 (light orange bars).

4.3.2.2. Mechanical Properties

The structures were also tested in a tensile test. Appendix D3 (Table 3.1) contains the values for this mechanical characterization. Compared to the reference samples, the IT fiber handsheets had a higher tensile index and elastic modulus values, 30,8 Nm/a, and 1650,43 MPa, respectively (Figure 4.28 and Figure 4.29).

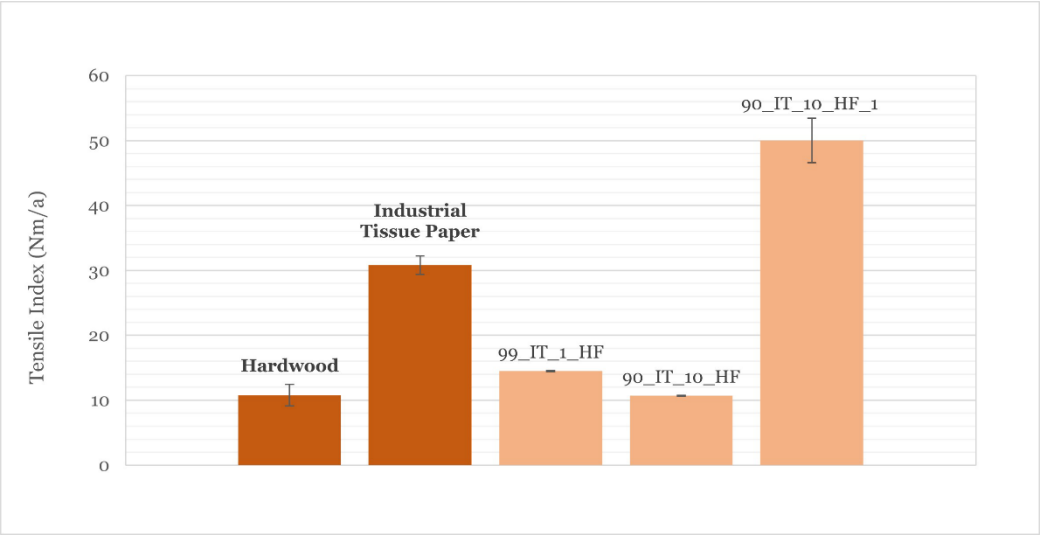

Figure 4.28 - Graphs of the tensile index (Mn/a) of the HW and IT handsheets (dark orange bars) and fiber mixture handsheets 99_IT_1_HF, 90_IT_10_HF and 90_IT_10_HF_1 (light orange bars).

Compared to HW fibers, IT fibers are smaller in length (Figure 4.24), which results in higher interfiber interactions and a higher tensile force. Comparing the IT reference sample to the mixture samples reveals a decrease in these two parameters. The increase in the percentage of HF in the sample, i.e., the increase in long fibers, reduced the handsheet strength. However, after PFI-refining the hemp fibers, the tensile index and elastic modulus values increased by 32% and 40%, respectively (Figures 2.28 and 4.29). The high interfiber bonds and fiber compaction caused by the high fibrillation percentage and high fine elements content improve tensile properties.

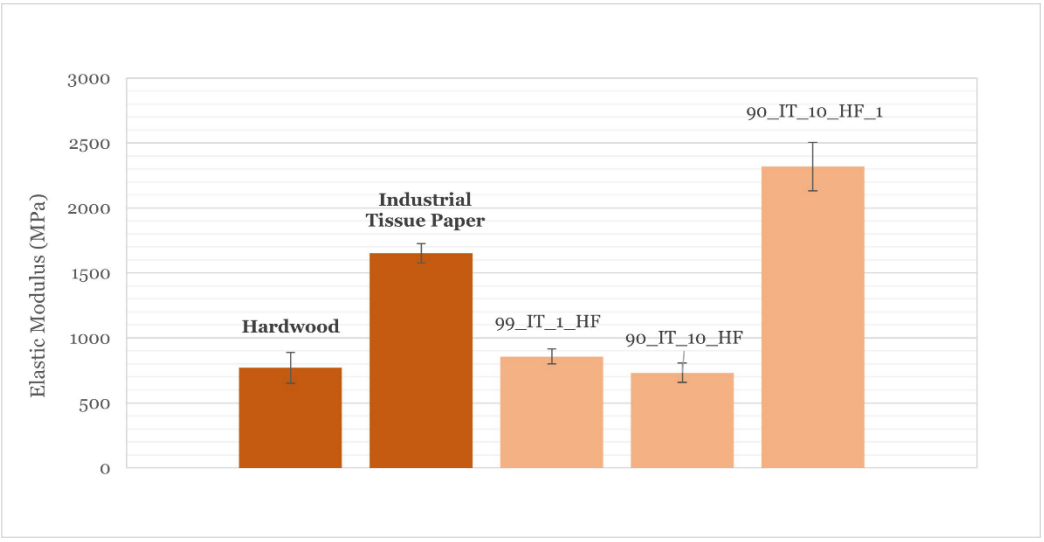

Figure 4.29 - Graphs of the tensile index (Mn/a) of the HW and IT handsheets (dark orange bars) and fiber mixture handsheets 99_IT_1_HF, 90_IT_10_HF and 90_IT_10_HF_1 (light orange bars).

4.3.2.3. Optical Properties

In addition to the previous characterizations, the optical of the handsheets produced in the laboratory with IT fibers and their respective mixtures with HF were evaluated. Table 4.4 provides the results that were obtained. The whiteness and opacity values of the HW and IT reference fibers are very similar. When the values of the mixtures are compared, an increase in HF by 10% in the mixture results in a decrease in whiteness and an increase in opacity. The structure's whiteness was affected by the fact that these fibers had some color. Additionally, light rays reflect more intensely inside the fibrous structure because the fibers are less compacted, increasing opacity. Cause of this, the 90_IT_10_HP_1 structure has a significantly lower opacity value than the others. After refinement ended, it promoted the homogenization of the entire sample, contributing to the handsheet darkness and lower whiteness.

Table 4. 4 - Graphs of the tensile index (Mn/a) of the HW and IT handsheets (dark orange bars) and handsheets 99_IT_1_HF, 90_IT_10_HF and 90_IT_10_HF_1 (light orange bars).

	Homogeneous Fibers	Heterogeneous Fibers		
	IT	99_IT_1_HP	90_IT_10_HP	90_IT_10_HP_1
Whiteness (%)	71,35 ± 0,23	71,15 ± 0,18	69,51 ± 0,55	61,69 ± 0,69
Opacity	82,19 ± 0,23	82,13 ± 0,32	82,89 ± 0,83	76,83 ± 0,90

4.4. Biodegradability Evaluation of Fibrous Structures

Companies have become interested in doing biodegradability testing to demonstrate that their products are biodegradable. A criterion that adds value to the product and differentiates it from competing companies (Itävaara & Vikman, 1996). There are different methodologies to assess the degree and rate of biodegradation. Materials can be degraded by enzymes or microbes in laboratory culture or biodegraded in soil, activated sludge, or compost. Composting, an aerobic biodegradation type, is one of the most widely used methods.

It is known for being a natural way of recycling because compost is a hummus-like substance made from decomposed organic material that decomposes material into biomass to complete the lifecycle. For these same reasons, this chapter serves as the final phase of the methodology proposed for investigating and assessing the biodegradation of structures created in the laboratory (Figure 3.5e).

The two evaluation methods chosen were (1) visual analysis, i.e., evaluating the material based on its appearance, and (2) analysis based on mass loss as time in days increased. For each type of sample, three samples were buried to improve the representativeness of the results; however, only one sample was buried for the control samples. Table 3.9 shows the selected samples as well as their designations. As mentioned in Chapter 3, structures containing hemp fiber were not considered in the present study because they were not yet produced, and the study itself required a two-month incubation period.

4.4.1. Visual Evaluation of Fibrous Structures

The results of biodegradation by composting the laboratory produced structures are shown in Figure 4.30 before and after being buried in the soil after 28 and 60 days, respectively. When looking at the images, keep in mind that the images were selected according to the most representative of the three submitted samples. Furthermore, because the images in Figure 4.30 are not at real scale, the length of the samples should not be considered when analyzing biodegradation. In other words, just because two samples appear the same length at first look does not mean they are, since the image is more compressed.

Starting with the control sample, the filter paper after 28 days showed some fragmentation between them, but with large areas still united. After 60 days, its original structure was relatively reduced and fragmented.

On the other hand, silicon coated paper after 60 days, maintained its structure reasonably intact. However, it was observed that the uncoated side layer was degrading more compared to the coated side layer, which appeared to be damaged. The fact that this side layer with coating is made with materials of fossil origin (plastic additives) decrease the biodegradation of this material.

Moving on to structures with a mixture of HW and SW fibers without mechanical treatment. Just like the filter, sample C, after 28 days, showed some fragments, but with large areas, only after 60 days was the structure significantly reduced. As mentioned before, the soil used in the tests is rich in enzymes or microbes that will degrade the cellulose. The fibers in this sample did not undergo mechanical treatment, so the polymeric cellulose chains are long and have few accesses. Consequently, the enzymes will have more difficulty in degrading them. For example, the same does not occur for samples that have gone through a mechanical treatment.

The three samples (D, E, F) were the ones that suffered the greatest degradation in a short time (28 days). However, sample E (SW_MT_3) did not degrade as quickly as the three. Despite having gone through a mechanical treatment process, it did not have the same effect on fiber polymerization as it had on the other two samples. As a result, the enzymes did not act as much on fiber degradation. In contrast, sample F, which contains 10% fiber, underwent an excessive refining process, so the cellulose units were smaller and simpler (high polymerization), easily degraded by enzymes in 28 days.

Finally, even 60 days later, the effects of structural degradation were less evident in the HW and SW samples that had not received any dry-sheet treatment. Due to the high basis weight and amount of compacted fibers present in the samples, it was difficult for the enzymes to degrade the material. It might take a few more months for it to disintegrate with more speed. Overall, the evaluation of the visual degradation results was positive and consistent with the literature (Itävaara & Vikman, 1996; Saha et al., 2019).

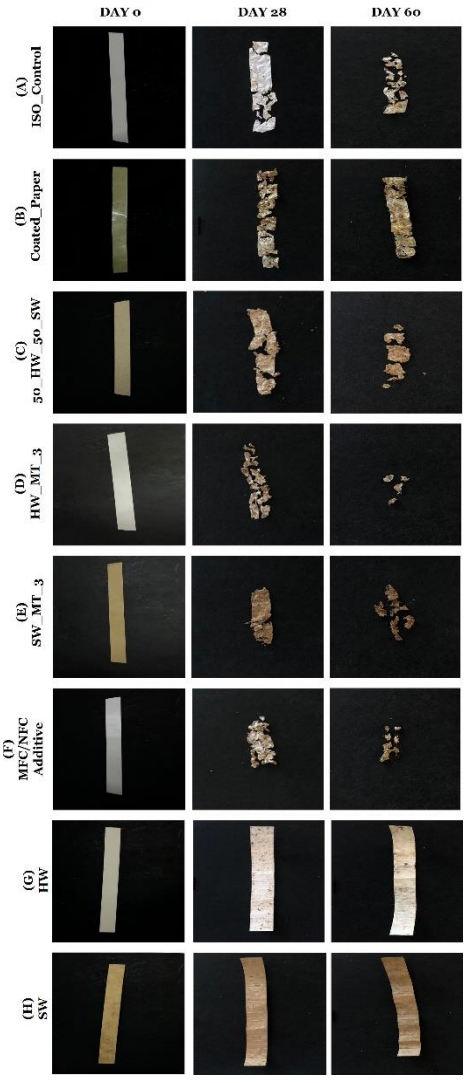

Figure 4.30 - Images of samples of handsheets that had undergone a biodegradation by composting test before and after being buried for 28 days and 60 days.

4.4.2. Evaluation by Loss of Mass of Fibrous Structures

For the evaluation of mass loss, equation 3.2 was used, and the results obtained were treated and graphed with the respective standard deviations, as shown in Figure 4.31. As can be seen, after 28 days, half of the samples (4 samples) had already lost 50% of their initial mass, and by 60 days, this value had increased to 80% of lost mass.

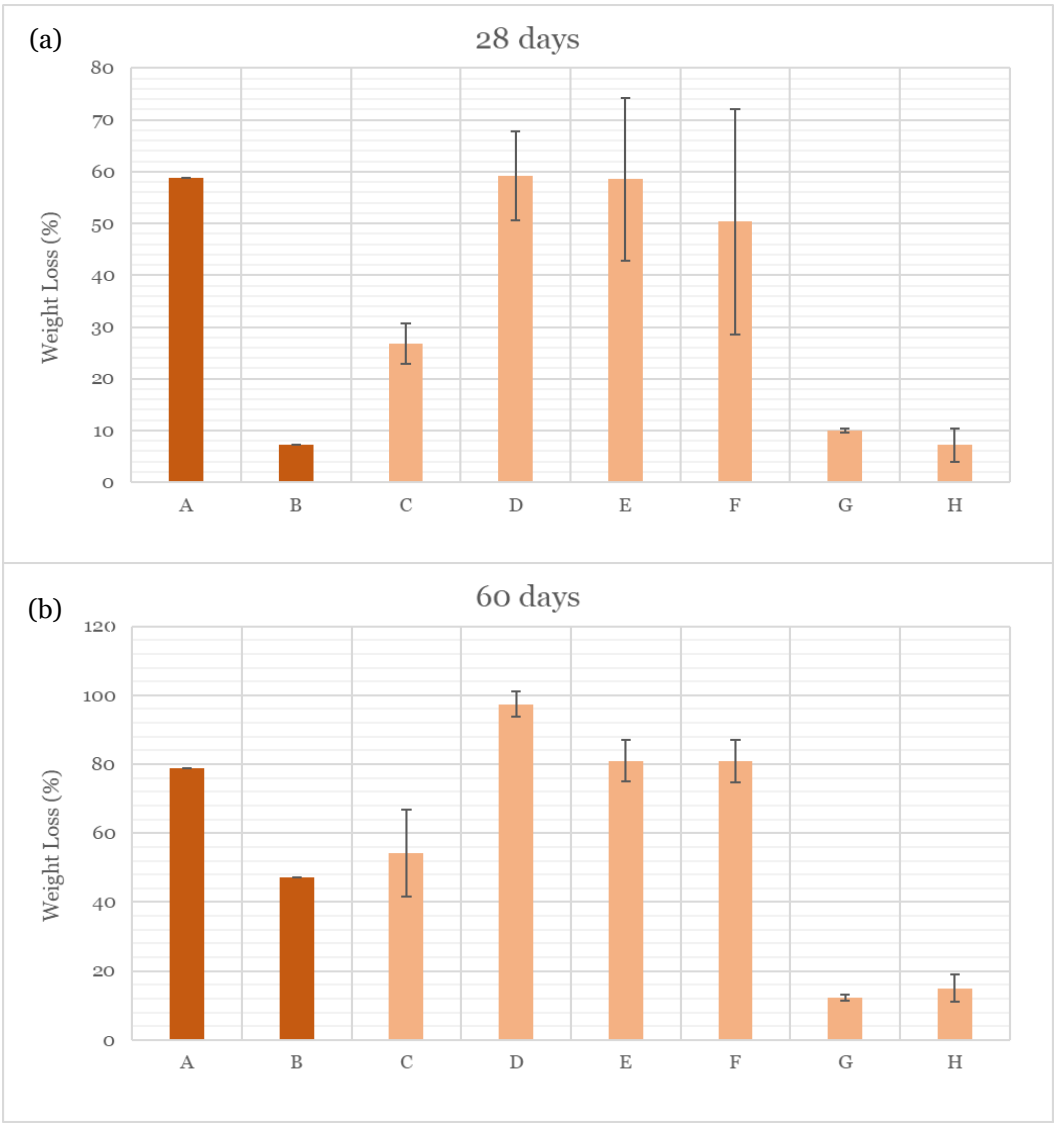

Figure 4.31 - Graphs evaluating the mass loss of the structures under study over time, (a) after 28 days and (b) after 60 days.

The HW_MT_3, D sample lost the most mass over the 28 and 60-day periods, with 59,18% and 97,41% of lost mass, respectively. Although it was previously stated that the HW and SW samples (G and H) did not appear to have suffered much degradation, the mass loss values indicate the opposite.

In fact, the HW sample lost 12,33% of its original mass in 60 days, while the SW sample lost 15,05% of its original mass. If the study was extended for another month, it is possible that at least 3/4 of the total samples would achieve 100% mass loss by composting. In three months, the total degradation of our samples in the environment could be guaranteed with high certainty.

Despite the positive results, this standard biodegradation test used has limitations because it is based on the quantitative measurement of the end product of metabolic degradation quantified by weight loss. Quantifying the biomass, volatile compounds, and the proportions of dissolved and undissolved polymer parts is also necessary. In this view, for this evaluation a respirometer, i.e., a device that measures O_2 and CO_2 concentrations in flow through the sample under controlled conditions, following **ISO1556**, will be used in the near future to measure the biodegradability of these materials in more detail.

In conclusion, these composting biodegradation test served as a baseline for the biodegradation studies of materials made from non-fossil raw materials and complementary research on this topic will be carried out in the future.

4.5. Optimization using Advanced Computational Tolls

4.5.1. Molecular Modeling

In the design and engineering of new materials for food packaging, the selection and optimization of the materials that constitute the main structure of the packaging is important. However, it becomes innovative when active compounds are used to release or absorb substances to extend the shelf life and preserve the quality and freshness of food, as is the example of active packages. In (Martins et al., 2018), bio-based active bi-layer film was developed where one of the layers was formed with cinnamaldehyde, which was used as an antimicrobial compound. Also (Atarés & Chiralt, 2016), essential oils were used in biodegradable active packaging due to their natural origin and functional antioxidant/antimicrobial properties. Therefore, molecular modeling enters this study as a computational tool to understand and study the chemical groups of 3D molecules and how they can interact with each other. The figures below show some 3D molecules attractive for current and future work due to their antioxidant/antimicrobial properties (Samba et al., 2023; Medeiros et al., 2023).

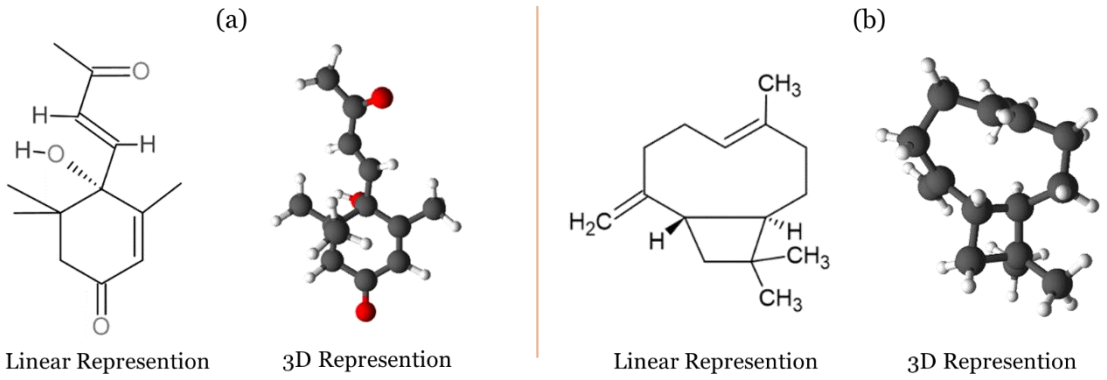

Figure 4.32 – Molecular structures in 2D and 3D of (a) dehydrovomifoliol (Samba et al., 2023) and (b) β-caryophyllene (Medeiros et al., 2023). Molecules made using ACD/ChemSketch by Mendes, J.A.S. and Medeiros, J.F.B.

4.5.2. Computational Simulation Studies for Structure Optimization

Once the values of the morphological characterization of the structures produced in the laboratory have been extrapolated, the conditions are met to move on to the stage of 3D computational simulations of the structures under study. As mentioned before, in the 3D simulator, it is important to select the inputs, considering the desired outputs to achieve a particular optimization objective. These same inputs can be: (1) length/width ratio, (2) wall thickness, (3) lumen thickness, (4) fiber flexibility, (5) resolution, i.e., number of layers in the thickness direction. However, for the simulations presented below, only two parameters were considered and varied: fiber length and flexibility. It is also necessary to convert actual measurements to simulator measurements because the simulator uses voxels as its measurement unit, and each voxel edge has a length of 20 μm. The values for this exact conversion are shown in Table 4.5.

Table 4.5 - Conversion of length weighted by length (real value) in number of voxels (simulated value) considering its dimensions. For Hardwood (HW), Softwood (HW), Hemp Fiber (HF) and Micro/nanofibrillated cellulose fibers (additive).

Fiber Sample	Length Weighted by Length (μm)	Lenght of a Voxel (μm)	Fiber Length Input (nº voxel)
HW	800	20	40
SW	2000		100
HF	2600		130
Additive	600		30

The fibers' flexibility was measured on a scale from 1 to 4. The 1 corresponds to a rigid fiber, while 4 represents a more flexible fiber. This attribution was made based on the previous structures' characterizations. Furthermore, for all simulation studies performed, three phases in fiber deposition were obtained: Initial: the first fibers to be deposited in the xOy plane; Intermediate: approximately half of the fibers have been deposited; and Final: the entire structure after all fibers have been deposited.

4.5.2.1. Simulation of Fiber Deposition of Reference Fibers without Mechanical Treatment

In the simulation of the reference fibers, the values referring to the length of the hardwood fibers and softwood fibers were considered. In Figure 4.33abc, the three moments in the hardwood fibers' deposition are referred to as the initial, intermediate, and final moments, respectively.

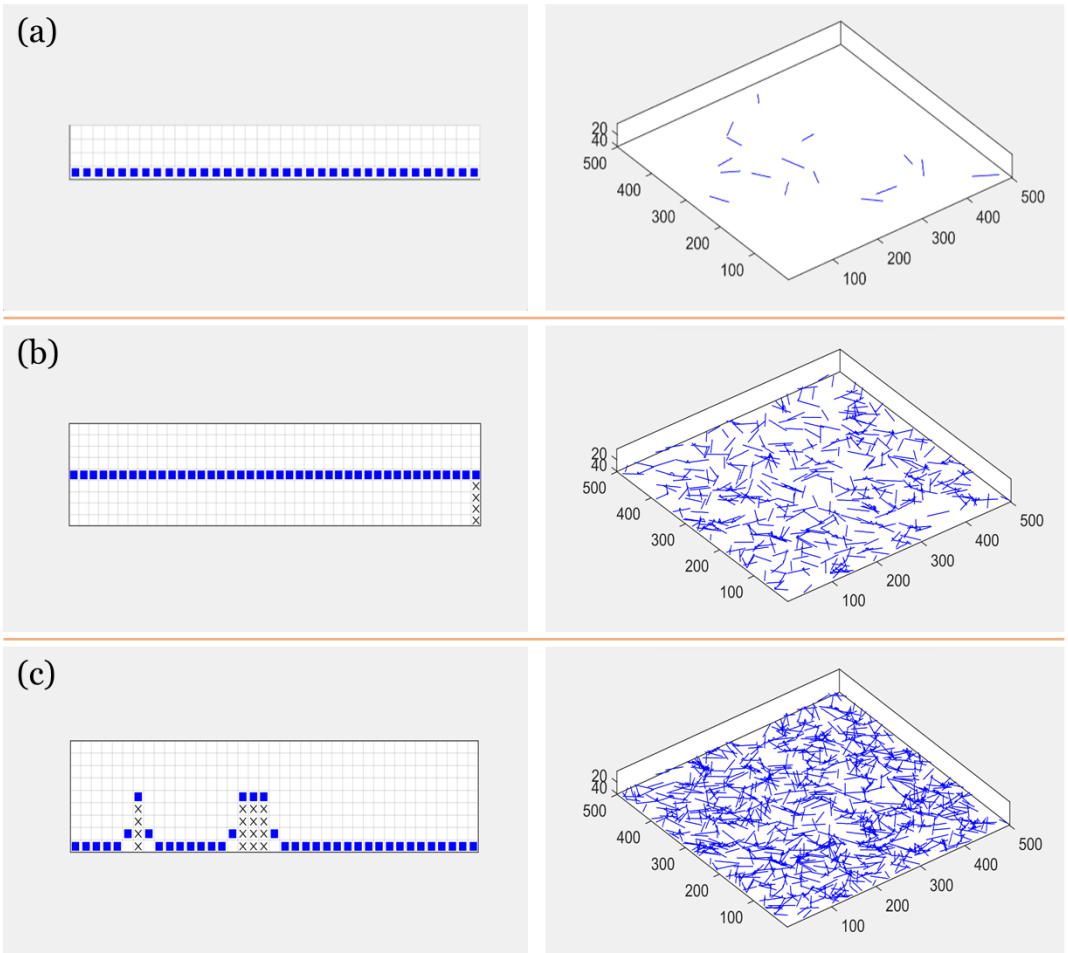

Figure 4.33 - The simulation represents the deposition process of HW fiber with a length of 40 voxels and flexibility 3. The left side is the fiber deposition in voxels, and the right side represents the visualization of 3D structures. In (a) the initial stage, (b) the intermediate stage, and (c) the final stage.

Since these fibers did not undergo mechanical treatment in the laboratory, they were assigned a flexibility value of 3, i.e., a fiber with a certain associated flexibility. The number of fibers deposited at the end was 750 fibers. On the left side of the figure, the fall of the voxels can be seen, which together form a fiber. The “x” symbols in the grid represent the positions occupied by previously deposited fibers (Figure 4.33c, left). On the right side (Figure 4.33), we can see the fiber-to-fiber deposition in the three-dimensional plane as the number of fibers increases, contributing to a more significant overlapping of fibers.

The fact that hardwood fibers have a short voxel length contributes to forming a spread 3D network with some empty spaces (porosity). The 3D simulator does, however, succeed in simulating the deposition of the fibers on top of one another without ever occupying the same position, as it did in the laboratory at producing the handsheets. In addition, it offers the viewer a global 3D image of the structure comparable to that created in the lab (Figure 4.34). It might also be necessary for determining the structure's porosity.

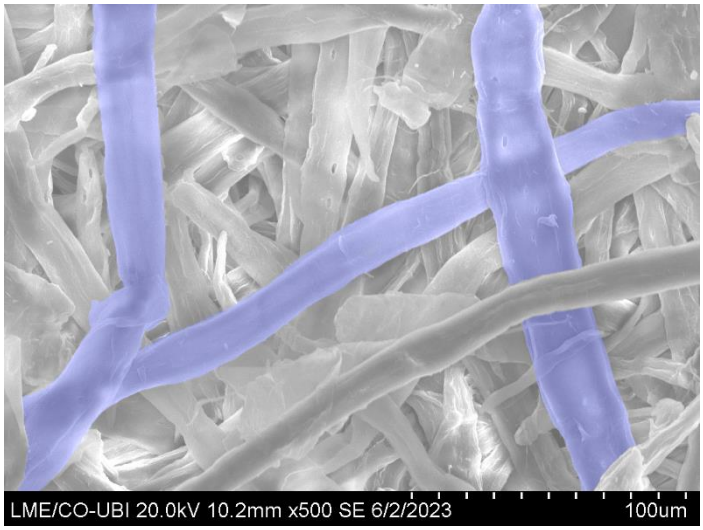

Figure 4.34 - SEM images of HW fibers, in blue are the deposition of fibers one by one, just like in the 3D simulation.

Moving on to the softwood fibers, they had the same analysis methodology as the previous ones. For this type of fiber, a length of 100 voxels and flexibility of 3 was chosen since they also did not undergo mechanical processes like hardwood fibers. Figure 4.35 represents the final stage in fiber deposition in the SW fiber simulator (blue).

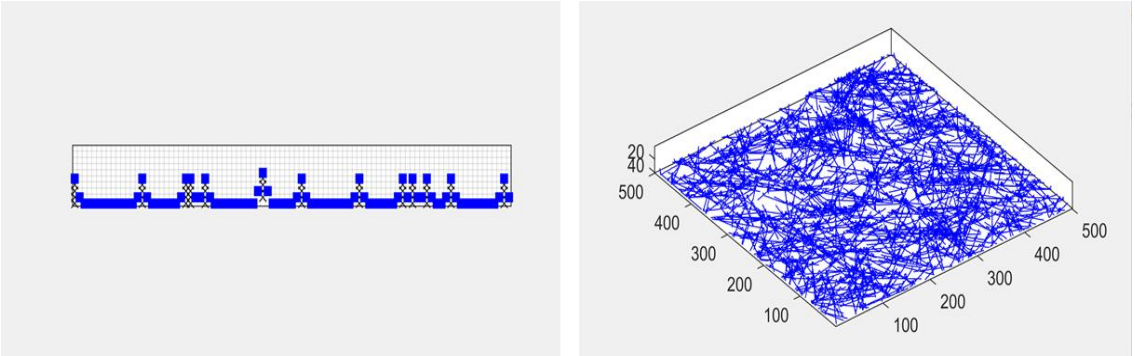

Figure 4.35 - The simulation represents the final stage in the deposition process of SW fiber with a length of 100 voxels and flexibility 3. The left side is the fiber deposition in voxels, and the right side represents the visualization of 3D structures.

As the length of the SW fibers is more remarkable compared to HW, it favored the formation of a 3D network, more compact and with fewer interstices between them. Furthermore, there are areas with higher fiber flocculation (areas with darker blue tones). In the paper industry, flocculation must be avoided, as it represents a paper whose fibers are not uniformly spread and easily break from each other.

4.5.2.2. Simulation of Fiber Deposition of Hemp Fibers without Mechanical Treatment

Figure 4.36 represents the simulation of hemp fibers, whose assigned dimensions were 130 voxels in length and type 2 flexibility. Since these fibers have undergone fewer treatments than reference fibers from industry, they have lower flexibility, therefore, they are more rigid. The 3D structure obtained on the right side is similar to that previously produced with SW fibers. A structure with few empty spaces and a high connection area between fibers due to increased crossing points between them. These similarities indicate that hemp fibers are a good option for replacing SW fibers.

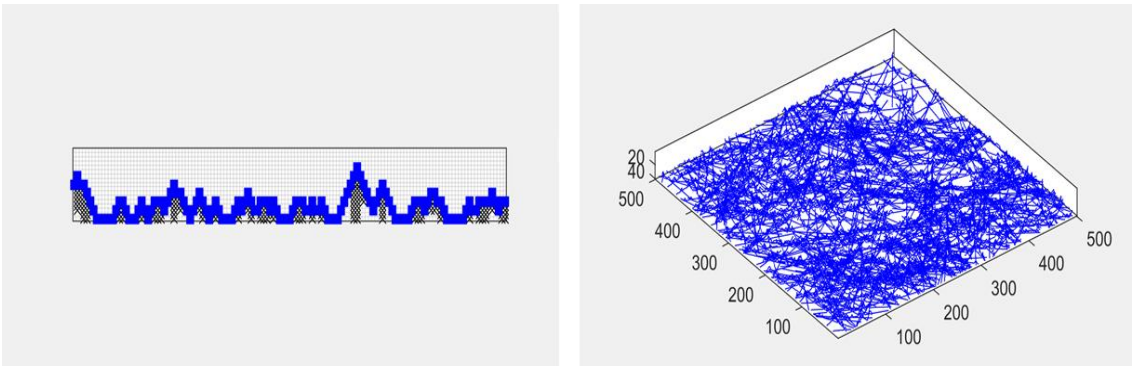

Figure 4.36 - The simulation represents the final stage in the deposition process of HF that has a length of 130 voxels and a flexibility of 2. The left side is the fiber deposition in voxels and the right side represent the visualization of 3D structures.

4.5.2.3. Simulation of Fiber Deposition of Reference Fibers Mixture

Similar to what was done in the laboratory, 3D structures were simulated with a mixture of HW fibers and SW fibers. The dimensions and flexibilities used were the same as those in the previously mentioned simulation studies. However, in this simulation, HW fibers are represented in blue, and softwood fibers in pink (Figure 4.37).

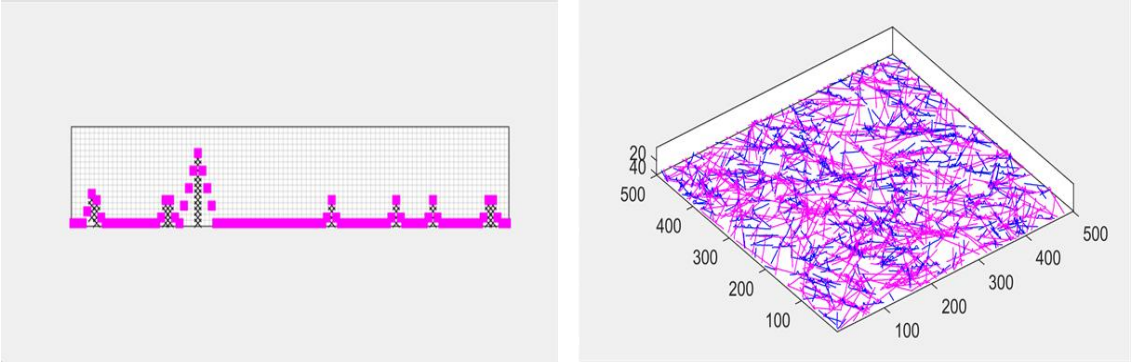

Figure 4.37 - The simulation represents the final stage in the deposition process of HF (blue) and SW (pink) mixture that has a length of 40 and 100 voxels, respectively and the same flexibility of 3. The left side is the fiber deposition in voxels and the right side represent the visualization of 3D structures.

Figure 4.38 highlights the 3D simulator's value as a tool with predictive capability in formulating and optimizing the studied fibrous structures.

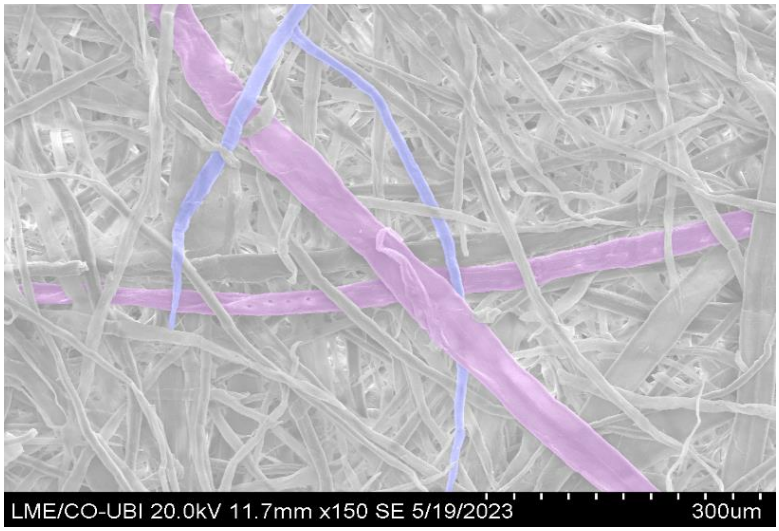

Figure 4.38 - SEM images of HW fibers (blue) and SW fibers (pink) are the deposition of fibers one by one, just like in the 3D simulation.

Given that the present study intends to study the replacement of SW fibers with hemp fibers, simulations were conducted with HW and hemp fiber mixtures. The length and flexibility dimensions were the same as those used in the fiber simulations separately. The results obtained can be seen in Figure 4.39, these are very similar to those obtained in Figure 4.37 were obtained.

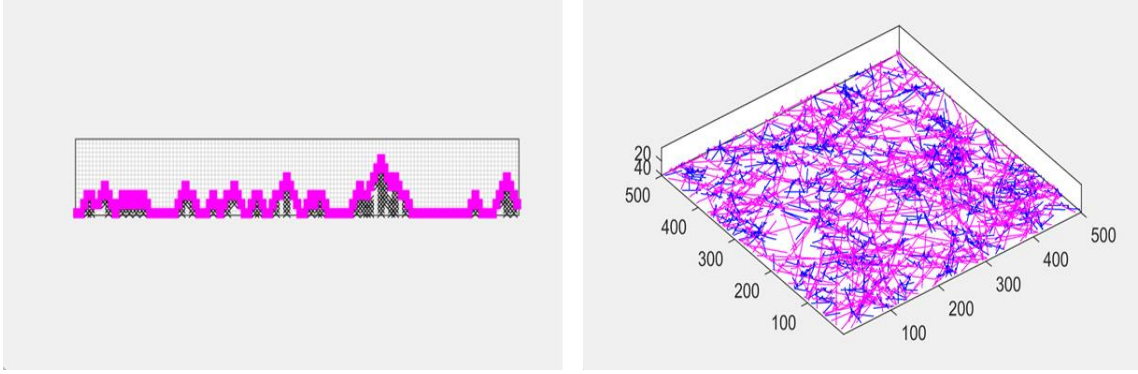

Figure 4.39 - The simulation represents the final stage in the deposition process of HW (blue) and HF (pink) mixture that has a length of 40 and 130 voxels and a flexibility of 3 and 2, respectively. The left side is the fiber deposition in voxels and the right side represent the visualization of 3D structures.

4.5.2.4. Simulation of Fiber Mixture Deposition of Reference Fibers with Hemp fibers and Micro/nano-fibrillated cellulose

A micro/nanofibrillated cellulose additive was added to the sample shown in the previous figure to optimize the structures. Because of its dimensions, a length of 30 voxels was used, and its flexibility received the highest value, which is 4. Because the production of micro/nanofibrillated cellulose is associated with a high degree of fibrillation, its fibers are very flexible. On the right side of Figure 4.40, the three-dimensional structure of this fiber mixture can be seen.

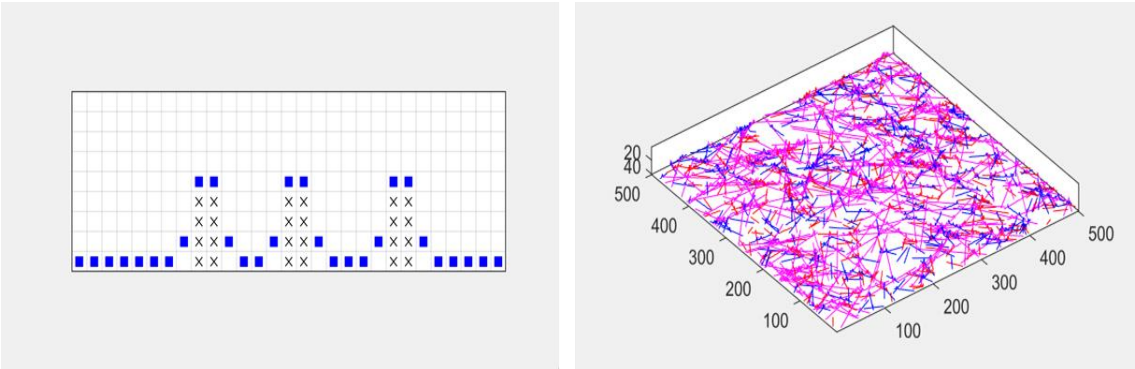

Figure 4.40 - The simulation represents the final stage in the deposition process of HW (blue), HF (pink), and the micro/nanofibrillated cellulose (red) mixture that has a length of 40, 130, and 30 voxels and flexibility of 3, 2 and 4, respectively. The left side is the fiber deposition in voxels, and the right side represents the visualization of 3D structures.

Combining the three types of fiber (HW, HF, and micro/nano-fibrillated cellulose) allows the design of an optimized material concerning its basic structural properties, which can later be experimentally validated. For the same reason, the scheme presented in Figure 3.1 is circular, presenting an experimental and computational methodology that complement each other. It evolves, considering the elaboration, characterization, and validation of the structures until the intended objectives are reached.

Considering this, the results obtained are still very preliminary, and it is necessary to continue their development. More complete results will be presented in future work with the multidisciplinary research team.

Chapter V
Conclusions and Futures Perspectives

5. Conclusions and Futures Perspectives

This project aimed to reinforce theoretical and practical concepts from both of my academic backgrounds, bioengineering and biotechnology. This goal was accomplished by combining computational and experimental approaches to develop and optimize cellulose-based fibrous structures. Furthermore, I was interested in developing innovative solutions that improve people's daily lives using environmentally friendly materials. This was achieved by incorporating this research into molded food packaging.

Since the 3D simulator would require input data, the first step was to characterize and comprehend the morphology and behavior of the reference fibers and then the hemp fibers. The same evaluation concluded that softwood fibers are approximately three times longer than hardwood fibers. Combining bleaching HW fibers with unbleached SW, without mechanical treatments, was necessary to establish a correlation between the increase in the proportion of unbleached SW and the decrease in sample brightness. This correlation is essential for benchmarking purposes. Today's consumers prefer valuable and safe products for the environment simultaneously. An environmentally friendly option is typically linked to a commercial paper product that is browner in color.

When a mechanical treatment (PFI-refinement) was applied to these fibers, it was noticed that as the revolutions increased, the fibrillation percentage increased proportionately. The best values were obtained for hardwood PFI-refined at 12000 revolutions (2,20%) and softwood refined at 6000 revolutions (2,86%). The increase in fine elements and fibrillation favored greater compaction and homogenization of the structures. In other words, it created a greater network of interconnections between fibers on a micro and nanoscale. The refined structures, in relation to the unrefined ones overall, showed a decrease in thickness (HW_MT_6 reduction of 62% and SW_MT_6 reduction of 60%) and also in porosity (HW_MT_12 reduction of 42% and SW_MT_6 reduction of 51%). The fact that the application of refinements changed the morphology of these two fibers allowed both HW and SW structures refined at 6000 revolutions to have the highest and similar tensile index values, 85,6 MPa and 86,8 MPa, respectively. That is, applying a mechanical treatment favor improving the mechanical characteristics of the structures, a significant factor in the design and engineering of new food packaging materials using cellulose fibers.

The hemp fibers obtained of high length reached values greater than 2000 μm. From PFI-refining industrial tissue paper fibers (IT) at 1000 revolutions, to which 10% hemp fibers were added, it was possible to obtain a 32% increase in the tensile index and a 40% increase in elastic modulus compared to IT fibers. The reinforcing capacity and stability of hemp fibers make them an ideal candidate for possibly replacing softwood fibers for cellulosic structures, which are currently imported at high costs.

The biodegradation results were highly encouraging. However, this test had limitations because it was based on the quantitative measurement of the end product of metabolic degradation by weight loss. Other parameters should also be considered, such as the quantitative measurement of biomass, volatile compounds, and the proportions of dissolved and undissolved polymer parts. Nonetheless, collecting this information and continuing this research in the future will be necessary for moving to an industrial level.

The computer simulation results include modeling the various 3D fibrous matrix, whose structures were characterized and compared to actual structures produced in the laboratory. The results agree with scanning electron microscopy images and experimental characterization methods. As supported by the data reported, this experimental work, supported by a computer simulation strategy, provided new optimized materials and outlines for future experimental explorations.

In conclusion, the results obtained from the structures made in the laboratory and through computational simulation are essential for designing and developing new renewable materials.

Chapter VI
Bibliography

Abdul Khalil, H. P. S., Davoudpour, Y., Islam, M. N., Mustapha, A., Sudesh, K., Dungani, R., and Jawaid, M. (2014). Production and modification of nanofibrillated cellulose using various mechanical processes: A review. *Carbohydrate Polymers*, 99, 649–665. https://doi.org/10.1016/J.CARBPOL.2013.08.069

Abitbol, T., Rivkin, A., Cao, Y., Nevo, Y., Abraham, E., Ben-Shalom, T., Lapidot, S., and Shoseyov, O. (2016). Nanocellulose, a tiny fiber with huge applications. *Current Opinion in Biotechnology*, 39, 76–88. https://doi.org/10.1016/J.COPBIO.2016.01.002

Agbor, V. B., Cicek, N., Sparling, R., Berlin, A., and Levin, D. B. (2011). Biomass pretreatment: Fundamentals toward application. *Biotechnology Advances*, 29(6), 675–685. https://doi.org/10.1016/J.BIOTECHADV.2011.05.005

Aguado, R., Tarrés, Q., Pèlach, M. À., Mutjé, P., de la Fuente, E., Sanchez-Salvador, J. L., Negro, C., and Delgado-Aguilar, M. (2022). Micro- and Nanofibrillated Cellulose from Annual Plant-Sourced Fibers: Comparison between Enzymatic Hydrolysis and Mechanical Refining. *Nanomaterials*, 12(9), 1612. https://doi.org/10.3390/nano12091612

Alava, M., and Niskanen, K. (2006). The physics of paper. *Reports on Progress in Physics*, 69(3), 669-723. https://doi.org/10.1088/0034-4885/69/3/R03

Andersson, T., and Djeflat, A. (2013). Basics on Benchmarking. In T. Andersson and A. Djeflat (Eds.), *The Real Issues of the Middle East and the Arab Spring*. *Innovation*. Technology, and Knowledge Management. 95–110. Springer. https://doi.org/10.1007/978-1-4614-5248-5_4

Atarés, L., and Chiralt, A. (2016). Essential oils as additives in biodegradable films and coatings for active food packaging. *Trends in Food Science & Technology*, 48, 51–62. https://doi.org/https://doi.org/10.1016/j.tifs.2015.12.001

Bajpai, P. (2014). Deinking with Enzymes. Recycling and Deinking of Recovered Paper. 139–153. *Elsevier*. https://doi.org/10.1016/B978-0-12-416998-2.00008-8

Bao, F., Liang, Z., Deng, J., Lin, Q., Li, W., Peng, Q., and Fang, Y. (2022). Toward intelligent food packaging of biosensor and film substrate for monitoring foodborne microorganisms: A review of recent advancements. *Critical reviews in food science and nutrition*, 1-12. https://doi.org/10.1080/10408398.2022.2137774

Barbash, V. A., Yashchenko, O. V, Yakymenko, O. S., Zakharko, R. M., and Myshak, V. D. (2022). Preparation of hemp nanocellulose and its use to improve the properties of paper for food packaging. *Cellulose*, 29(15), 8305–8317. https://doi.org/10.1007/s10570-022-04773-6

Begley, T. H., Hsu, W., Noonan, G., and Diachenko, G. (2008). Migration of fluorochemical paper additives from food-contact paper into foods and food simulants. *Food additives & contaminants*, 25(3), 384–390. https://doi.org/10.1080/02652030701513784

Bento, R., Pagán, E., Berdejo, D., de Carvalho, R. J., García-Embid, S., Maggi, F., Magnani, M., de Souza, E. L., García-Gonzalo, D., and Pagán, R. (2020). Chitosan nanoemulsions of cold-pressed orange essential oil to preserve fruit juices. *International Journal of Food Microbiology*, 331, 108786. https://doi.org/10.1016/j.ijfoodmicro.2020.108786

Biji, K. B., Ravishankar, C. N., Mohan, C. O., and Srinivasa Gopal, T. K. (2015). Smart packaging systems for food applications: a review. *Journal of Food Science and Technology*, 52(10), 6125–6135. https://doi.org/10.1007/S13197-015-1766-7

Bronkhorst, C. A. (2003). Modelling paper as a two-dimensional elastic–plastic stochastic network. *International Journal of Solids and Structures*, 40(20), 5441–5454. https://doi.org/10.1016/S0020-7683(03)00281-6

Carrillo, I., Mendonça, R. T., Ago, M., and Rojas, O. J. (2018). Comparative study of cellulosic components isolated from different Eucalyptus species. *Cellulose*, 25(2), 1011–1029. https://doi.org/10.1007/s10570-018-1653-2

Chauhan, V., and Bhardwaj, N. (2013). Effect of particle size and preflocculation of talc filler on sizing characteristics of paper. *Appita Journal*, 66, 66–72.

Conceição, E. L. T., Curto, J. M. R., Simões, R. M. S., and Portugal, A. A. T. G. (2010). Coding a Simulation Model of the 3D Structure of Paper. In R.P. Barneva, V.E. Brimkov, H.A. Hauptman, R.M. Natal Jorge, and J.M.R.S. Tavares (Eds.), Computational Modeling of Objects Represented in Images. Lecture Notes in Computer Science, 6026, 27-38. *Springer*. https://doi.org/10.1007/978-3-642-12712-0_27

Cornelissen, M., Małyska, A., Nanda, A. K., Lankhorst, R. K., Parry, M. A. J., Saltenis, V. R., Pribil, M., Nacry, P., Inzé, D., and Baekelandt, A. (2021). Biotechnology for Tomorrow's World: Scenarios to Guide Directions for Future Innovation. *Trends in Biotechnology*, 39(5), 438–444. https://doi.org/10.1016/J.TIBTECH.2020.09.006

Curto, J. M. R. (2012). 3D Computational Simulation and Experimental Characterization of Polymeric Stochastic Network Materials: Case Studies in Reinforced Eucalyptus Office Paper and Nanofibrous Materials. PhD Thesis in Paper Engineering. University of Beira Interior, Covilhã, Portugal. http://hdl.handle.net/10400.6/4411

Curto, J. M. R., Conceição, E. L. T., Portugal, A. T. G., and Simões, R. M. S. (2011). Three-dimensional modelling of fibrous materials and experimental validation. *Materialwissenschaft Und Werkstofftechnik*, 42(5), 370–374. https://doi.org/10.1002/MAWE.201100790

Curto, J. M. R., Mendes, A. O., Conceição, E. L. T., Portugal, A. T. G., Fiadeiro, P. T., Ramos, A. M. M., Simões, R. M. S., and Santos Silva, M. J. (2015). Development of an innovative 3D simulator for structured polymeric fibrous materials and liquid droplets: Contribution to the experimental characterization and optimization of deposition time and spreading area using an innovative 3D optic system and a fibrous porous materials simulator. *Advanced Structured Materials*, 70, 301–321. https://doi.org/10.1007/978-3-319-19443-1_25

Das, P. P., Kalyani, P., Kumar, R., and Khandelwal, M. (2023). Cellulose-based natural nanofibers for fresh produce packaging: current status sustainability and future outlook. *Sustainable Food Technolgy*, 1(4), 528–544. https://doi.org/10.1039/D3FB00066D

Debnath, M., Sarder, R., Pal, L., and Hubbe, M. A. (2022). Molded Pulp Products for Sustainable Packaging: Production Rate Challenges and Product Opportunities. *BioResources*, 17(2), 3810–3870. https://doi.org/10.15376/BIORES.17.2.DEBNATH

Didone, M., Saxena, P., Brilhuis-Meijer, E., Tosello, G., Bissacco, G., Mcaloone, T. C., Pigosso, D. C. A., and Howard, T. J. (2017). Moulded Pulp Manufacturing: Overview and Prospects for the Process Technology. *Packaging Technology and Science*, 30(6), 231–249. https://doi.org/10.1002/PTS.2289

Eichhorn, S. J., Dufresne, A. A., Aranguren, A. M., Marcovich, A. N. E., Capadona, A. J. R., Rowan, A. S. J., Weder, A. C., Thielemans, A. W., Roman, A. M., Renneckar, A. S., Gindl, A. W., Veigel, A. S., Keckes, A. J., Yano, A. H., Abe, A. K., Nogi, A. M., Nakagaito, A. A. N., Mangalam, A. A., Simonsen, A. J., Nakagaito, Á. A. N. (2010). Review: current international research into cellulose nanofibres and nanocomposites. *Journal of Materials Science*, 45(1), 1–33. https://doi.org/10.1007/s10853-009-3874-0

Enescu, D., Cerqueira, M. A., Fucinos, P., and Pastrana, L. M. (2019). Recent advances and challenges on applications of nanotechnology in food packaging. A literature review. *Food and Chemical Toxicology*, 134, 110814. https://doi.org/10.1016/J.FCT.2019.110814

Erdal, N. B., and Hakkarainen, M. (2022). Degradation of Cellulose Derivatives in Laboratory, Man-Made, and Natural Environments. *Biomacromolecules*, 23(7), 2713–2729. https://doi.org/10.1021/acs.biomac.2c00336

Eurostat. (2022). Plastic packaging waste: 38% recycled in 2020. https://ec.europa.eu/eurostat/web/products-eurostat-news/-/ddn-20221020-1. (Accessed 20 March 2023).

Fiadeiro, P. T., de O. Mendes, A., Ramos, A. M. M., and de Sousa, S. C. L. (2013). Study of the ink-paper interaction by image analysis: surface and bulk inspection. *In* Proceedings of the SPIE 8th Iberoamerican optics meeting and 11th Latin American meeting on optics, lasers and applications, 8785BV-1/8785BV-8. https://doi.org/10.1117/12.2024991

Flauzino Neto, W.P. (2017). Morphological investigation of cellulose nanocrystals and nanocomposite applications. PhD Thesis in Chemistry. Federal University of Uberlândia, Uberlândia. https://repositorio.ufu.br/handle/123456789/18105

García-Guzmán, L., Cabrera-Barjas, G., Soria-Hernández, C. G., Castaño, J., Guadarrama-Lezama, A. Y., and Llamazares, S. R. (2022). Progress in Starch-Based Materials for Food Packaging Applications. *Polysaccharides*, 3(1), 136-177. https://doi.org/10.3390/POLYSACCHARIDES3010007

Ghaani, M., Cozzolino, C. A., Castelli, G., and Farris, S. (2016). An overview of the intelligent packaging technologies in the food sector. *Trends in Food Science & Technology*, 51, 1–11. https://doi.org/10.1016/J.TIFS.2016.02.008

Ginebreda, A., Guillén, D., Barceló, D., and Darbra, R.M. (2011). Additives in the Paper Industry. In Bilitewski, B., Darbra, R., Barceló, D. (Eds.), Global Risk-Based Management of Chemical Additives I. *The Handbook of Environmental Chemistry*, 18, 11-34. Springer. https://doi.org/10.1007/698_2011_109

Giordano, L., Gonthier, P., Negro, F., Zanuttini, R., and Cremonini, C. (2021). Effectiveness of new molecules against widespread moulds for food-safe hardwood and softwood packaging. *European Journal of Wood and Wood Products,* 79(1), 227–236. https://doi.org/10.1007/s00107-020-01626-6

Gupta, B., Rawat, A., Jain, A., Arora, A., and Dhami, N. (2017). Analysis of Various Decision Tree Algorithms for Classification in Data Mining. *International Journal of Computer Applications*, 163, 15–19. https://doi.org/10.5120/ijca2017913660

Han, G. (2022). Characterization and properties of nanocellulose-enhanced pulp-molded lunch boxes. *Journal of Physics: Conference Series*, 2393(1), 12006. https://doi.org/10.1088/1742-6596/2393/1/012006

Hann, Simon; Ettlinger, Sarah; Gibbs Adrian; Hogg, Dominic; Ledingham, B. (2017). Study to provide Information supplementing the Study on the Impact of the Use of "oxo-degradable" plastic on the Environment. Final report, Publications Office. https://doi.org/https://doi.org/10.2779/081633

Heinze, T. (2015). Cellulose: Structure and properties. *Advances in Polymer Science*, 271, 1–52. https://doi.org/10.1007/12_2015_319/COVER

Heyden, S. (2000). Network Modelling for Evaluation of Mechanical Properties of Cellulose Fibre Fluff. PhD Thesis in Structural Mechanics. Lund University, Lund, Sweden. https://lup.lub.lu.se/record/19648

Isogai, A., Hänninen, T., Fujisawa, S., and Saito, T. (2018). Review: Catalytic oxidation of cellulose with nitroxyl radicals under aqueous conditions. *Progress in Polymer Science*, 86, 122–148. https://doi.org/10.1016/J.PROGPOLYMSCI.2018.07.007

Isogai, A., Saito, T., and Fukuzumi, H. (2011). TEMPO-oxidized cellulose nanofibers. *Nanoscale*, 3(1), 71–85. https://doi.org/10.1039/C0NR00583E

Itävaara, M., and Vikman, M. (1996). An overview of methods for biodegradability testing of biopolymers and packaging materials. *Journal of Environmental Polymer Degradation*, 4(1), 29–36. https://doi.org/10.1007/BF02083880

Jackson, C., Mercy Obiakor, N., Okokon Ita, O., Clement Jackson, T., Nkwachi Iheanyichukwu, I., and Salome Ucheokoro, A. (2021). Biotechnology and Nanotechnology Drug Delivery: A Review. *Journal of Pharmacy and Pharmacology*, 9, 127-132. https://doi.org/10.17265/2328-2150/2021.04.001

Jafari, M. (2017). Application of Vibrational Spectroscopy in Organic Electronics. PhD Thesis in Molecular Physics. Linköping University Electronic Press. https://urn.kb.se/resolve?urn=urn:nbn:se:liu:diva-142216

Kallmes, O. J., and Corte, H. (1960). Statistical Geometry of a Fibrous Network, Formation and Structure of Paper. 13–46.

Kallmes, O. J., and Corte, H. (1962). The Interpretation of Paper Properties in Terms of Structure, Formation and Structure of Paper 2. 351–368.

Kerekes, R. J., McDonald, D., and Zhao, J. (2020). Perspectives on deriving mathematical models in pulp and paper science. *Bioresources*, 15, 7319–7329. https://doi.org/10.15376/biores.15.4.7319-7329

Klemm, D., Heublein, B., Fink, H. P., and Bohn, A. (2005). Cellulose: Fascinating Biopolymer and Sustainable Raw Material. *Angewandte Chemie* International Edition, 44(22), 3358–3393. https://doi.org/10.1002/ANIE.200460587

Kostić, M. (2021). Development of novel cellulose-based functional materials. *Advanced Technologies*, 10(2), 73–83. https://doi.org/10.5937/SAVTEH2102073K

Kovalenko, V. I. (2010). Crystalline cellulose: structure and hydrogen bonds. *Russian Chemical Reviews,* 79(3), 231–241. https://doi.org/10.1070/RC2010v079n03ABEH004065

Lavrykov, S., Lindström, S. B., Singh, K. M., and Ramarao, B. V. (2012). 3D network simulations of paper structure. *Nordic Pulp and Paper Research Journal*, 27(2), 256–263. https://doi.org/10.3183/npprj-2012-27-02-p256-263

Li, A., Xu, D., Luo, L., Zhou, Y., Yan, W., Leng, X., Dai, D., Zhou, Y., Ahmad, H., Rao, J., and Fan, M. (2021). Overview of nanocellulose as additives in paper processing and paper products. *Nanotechnology Reviews*, 10(1), 264–281. https://doi.org/10.1515/NTREV-2021-0023

Li, L., Kim, S. M., Song, S. H., Ku, T. W., Song, W. J., Kim, J., Chong, M. K., Park, J. W., and Kang, B. S. (2008). Finite element modeling and simulation for bending analysis of multi-layer printed circuit boards using woven fiber composite. *Journal of Materials Processing Technology*, 201(1), 746–750. https://doi.org/https://doi.org/10.1016/j.jmatprotec.2007.11.190

Li, T., Chen, C., Brozena, A. H., Zhu, J. Y., Xu, L., Driemeier, C., Dai, J., Rojas, O. J., Isogai, A., Wågberg, L., and Hu, L. (2021). Developing fibrillated cellulose as a sustainable technological material. *Nature*, 590, 47-56. https://doi.org/10.1038/s41586-020-03167-7

Lin, N., and Dufresne, A. (2014). Nanocellulose in biomedicine: Current status and future prospect. *European Polymer Journal*, 9, 302–325. https://doi.org/10.1016/j.eurpolymj.2014.07.025

Martins, V. D. F., Cerqueira, M. A., Fuciños, P., Garrido-Maestu, A., Curto, J. M. R., and Pastrana, L. M. (2018). Active bi-layer cellulose-based films: development and characterization. *Cellulose*, 25(11), 6361–6375. https://doi.org/10.1007/S10570-018-2021-Y/TABLES/3

Medeiros, J. F. B., Mendes, J. A. S., Samba, N., Fiadeiro, P. T., Silva, L., and Curto, J. M. R. (2023). Biodegradable Cannabis sativa L. combined with the Ageratum conyzoides L. Essential Oil Drug Delivery System (DDS) for Dermic Application. Proceedings of the 71st International Congress and Annual Meetings of the Society for Medicinal Plant and Natural Products Research (GA), 2-5 July 2023, Trinity College, Dublin, Irland.

Mendes, A. M., Fiadeiro, P. T., Ramos, A. M. M., and de Sousa, S. C. L. (2013). Development of an optical system for analysis of the ink–paper interaction. *Machine Vision and Applications*, 24(8), 1733–1750. https://doi.org/10.1007/s00138-013-0496-y

Mendes, J. A. S., and Curto, J. M. R. (2021). Development of Multi Layer Protection Masks Made from Polymer Based Materials. Proceedings of Polymer Connect: Polymer Science and Composite Materials Conference, 5-7 July 2021, Virtual.

Michelin, M., Marques, A. M., Pastrana, L. M., Teixeira, J. A., and Cerqueira, M. A. (2020). Carboxymethyl cellulose-based films: Effect of organosolv lignin incorporation on physicochemical and antioxidant properties. *Journal of Food Engineering,* 285, 110107. https://doi.org/10.1016/J.JFOODENG.2020.110107

Monga, S., Thapliyal, B. P., Tyagi, S., and Naithani, S. (2017a). Relationship between Strength Properties and Fiber Morphological Characteristics of E. tereticornis –Part-2. Regression and Artificial Neural Networks Analysis. *International Journal of Science and Research*, 6(1), 1557.

Monga, S., Thapliyal, B., Tyagi, S., and Naithani, S. (2017b). Relationship between Strength Properties and Fiber Morphological Characteristics of S. officinarum – Part-1: Regression and Artificial Neural Networks Analysis. *International Journal of Science and Research*, 6 (1), 6–391.

Morais, F. P. (2017). Desenvolvimento de Sistemas de Entrega de Fármacos Inovadores utilizando Materiais Poliméricos Porosos contendo Nanocelulose. Master Thesis in Medicinal Chemistry. University of Beira Interior, Covilhã, Portugal. http://hdl.handle.net/10400.6/9468

Morais, F. P., Carta, A. M. M. S., Amaral, M. E., and Curto, J. M. R. (2021). Micro/nano-fibrillated cellulose (MFC/NFC) fibers as an additive to maximize eucalyptus fibers on tissue paper production. *Cellulose*, 28(10), 6587–6605. https://doi.org/10.1007/s10570-021-03912-9

Morais, F. P., Carta, A. M. M. S., Amaral, M. E., Curto, J. M. R., Ferri, J. M., Fombuena Borràs, V., Fernando, M., and Carrasco, A. (2021). An Innovative Computational Strategy to Optimize Different Furnish Compositions of Tissue Materials Using Micro/Nanofibrillated Cellulose and Biopolymer as Additives. *Polymers* 13(15), 2397. https://doi.org/10.3390/POLYM13152397

Morais, F. P., and Curto, J. M. R. (2022a). 3D Computational Simulation and Experimental Validation of Structured Materials: Case Studies of Tissue Papers. *BioResource*s, 17(3), 4206–4225. https://doi.org/10.15376/BIORES.17.3.4206-4225

Morais, F. P., and Curto, J. M. R. (2022b). Challenges in Computational Materials Modelling and Simulation: A case-study to predict tissue paper properties. *Heliyon*, 8(5), e09356. https://doi.org/10.1016/j.heliyon.2022.e09356

Morais, F. P., and Curto, J. M. R. (2022c). Design and Engineering of Natural Cellulose Fiber-Based Biomaterials with Eucalyptus Essential Oil Retention to Replace Non-Biodegradable Delivery Systems. *Polymers*, 14(17), 3621. https://doi.org/10.3390/POLYM14173621

Morais, F. P., and Curto, J. M. R. (2023). 3D simulation of nano/micro cellulose delivery systems for dermic and respiratory applications: Case study of eucalyptus essential oil incorporation. *Materialwissenschaft Und Werkstofftechnik*, 54(4), 450–458. https://doi.org/https://doi.org/10.1002/mawe.202200284

Morais, F. P., Mendes, A. O., Carta, A. M. M. S., Fiadeiro, P. T., Amaral, M. E., and Curto, J. M. R. (2023). A 3D Fiber-Based Strategy for Optimization of Tissue Materials Using a Combination of Liquid Absorbency/Retention Methods. A. Öchsner and H. Altenbach (Eds.), Engineering Design Applications V: Structures, Materials and Processes, 81–11. *Springer*. https://doi.org/10.1007/978-3-031-26466-5_6

Moreira, J. M. H. P. (2023). Development of dermic application systems made from micro/nano cellulose biopolymeric materials with 3D porosity simulation to optimize the retention and release of essential oils biomolecules. Master Thesis in Biotechnology. University of Beira Interior, Covilhã, Portugal. http://hdl.handle.net/10400.6/13327

Muddasar, M., Beaucamp, A., Culebras, M., and Collins, M. N. (2022). Cellulose: Characteristics and applications for rechargeable batteries. *International Journal of Biological Macromolecules*, 219, 788–803. https://doi.org/10.1016/J.IJBIOMAC.2022.08.026

Myers, R.H., Montgomery, D.C., and Anderson-Cook, C.M. (2016). Response Surface Methodology: Process and Product Optimization Using Designed Experiments. 4th edition, *Wiley*.

Nascimento, E. S., Barros, M. O., Cerqueira, M. A., Lima, H. L., Borges, M. de F., Pastrana, L. M., Gama, F. M., Rosa, M. F., Azeredo, H. M. C., and Gonçalves, C. (2021). All-cellulose nanocomposite films based on bacterial cellulose nanofibrils and nanocrystals. *Food Packaging and Shelf Life*, 29, 100715. https://doi.org/10.1016/J.FPSL.2021.100715

Nasrollahzadeh, M., Sajadi, S. M., Sajjadi, M., and Issaabadi, Z. (2019). Applications of Nanotechnology in Daily Life. *Interface Science and Technology*, 28, 113–143. https://doi.org/10.1016/B978-0-12-813586-0.00004-3

Nguyen, S. Van, and Lee, B.-K. (2022). Polyvinyl alcohol/alkyl ketene dimer films with excellent water resistance and water vapor barrier properties. *Materials Letters*, 307, 131045. https://doi.org/https://doi.org/10.1016/j.matlet.2021.131045

Nida, S., Moses, J. A., and Anandharamakrishnan, C. (2021). 3D printed food package casings from sugarcane bagasse: a waste valorization study. *Biomass Conversion and Biorefinery*, 1, 1–11. https://doi.org/10.1007/s13399-021-01982-0

Niskanen, K. J., and Alava, M. J. (1994). Planar Random Networks with Flexible Fibers. *Physical Review Letters*, 73(25), 3475–3478. https://doi.org/10.1103/PhysRevLett.73.3475

Niskanen, K.J., Nilsen, N., Hellen, E., and Alava, M.J. (1997). KCL-PAKKA: Simulation of the 3D structure of paper. In Proceedings of The Fundametals of Papermaking Materials, Trans. of the XI Fund. Res. Symp. Cambridge. 1273–1291. https://doi.org/10.15376/frc.1997.2.1273.

Oliaei, E., Lindström, T., and Berglund, L. A. (2021). Sustainable development of hot-pressed all-lignocellulose composites—comparing wood fibers and nanofibers. *Polymers*, 13(16), 2747. https://doi.org/10.3390/POLYM13162747/S1

Oprea, M., and Voicu, S. I. (2020). Recent advances in composites based on cellulose derivatives for biomedical applications. *Carbohydrate Polymers*, 13(11), 2481. https://doi.org/10.1016/J.CARBPOL.2020.116683

Oshani Nayanathara, R. M., Leng, W., Liyanage, S. D., Wang, X., Wang, L., Wang, J., Tian, Z., Pittman, C. U., Gwaltney, S. R., and Zhang, X. (2023). A general Metal-Ion-Modification route for preparing hydrophobic paper and tableware from lignocellulose fibers. *Chemical Engineering Journal*, 459, 141596. https://doi.org/https://doi.org/10.1016/j.cej.2023.141596

Osong, S. H., Norgren, S., and Engstrand, P. (2016). Processing of wood-based microfibrillated cellulose and nanofibrillated cellulose, and applications relating to papermaking: a review. *Cellulose*, 23(1), 93–123. https://doi.org/10.1007/s10570-015-0798-5

Phanthong, P., Reubroycharoen, P., Hao, X., Xu, G., Abudula, A., and Guan, G. (2018). Nanocellulose: Extraction and application. *Carbon Resources Conversion*, 1(1), 32–43. https://doi.org/10.1016/J.CRCON.2018.05.004

Picheth, G. F., Pirich, C. L., Sierakowski, M. R., Woehl, M. A., Sakakibara, C. N., de Souza, C. F., Martin, A. A., da Silva, R., and de Freitas, R. A. (2017). Bacterial cellulose in biomedical applications: A review. *International Journal of Biological Macromolecules,* 104, 97–106. https://doi.org/https://doi.org/10.1016/j.ijbiomac.2017.05.171

Rokach, L., and Maimon, O. (2005). Decision Trees. In O. Maimon and L. Rokach (Eds.), Data Mining and Knowledge Discovery Handbook, 165–192. *Springer*. https://doi.org/10.1007/0-387-25465-X_9

Saha, N., Kadu, D., and Madhu, G. (2019). Evaluation of Biodegradability Characteristics of Cellulose-based Film as per IS/ISO 14855-1 Evaluation of Biodegradability Characteristic. *Journal of Applied Packaging Research*, 12(3), 12-23. https://scholarworks.rit.edu/japr/vol11/iss3/2/

Sahu, T., Ratre, Y. K., Chauhan, S., Bhaskar, L. V. K. S., Nair, M. P., and Verma, H. K. (2021). Nanotechnology based drug delivery system: Current strategies and emerging therapeutic potential for medical science. *Journal of Drug Delivery Science and Technology*, 63, 102487. https://doi.org/10.1016/J.JDDST.2021.102487

Salgado, P. R., Di Giorgio, L., Musso, Y. S., and Mauri, A. N. (2021). Recent Developments in Smart Food Packaging Focused on Biobased and Biodegradable Polymers. *Frontiers in Sustainable Food Systems*, 5, 125. https://doi.org/10.3389/fsufs.2021.630393

Samba, N., Medeiros, J. F. B., Guerrero De León, E., Morán-Pinzón, J., Mondolis, E., Mero-Ríos, A., Díaz-Rodríguez, M., Morales-Barrios, A., Mendes, J. A. S., López Rodilla, J. M., Gomes, A., Silva, L., and Curto, J. M. R. (2023). Antioxidant Activity of Cochlospermum angolense Welw. ex Oliv Leaves. Proceedings of the 71st International Congress and Annual Meetings of the Society for Medicinal Plant and Natural Products Research (GA), 2-5 July 2023, Trinity College, Dublin, Irland.

Schenker, U., Chardot, J., Missoum, K., Vishtal, A., and Bras, J. (2021). Short communication on the role of cellulosic fiber-based packaging in reduction of climate change impacts. *Carbohydrate Polymers*, 254, 117248. https://doi.org/10.1016/J.CARBPOL.2020.117248

Semple, K. E., Zhou, C., Rojas, O. J., Nkeuwa, W. N., and Dai, C. (2022). Moulded pulp fibers for disposable food packaging: A state-of-the-art review. *Food Packaging and Shelf Life*, 33, 100908. https://doi.org/10.1016/J.FPSL.2022.100908

Seppänen, R. (2007). On the internal sizing mechanisms of paper with AKD and ASA related to surface chemistry, wettability and friction. PhD Thesis in Physical Chemistry. KTH Royal Institute of Technology, Stockholm, Sweden. https://urn.kb.se/resolve?urn=urn:nbn:se:kth:diva-4537

Shahcheraghi, N., Golchin, H., Sadri, Z., Tabari, Y., Borhanifar, F., and Makani, S. (2022). Nano-biotechnology, an applicable approach for sustainable future. *3 Biotech*, 12(3), 1–24. https://doi.org/10.1007/s13205-021-03108-9

Sharma, A., Thakur, M., Bhattacharya, M., Mandal, T., and Goswami, S. (2019). Commercial application of cellulose nano-composites – A review. *Biotechnology Reports*, 21, e00316. https://doi.org/10.1016/J.BTRE.2019.E00316

Silva, F. A. G. S., Dourado, F., Gama, M., and Poças, F. (2020). Nanocellulose Bio-Based Composites for Food Packaging. *Nanomaterials*, 10(10), 2041. https://doi.org/10.3390/NANO10102041

Simon, J. W. (2021). A Review of Recent Trends and Challenges in Computational Modeling of Paper and Paperboard at Different Scales. *Archives of Computational Methods in Engineering*, 28(4), 2409–2428. https://doi.org/10.1007/s11831-020-09460-y

Somvanshi, M., Chavan, P., Tambade, S., and Shinde, S. V. (2016). A review of machine learning techniques using decision tree and support vector machine. International Conference on Computing Communication Control and Automation (ICCUBEA), 1–7 August. https://doi.org/10.1109/ICCUBEA.2016.7860040

Sousa, S. (2012). Estudo da interação tinta/papel na impressão inkjet. PhD Thesis.in Paper Engineering University of Beira Interior, Covilhã, Portugal. http://hdl.handle.net/10400.6/2776

Sousa, S., Mendes, A., Fiadeiro, P., and Ramos, A. (2014). Dynamic Interactions of Pigment-Based Inks on Chemically Modified Papers and Their Influence on Inkjet Print Quality. *Industrial and Engineering Chemistry Research*, 53(12), 4660–4668. https://doi.org/10.1021/ie403595f

Tahir ul Qamar, M., Alqahtani, S. M., Alamri, M. A., and Chen, L. L. (2020). Structural basis of SARS-CoV-2 3CLpro and anti-COVID-19 drug discovery from medicinal plants. *Journal of Pharmaceutical Analysis*, 10(4), 313–319. https://doi.org/10.1016/j.jpha.2020.03.009

Tingaut, P., Zimmermann, T., and Ebe Bc, G. S. (2012). Cellulose nanocrystals and microfibrillated cellulose as building blocks for the design of hierarchical functional materials.*Journal of Materials Chemistry*, 22, 20105-20111 https://doi.org/10.1039/c2jm32956e

Trache, D., Tarchoun, A. F., Derradji, M., Hamidon, T. S., Masruchin, N., Brosse, N., and Hussin, M. H. (2020). Nanocellulose: From Fundamentals to Advanced Applications. *Frontiers in Chemistry*, 8, 392. https://doi.org/10.3389/fchem.2020.00392

United Nations. (2021). Goal 12: Ensure sustainable consumption and production patterns. https://www.un.org/sustainabledevelopment/sustainable-consumption-production/ (Accessed 15 May 2023).

Usman, M., Farooq, M., Wakeel, A., Nawaz, A., Cheema, S. A., Rehman, H. ur, Ashraf, I., and Sanaullah, M. (2020). Nanotechnology in agriculture: Current status, challenges and future opportunities. Science of The Total Environment, 721, 137778. https://doi.org/10.1016/j.scitotenv.2020.137778

Vanderroost, M., Ragaert, P., Devlieghere, F., and De Meulenaer, B. (2014). Intelligent food packaging: The next generation. *Trends in Food Science & Technology*, 39(1), 47–62. https://doi.org/10.1016/J.TIFS.2014.06.009

Velosa, J. C., Mendes, J. A. S., Medeiros, J. F. B., Mitchell, G., Fiadeiro, P. T., and Curto, J. M. R. (2023). Design and Optimization of Printed Circuit Boards Reinforced with Natural Fibers using Computational Finite Element Modeling. Proceedings of the XXVI International Conference – Forest Biobased Materials – TECNICELPA 2023, 11-13 October 2023, Coimbra, Portugal.

Vieira, J. C., Morais, F., de Oliveira Mendes, A., Ribeiro, M. L., Carta, A. M., Curto, J., Amaral, M. E., Fiadeiro, P. T., and Costa, A. P. (2022). Mechanical and softness characterization of “deco” and “micro” embossed tissue papers using finite element model (FEM) validation. *Cellulose*, 29(10), 5895–5912. https://doi.org/10.1007/s10570-022-04618-2

Vijayakumar, M. D., Surendhar, G. J., Natrayan, L., Patil, P. P., Ram, P. M. B., and Paramasivam, P. (2022). Evolution and Recent Scenario of Nanotechnology in Agriculture and Food Industries. *Journal of Nanomaterials*, 2022(5), 1-17 https://doi.org/10.1155/2022/1280411

von Sivers, M., and Zacchi, G. (1995). A techno-economical comparison of three processes for the production of ethanol from pine. *Bioresource Technology*, 51(1), 43–52. https://doi.org/10.1016/0960-8524(94)00094-H

Wan, Y. Z., Luo, H., He, F., Liang, H., Huang, Y., and Li, X. L. (2009). Mechanical, moisture absorption, and biodegradation behaviours of bacterial cellulose fibre-reinforced starch biocomposites. *Composites Science and Technology*, 69(7), 1212–1217. https://doi.org/https://doi.org/10.1016/j.compscitech.2009.02.024

Xi, J., Du, W., Zhong, and L., Xi, J., Du, W., and Zhong, and L. (2013). Probing the Interaction Between Cellulose and Cellulase with a Nanomechanical Sensor. *Cellulose*, 7, 125 – 140 https://doi.org/10.5772/50285

Xu, Y., Noonan, G. O., and Begley, T. H. (2013). Migration of perfluoroalkyl acids from food packaging to food simulants. *Food Additives & Contaminants*, 30(5), 899–908. https://doi.org/10.1080/19440049.2013.789556

Yildirim, S., Röcker, B., Pettersen, M. K., Nilsen-Nygaard, J., Ayhan, Z., Rutkaite, R., Radusin, T., Suminska, P., Marcos, B., and Coma, V. (2018). Active Packaging Applications for Food. *Comprehensive Reviews in Food Science and Food Safety*, 17(1), 165–199. https://doi.org/10.1111/1541-4337.12322

Zhang, Y., Duan, C., Bokka, S. K., He, Z., and Ni, Y. (2022). Molded fiber and pulp products as green and sustainable alternatives to plastics: A mini review. *Journal of Bioresources and Bioproducts*, 7(1), 14–25. https://doi.org/10.1016/J.JOBAB.2021.10.003

Zhou, W., Fang, J., Tang, S., Wu, Z., and Wang, X. (2021). 3D-Printed Nanocellulose-Based Cushioning–Antibacterial Dual-Function Food Packaging Aerogel. *Molecules*, 26(12), 3543. https://doi.org/10.3390/MOLECULES26123543

Zinge, C., and Kandasubramanian, B. (2020). Nanocellulose based biodegradable polymers. *European Polymer Journal*, 133, 109758. https://doi.org/10.1016/J.EURPOLYMJ.2020.109758

Appendix

Appendix A. Publication List

Silva, S.J., Samba N., Mendes, J. A. S., Pires, J. R. A., Rodrigues, C., Curto, J. M. R., Gomes, A. C., Fernando, A.L and Silva, L. (2023). Sustainable food packaging with chitosan biofilm reinforced with nanocellulose and essential oils. *Macromol*. Accepted for Publication.

Medeiros, J. F. B., Mendes, J. A. S. and Curto, J. M. R. Extraction of cellulose from Cannabis sativa L. evaluation and comparison of its fibers with Eucalyptus globulus and Pinus pinaster fibers. Submitted for review.

Mendes, J.A.S. and Curto, J.M.R. (2021). Development of Multi-Layer Protection Masks Made from Polymer Based Materials. Proceedings of the Polymer Science and Composite Materials Conference, Polymer Connect on 05-07 July 2021, Virtual.

Curto, J. M. R., Medeiros, J. F. B., Mendes, J. A. S., Samba, N., Oliveira, S., Videira, P., Silva, L., Amaral, M. E., Fiadeiro, P. T and Costa, A. P. (2023). Engineering of Eucalyptus and Cannabis Biobased Materials for Dermic Applications using 3D Simulation. Proceedings of the XXVI International Conference – Forest Biobased Materials – TECNICELPA 2023, 11-13 October 2023, Coimbra, Portugal

Velosa, J. C., Mendes, J. A. S., Medeiros, J. F. B., Mitchell, G., Fiadeiro, P. T., and Curto, J. M. R. (2023). Design and Optimization of Printed Circuit Boards Reinforced with Natural Fibers using Computational Finite Element Modeling. Proceedings of the XXVI International Conference – Forest Biobased Materials – TECNICELPA 2023, 11-13 October 2023, Coimbra, Portugal

Medeiros, J. F. B., Mendes, J. A. S., Samba, N., Fiadeiro, P. T., Silva, L., and Curto, J. M. R. (2023). Biodegradable Cannabis sativa L. combined with the Ageratum conyzoides L. Essential Oil Drug Delivery System (DDS) for Dermic Application. Proceedings of the 71st International Congress and Annual Meetings of the Society for Medicinal Plant and Natural Products Research (GA), 2-5 July 2023, Trinity College, Dublin, Irland.

Samba, N., Medeiros, J. F. B., Guerrero De León, E., Morán-Pinzón, J., Mondolis, E., Mero-Ríos, A., Díaz-Rodríguez, M., Morales-Barrios, A., Mendes, J. A. S., López Rodilla, J. M., Gomes, A., Silva, L., and Curto, J. M. R. (2023). Antioxidant Activity of Cochlospermum angolense Welw. ex Oliv Leaves. Proceedings of the 71st International Congress and Annual Meetings of the Society for Medicinal Plant and Natural Products Research (GA), 2-5 July 2023, Trinity College, Dublin, Irland.

Velosa, J. C., Mendes, J. A. S., Medeiros, J. F. B., Mitchell, G., Fiadeiro, P. T., and Curto, J. M. R. (2023). Design and Optimization of Printed Circuit Boards Reinforced with Natural Fibers using Computational Finite Element Modeling. Proceedings of Ciência 2023 – Portuguese Science Summit, Science and Ocean Beyond the Horizon, 5-7 July 2023, University Campus of Santiago, Aveiro, Portugal.

Mendes, J. A. S., Videira, P., Velosa, J. C. and Curto, J.M.R. (2023). Design and engineering of multi-layer protection masks natural cellulose fiber-based biomaterials. Proceedings of VIII Faculty of Science Conference Cycle - A avaliação no Ensino: Os novos paradigmas, 29-30 September 2023, University of Beira Interior, Covilhã, Portugal.

Mendes, J. A. S. and Curto, J.M.R. (2022). Design and engineering of multi-layer protection masks natural cellulose fiber-based biomaterials Proceedings of VIII Faculty of Science Conference Cycle - Ensino Pós-Pandemia: O Novo Amanhã,23-24 September 2022, University of Beira Interior, Covilhã, Portugal.

Appendix B. Data obtained from the Characterization of the Reference Fibers

B1. Morphological Characterization

Table B1.1 - Morphological characterization using Morfi® in homogeneous fibers (HW or SW) and in mixtures with each other (heterogeneous fibers) in the proportions HW:SW - 90:10, 80:20, 50:10, respectively.

	Homogeneous Fibers		Heterogeneous Fibers		
	HW	SW	90_HW_10SW	80_HW_20SW	50_HW_50SW
Fibers Population (million/g)	1,5	3,8	18,9	16,1	11,32
Length weighted by length (µm)	749	2270	834	943	1148
Width (µm)	15,5	27,2	16,5	17,1	18,1
Coarseness (mg/m)	1,00	0,26	0,08	0,09	0,13
Fibrillation (%)	0,42	0,97	0,67	0,75	0,76
Broken Ends (%)	17,7	35,6	25,6	26,07	26,89
Kinked fibers (%)	44,1	44,7	43,7	46,5	47,9

Table B1.2 - Morphological characterization using Morfi® on homogeneous fibers (HW or SW) to which a mechanical process (PFI-refined) has been applied.

	Hardwood					Softwood		
	HW_MT_1	HW_MT_3	HW_MT_6	HW_MT_12	Additive	SW_MT_1	SW_MT_3	SW_MT_6
Fibers Population (million/g)	22,9	22,2	22,6	22,7	21,75	4,1	7,1	5,4
Length weighted by lengt (µm)	773	754	722	664	761	2284	2215	1977
Width (µm)	17,1	17,9	18,6	20,2	17,4	28,2	29,7	29,7
Coarseness (mg/m)	0,07	0,07	0,07	0,07	0,07	0,24	0,15	0,22
Fibrillation (%)	0,79	1,04	1,41	2,20	0,88	1,18	2,14	2,86
Broken Ends (%)	25,8	28,3	29,1	31,8	26,8	36,0	36,1	37,8
Kinked fibers (%)	34,7	36,6	37,4	45,4	35,0	32,2	32,9	36,7

B2. Structural Characterization

Table B2.1 - Structural characterization of homogeneous fibers (HW or SW) and mixtures with each other (heterogeneous fibers) in the proportions HW:SW - 50:50, 90:10, 80:20, 50:10, respectively.

	Homogeneous Fibers		Heterogeneous Fibers		
	HW	SW	90_HW_10SW	80_HW_20SW	50_HW_50SW
Weight (g)	1,24 ± 0,11	1,29 ± 0,17	1,35 ± 0,011	1,34 ± 0,022	1,47 ± 0,19
Area (m^2)	0,02138 ± 0				
Grammage (g/m^2)	57, 99 ± 5,22	60, 67 ± 8,15	63,06 ± 0,52	62,57 ± 1,04	67, 76 ± 0,87
Thickness (mm)	0,175 ± 0,15	0,211 ± 0,30	0,18 ± 0,0065	0,19 ± 0,0081	0,211 ± 0,0064
Bulk (cm^3/g)	3,02 ± 0,11	3,47 ± 0,10	2,904 ± 0,11	3,01±0,12	3,11 ± 0,12
Structure Density (g/cm^3)	0,331 ± 0,13	0,288 ± 0,01	0,34 ± 0,013	0,33 ± 0,13	0,32 ±0,012
Porosity (%)	77,92 ± 0,85	80,80 ± 0,56	77,01 ± 0,88	77,82 ± 0,86	78,54 ± 0,78

Table B2.2 - Structural characterization of homogeneous fibers (HW or SW) to which a mechanical process (PFI-refinement) has been applied.

	Hardwood				Softwood		
	HW_MT_1	HW_MT_3	HW_MT_6	Additive	SW_MT_1	SW_MT_3	SW_MT_6
Weight (g)	1,31 ± 0,16	1,33 ± 0,011	1,37 ± 0,084	1,37 ± 0,0089	1,31 ± 0,016	1,42 ± 0,033	1,34 ± 0,40
Area (m^2)	0,02138 ± 0						
Grammage (g/m^2)	61,31 ± 0,77	62,23 ± 0,54	64,15 ± 0,40	63,98 ± 0,42	61,31 ± 0,77	66,57 ± 1,55	62,68 ± 1,89
Thickness (mm)	0,090 ± 0,0016	0,074 ± 0,0017	0,066 ± 0,0011	0,088 ± 0,015	0,91 ± 0,0016	0,097 ± 0,0026	0,085 ± 0,0029
Bulk (cm^3/g)	1,47 ± 0,028	1,19 ± 0,033	1,03 ± 0,018	1,19 ± 0,033	1,48 ± 0,0qew24	1,46 ±0,034	1,36 ±0,046
Structure Density (g/cm^3)	0,68 ± 0,013	0,84 ± 0,023	0,97 ± 0,17	0,73 ± 0,13	0,68 ±0,011	0,68 ± 0,16	0,74 ± 0,024
Porosity (%)	54,76 ± 0,87	43,91 ±1,55	35,43 ± 1,11	51,40 ± 0,86	54,88 ± 0,73	54,40 ± 1,10	50,99 ± 1,57

B3. Mechanical Characterization

Table B3.1 – Mechanical characterization of homogeneous fibers (HW or SW) and mixtures with each other (heterogeneous fibers) in the proportions HW:SW - 90:10, 80:20, 50:10, respectively

	Homogeneous Fibers		Heterogeneous Fibers		
	HW	SW	90_HW_10SW	80_HW_20SW	50_HW_50SW
Tensile Index (Nm/a)	10,8 ± 1,67	9,6 ± 1,3	11,6 ± 2,2	10,2 ± 0,8	11,3 ± 0,8
Elastic Modulus (MPa)	770,02 ± 117,56	483,09 ± 78,92	763, 23 ± 115,22	671,39 ± 60,86	671,39 ± 60,86

Table B3.2 - Structural characterization of homogeneous fibers (HW or SW) to which a mechanical process (PFI-refinement) has been applied.

	Hardwood				Softwood		
	HW_MT_1	HW_MT_3	HW_MT_6	Additive	SW_MT_1	SW_MT_3	SW_MT_6
Tensile Index (Nm/a)	48,7 ± 3,9	71,9 ± 6,2	85,6 ± 5,8	57,8 ± 3,6	44,3 ± 2,8	71 ± 4,1	86,8 ± 3,4
Elastic Modulus (MPa)	4261,15 ± 160,07	5365,95 ± 478,04	5959,98 ± 431,63	4661,58 ± 255,07	3048,31 ± 143,97	4707,97 ± 205,38	5131,51 ± 494,22

Appendix C. Data obtained from the Characterization of the Hemp Fibers

C1. Morphological characterization of hemp fibers

Table C1.1 - Morphological characterization using Morfi® on hemp fibers.

	Hemp Fiber				
	HF_C_0.5M	HF_C_1M	HF_C_2M	HF_G_1M	HF_G_2M
Fibers Population (million/g)	7,32 ± 1,06	8,8 ± 0,31	7,10 ± 0,42	7,31 ± 0	9,97 ± 1,28
Length weighted by Length (µm)	2,72 ± 211	2,39 ± 36	2,38 ± 37	2,68 ± 23	1,46 ± 26
Width (µm)	24,2 ± 0,12	24,2 ± 0,33	19,6 ± 0,05	22 ± 0	23,7 ± 0,19
Coarseness (mg/m)	0,18 ± 0,03	0,14 ± 0,01	0,19 ± 0,01	0,17 ± 0	0,18 ± 0,02
Fibrillation (%)	1,12 ± 0,03	1,17 ± 0,07	0,94 ± 0,02	1.04 ± 0,02	1,51 ± 0,04
Broken Ends (%)	46,48 ± 0,36	46,3 ± 0,35	36,6 ± 0,55	42,1 ± 0,31	44,34 ±0,59
Kinked fibers (%)	43,77 ± 1,06	41,9 ± 0,43	51,05 ± 0,10	50,6 ± 0,42	47,52 ± 0,20

Appendix D. Data obtained from the Characterization of the Industrial Tissue Paper with Hemp Fibers

D1. Morphological Characterization

Table D1.1 - Structural characterization of homogeneous fibers (IT) and mixtures with hemp fiber (heterogeneous fibers) in the proportions IT:HF .

	Homogeneous Fibers	Heterogeneous Fibers		
	IT	99_IT_1_HF	90_IT_10_HF	90_IT_10_HF_1
Fibers Population (million/g)	17,4	17,6	18	18,5
Length weighted by Length (µm)	695	702	744	728
Width (µm)	17,4	17,6	18	18,5
Coarseness (mg/m)	0,0832	0,0839	0,0814	0,0,0862
Fibrillation (%)	1,08	1,06	1,09	1,12
Broken Ends (%)	29,19	30,06	32,15	31,63
Kinked fibers (%)	74,74	73,46	72,97	48,83

D2. Structural Characterization

Table D2.1 - Structural characterization of homogeneous fibers (IT) and mixtures with hemp fiber (heterogeneous fibers) in the proportions IT:HF .

	Homogeneous Fibers	Heterogeneous Fibers		
	IT	99_IT_1_HF	90_IT_10_HF	90_IT_10_HF_1
Weight (g)	1,34 ± 0,12	1,34 ± 0,008	1,37 ± 0,05	1,24 ± 0,02
Area (m^2)	0,02138 ± 0			
Grammage (g/m^2)	62,79 ± 0,5	62,86 ± 0,35	64,04 ± 2,35	58,13 ± 0,73
Thickness (mm)	0,168 ± 0,005	0,169 ± 0,003	0,185 ± 0,03	0,121 ± 0,005
Bulk (cm^3/g)	2,66 ± 0,024	2,70 ± 0,041	2,88 ± 0,36	2,08 ± 0,10
Structure Density (g/cm^3)	0,38 ± 0,003	0,37 ± 0,006	0,35 ± 0,038	0,48 ± 0,023
Porosity (%)	75,12 ± 0,46	75,32 ± 0,37	76,59 ± 2,52	67,93 ± 1,55

D3. Mechanical Characterization

Table D3.1 - Mechanical characterization of homogeneous fibers (IT) and mixtures with hemp fiber (heterogeneous fibers) in the proportions IT:HF .

	Homogeneous Fibers	Heterogeneous Fibers		
	IT	99_IT_1_HF	90_IT_10_HF	90_IT_10_HF_1
Tensile Index (Nm/a)	30,8 ± 1,4	14,5 ± 0,072	10,7 ± 0,077	50 ± 3,4
Elastic Modulus (MPa)	1650,43 ± 76,04	852,82 ± 58,09	731,7 ± 75,3	2318,94 ± 185,79